The Dissertation Committee for Christina Marie Davis Certifies that this is the approved version of the following dissertation:

Electron Transfer within Tetrathiafulvalene Calix[4]pyrrole Supramolecular Ensembles

Committee:

Jonathan L. Sessler, Supervisor

Michael J. Krische

Dionicio R. Siegel

David W. Hoffman

Jennifer S. Brodbelt

Eric V. Anslyn

Electron Transfer within Tetrathiafulvalene Calix[4]pyrrole Supramolecular Ensembles

by

Christina Marie Davis, B.S.

Dissertation

Presented to the Faculty of the Graduate School of

The University of Texas at Austin

in Partial Fulfillment

of the Requirements

for the Degree of

Doctor of Philosophy

The University of Texas at Austin

December 2014

Dedication

This dissertation is dedicated to Kinta B. and Frederic J. Delamain,
my loving grandparents, who have always been my biggest supporters.

Acknowledgements

Firstly, I would like to thank my advisor, Professor Jonathan L. Sessler, for allowing me to join his amazing research group where I was able to work on the chemistry that most interested me over my time in Austin. Prof. Sessler is one of the most uplifting, inspiring people I have ever known and it was an absolute pleasure to work under his guidance. I would like to thank him for all of his unconditional support and advice over the years as well as for his time and hard work editing our coauthored manuscripts as well as this dissertation.

I would also like to thank the chemist who sparked my interest in research, Prof. Elizabeth J. Harbron of The College of William and Mary. I cannot thank her enough for the experience and life lessons she bestowed upon me prior to graduate school.

Throughout my time at UT I had the pleasure of working with many collaborators from all over the world. I would like to thank Prof. Dongho Kim and Prof. Shunichi Fukuzumi not only for their academic expertise but also for their hospitality during my visits to their laboratories.

I am forever grateful for the privilege of working in the Sessler group with some of the most remarkable people I have ever known. I would especially like to thank: Christian Preihs for always being there during my many freak-outs over chemistry and being a wonderful life-long friend. Christopher Bejger and Nathan Bill for being my mentors and "big brothers" during my time at UT. Jung Su Park for taking me under his wing almost immediately after I arrived at UT and being like a second advisor to me, without whom I never would have learned so much supramolecular electron transfer chemistry so fast. Eric Silver for listening to me complain and always answering my relentless questions. Dong Sub Kim for being my TTF "partner in crime." Yerim Yeon

for being a wonderful friend and lab-mate, especially during our semester in Korea together. Aaron Lammer and Byung Joon Lim for being some of the best office mates a person imagine. Vladimir Roznyatovskiy for helping me with synthetic issues even after he graduated from UT. JuHoon Lee, my "work husband," for helping me get settled in to life at UT and in the Sessler lab. The post docs Zhan Zhang, I-Ting Ho, Dani Lyons, Ian Jones, Sungkuk Kim, Gregory Thiabaud, and Jonathan Arambula for being kind and helpful during my time at UT. The rest of the Sessler lab members who were on this journey with me over the last 4.5 years, Murat Deliomeroglu, Ren-Tsung Wu, Min Hee Lee, Jia Jia Cai, Gabriela Vargas-Zúñiga, Elizabeth Karnas, Soo Jung Leem, and Hao Li.

And last but not least, my parents, Marie D. and David W. Davis, sister Ashley E. Davis-Shick, fiancé Jeff Pruet, and sweet kitty Magnesium Davis for supporting me unconditionally throughout my studies, without whom none of this was possible.

Electron Transfer within Tetrathiafulvalene Calix[4]pyrrole Supramolecular Ensembles

Christina Marie Davis, Ph.D.

The University of Texas at Austin, 2014

Supervisor: Jonathan L. Sessler

Over the last decade, the ecological need for clean and renewable energy sources has resulted in considerable resources being directed toward the development of systems capable of converting light energy into chemical energy. This has led to a focus on artificial photosynthetic systems and solar cell devices. These types of devices are desirable since they do not contribute to greenhouse gas emissions, as compared with fossil fuels. Organic solar cells (OSCs) are able to convert solar energy into chemical energy via photon absorption that creates a potential difference in the medium and results in electron transfer. The evolution and lifetime of the charge-separated state produced upon this electron transfer has proved difficult to mimic with synthetic materials. One well recognized problem is that to achieve efficient electron transfer, the rate of back electron transfer must be slower than that of forward electron transfer. Creating a molecular dyad that undergoes rapid electron transfer and results in a long lifetime is a key step in the creation of an organic solar cell that permits efficient solar energy conversion. One such way to achieve these systems is to employ supramolecular interactions to pre-organize the donors and acceptors in solution.

The goal of the studies depicted in this dissertation was to explore whether tetrathiafulvalene substituted calix[4]pyrroles (TTF–C4Ps) paired with suitable electron

acceptors would lead to systems that undergo electron transfer, either thermal or photoinduced, followed by the formation of stable charge-separated states. We chose to employ fullerenes (Chapter 2) and a porphyrin substituted with a carboxylate functional group (Chapter 3) as the acceptors in the putative electron transfer complexes since both are well known as photoabsorbers that have been extensively studied in photosynthetic model systems. The electron transfer from a TTF moiety of the calix[4]pyrrole to either fullerene or porphyrin was studied via UV-Vis-NIR, fluorescence, and electron spin resonance spectroscopies as well as with laser flash photolysis measurements and theoretical calculations. Chapter 4 details work in which TTF oxidation states were used to create a stable TTF mixed-valence dimer as well as a redox switched "on—off—on" fluorescent system.

Table of Contents

List of Tables

List of Figures

List of Illustrations

Chapter 1

Historical Overview and Introduction to Electron Transfer and Tetrathiafulvalene Calix[4]pyrroles

1.1 Electron Transfer

Electron transfer (ET), one of the most elementary properties in life, is ubiquitous in both chemistry and biology. The most well known ET reactions in chemistry involve reduction-oxidation (redox) reactions as well as photochemical measurements.[1,2] Nature utilizes ET for such processes as photosynthesis, nitrogen fixation, cellular respiration, and fermentation.[2,3] Photosynthesis, arguably the most important biological process, utilizes solar energy in the form of light to produce nearly all the free energy utilized by biological systems,[3] excluding those that utilize chemosynthesis. The process of photosynthesis exploits potential differences across membranes and electron transfer reactions to produce energy as well as carbon compounds and oxygen. The general equation for the reduction of carbon dioxide and oxidation of water to form hydrocarbons and oxygen, respectively, via photosynthesis is represented in Figure 1.1 wherein CH_2O represents a carbohydrate.

$$CO_2 + H_2O \xrightarrow{\text{light}} (CH_2O) + O_2$$

Figure 1.1 The overall equation for photosynthesis.

In green plants, photosynthesis takes place in the chloroplasts, compartmentalized sacs resembling mitochondria. Chlorophyll, a cyclic magnesium tetrapyrrole located within the chloroplast, acts as a chromophore and absorbs light from the sun, which excites an electron from the ground state to an excited state.[3] Once in an excited state, an electron has multiple pathways by which it may return to the ground state, most of which will be discussed later on in this chapter. In the case of chlorophyll, there are suitable electron acceptors near by, which accept the electron resulting in the creation of a potential difference. This electron continues to move along a well-defined electron transport chain, reducing other molecules along the way. The end result of this electron transport pathway, initiated by the absorption of light, is the formation of a proton gradient, which allows for the production of chemical energy and the oxidation of water to form molecular oxygen.[3]

Individual reactions in the electron transport chain are examples of bimolecular ET. Bimolecular ET takes place between two molecules, a donor (D) and an acceptor (A), which are not covalently bound. The ET from D to A forms the oxidized donor ($D^{\bullet+}$) and the reduced acceptor ($A^{\bullet-}$). This transfer can be broken down into three main steps depicted in Figure 1.2. The first step involves the donor and acceptor associating through diffusion to form an encounter complex [D, A]. This complex then undergoes ET to form [$D^{\bullet+}$, $A^{\bullet-}$], also referred to as a charge transfer complex, which subsequently dissociates via diffusion into free ions as the radical cation $D^{\bullet+}$ and radical anion $A^{\bullet-}$.[4] The ET step can either occur spontaneously (thermal electron transfer) or as the result of photon absorption (photoinduced electron transfer).

Figure 1.2 Steps for the bimolecular electron transfer between a donor (D) and an acceptor (A).

The mechanism and mathematics behind ET was not elucidated until the 1950's when Rudolph A. Marcus published his theory, the Marcus Theory of Electron Transfer. This theory, most of which centers around the outer-sphere electron transfer seen in bimolecular ET reactions, coupled with the increased instrument developments have allowed our understanding of ET to increase exponentially in recent years. The following sections summarize the Marcus Theory and discuss ET events that occur as a result of photon absorption.

1.1.1 Marcus Theory of Electron Transfer

In 1956, Marcus published his theory on the mechanism of electron transfer.[4] In this paper, which consisted of a semi-empirical theory for ET, he stated that only a slight overlap of electronic orbitals of the donor and acceptor is necessary for ET to occur between reacting molecules. His theory on electron transfer and conceptualization of an activated complex electronic configuration in which no bonds are broken or formed is based on this small overlap assumption. Since he first published his theory on ET, Marcus produced many papers on the subject and subsequently was awarded the Nobel Prize in Chemistry in 1992.[5] A brief introduction to the Marcus Theory collated from Marcus's 1956 paper,[4] as well as others,[1,2,6] is given below.

For a wave function (ϕ) describing the electrons of reacting particles there are two valid solutions, one for the wave function of the electronic configuration of the two reactants (ϕ_x*) and one for the wave function of the electronic configuration of the

products (ϕ_x). If the two reactants only weakly interact, following the small overlap assumption, the correct wave function for the activated complex would be a linear combination of the two solutions, namely $\phi_x + c\phi_x^*$ where c is a constant. This linear combination is correct only if the two wave function solutions have the same total energy in any given atomic configuration. This is because the electron does not change energy upon transferring. Therefore, the molecular orbitals of the reactants and products must be degenerate. For this equilibrium system described, there are two hypothetical thermodynamic states which can be deemed X^* for the reactants and X for the products.

In solution, the two reactants are freely moving and the solvent configuration is fluctuating. It is pertinent that the configuration of the solvent in the activated complex allows for the total energy of the system to remain equal. Therefore, solvent–reactant and/or solvent–product assemblies must be manipulated such that they become energetically degenerate. The energy required to arrange the donor and acceptor orbitals within the solvent into a viable position for ET is referred to as the reorganization energy. It is one barrier to ET. Here, the Frank-Condon principle becomes significant. This principle states that electron transfer is a vertical transition because the nuclear geometry of the molecule does not change during the absorption of a photon since electronic transitions occur much faster than typical nuclear vibrations.[7] Therefore, solvent molecules do not have time to rearrange during the electronic transitions that occur during ET and neither do the nuclei of the reactant molecules. With that being said, if the two reactants approach each other under conditions where the solvent configuration is such that the total energy of the system is the same, an activated complex can be formed. Upon formation of this activated complex, the reactants can form state X^* which then can reform reactants upon disorganization or form state X leading to ET product formation.

The overall scheme for the conversion of reactants to products following the Marcus Theory is shown in Figure 1.3.

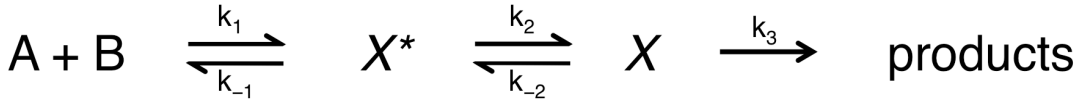

Figure 1.3 Reaction scheme for the conversion of reactants A and B to ET products in accordance with the Marcus Theory on electron transfer.

The equation derived by Marcus that represents the rate constant of ET within a nonadiabatic intramolecular system is as follows:

$$k_{ET} = \left(\frac{4\pi^3}{h^2 \lambda k_B T}\right)^{1/2} V^2 \exp\left[-\frac{(\Delta G_{ET} + \lambda)^2}{4\lambda k_B T}\right] \qquad (1)$$

wherein k_{ET} is the rate constant of ET, V is the electronic coupling constant, T is temperature, ΔG_{ET} is the Gibb's free energy, λ is the reorganization energy, k_B is the Boltzmann constant, and h is Planck's constant. The Marcus theory predicts that the rate of ET should decrease as the driving force for ET increases. This apparent dichotomy is referred to as the Marcus inverted region. Without this inverted region, efficient charge separation would be impossible because the back electron transfer would be rapid, causing the energy created via photon absorption to be lost as heat upon back electron transfer.

1.1.2 Photoinduced Electron Transfer

Electron transfer in Nature results from the absorption of a photon, as seen in photosynthesis. The ability of the photosynthetic apparatus to take light energy from the

sun and transform it into chemical energy has resulted in considerable scientific effort aimed at the development of artificial systems capable of such energy conversion. As discussed in the previous section, for bimolecular ET to take place, there needs to be donor (D) and suitable acceptor (A) within close proximity. Upon absorption of a photon of suitable energy, the D will be converted to an excited state. From this excited state, the electron has many different pathways it can move through in order to return to the ground state. The pathways that are available for the D in absence of an A are shown in Figure 1.4, commonly referred to as a Jablonski diagram.[1]

Upon absorption of a photon of suitable energy, an electron is excited to the singlet-excited state S_1 from the ground state S_0. This transition is quantized, meaning the energy of the photon must match the energy needed for the specific transition. The electronic transition occurs from the zero vibration level of the ground state and can go to any number of vibrational levels within the excited state, as dictated by the energy of the photon. If the electron is excited to a vibrational level above $v = 0$, the electron typically relaxes quickly down to the $v= 0$ level of the S_1 state. To return to S_0 directly from S_1, the electron can undergo a radiative or a radiationless transition. The radiative process is known as fluorescence and upon electronic transition to the ground state a photon is released whose energy matches that of the quantized transition. This transition will take place from the $v = 0$ level of S_1 to the vibrational level of S_0 that matches the vibrational level reached upon excitation. For example, if the electron is excited from S_0, $v = 0$ to S_1, $v = 3$, the transition from the excited state to the ground state will occur from S_1, $v = 0$ to S_0, $v = 3$. This difference results in what is known as a Stokes Shift, where the absorption λ_{max} is at a lower wavelength, of more energy, than the fluorescence λ_{max}. This is shown by the differences in magnitude illustrated by the arrows corresponding to process 1 and process 4 in the Jablonski diagram of Figure 1.4. Fluorescence is a rather fast process and

usually takes place on the order of nanoseconds. The radiationless process, also known as internal conversion, results in the electron relaxing to S_0 without the release of a photon.[1]

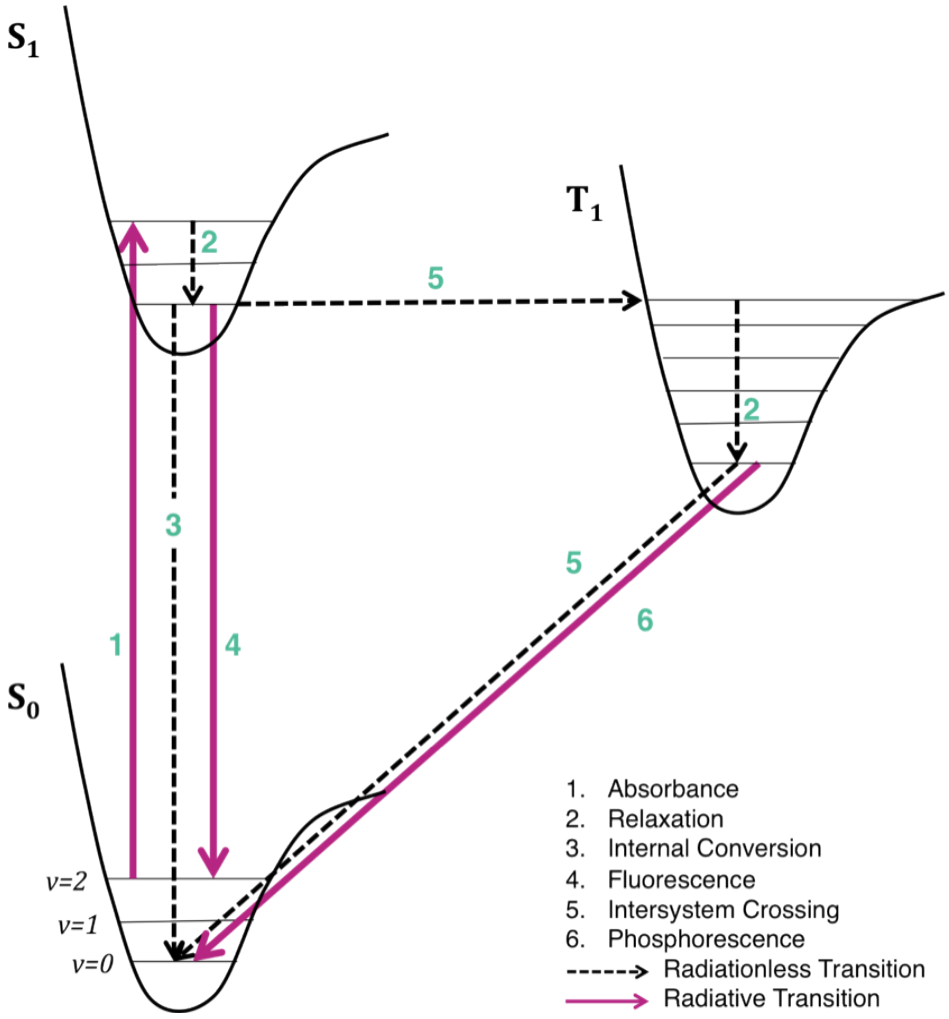

Figure 1.4 Jablonski diagram summarizing the electronic transitions an electron can undergo upon excitation via absorption of a photon.

To reach the triplet excited state T_1, the electron must undergo intersystem crossing. Intersystem crossing refers to a process where the spin of the electron is flipped from a +½ to a –½ spin state or visa versa. From T_1, the electron can relax back down to

ground state via radiationless means or it can undergo a phosphorescence transition, wherein a photon is emitted. The time-course of this latter transition is slower than that of fluorescence, resulting in phosphorescence being a longer-lived luminescence feature. It can take anywhere from seconds to a couple of minutes for this transition to occur.[1]

If a second molecule is in close proximity or electronically coupled to a photoexcited moleucle, the pathways the electron may take back to the ground state become more complex. For example, if a fluorophore undergoes a collision with a second molecule after being excited, its fluorescence may be quenched as the energy is transferred to the colliding molecule. This is referred to as dynamic quenching and is highly dependent on the concentration of solutions. However, if the electronic characteristics of the second molecule are appropriate and it is within a close proximity, the fluorescence of the first photoexcited molecule may be quenched through static quenching methods, such as energy or electron transfer. One such energy transfer method is through fluorescence resonance energy transfer, or FRET. This involves two fluorophores, D and A, wherein the fluorescence of the first (D) overlaps with the absorbance of the second (A). After the first fluorophore is excited, the photon that is emitted upon the S_1 to S_0 transition is absorbed by the second fluorophore, which undergoes photoexcitation. Relaxation of the second molecule to the ground state then gives rise to fluorescence. The net result is that excitation of the first fluorophore is followed by fluorescence emission from the second (Figure 1.5).[1]

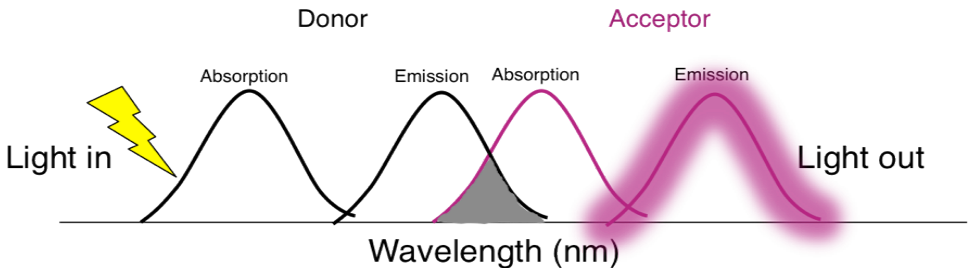

Figure 1.5 Depiction of energy transfer via fluorescence resonance energy transfer (FRET).

Photoinduced electron transfer (PET) takes place when the electron itself is transferred, rather than the energy as seen in processes such as FRET. Under conditions of PET, the excited molecule will either act as an acceptor or as a donor. However, the later is more prevalent. This is because upon excitation an electron moves from the highest occupied molecular orbital (HOMO) to the lowest unoccupied molecular orbital (LUMO). When the electron is in the LUMO, which is normally an anti-bonding orbital, the molecule generally has a lower oxidation potential allowing it to be more easily oxidized. [1]

Photoinduced electron transfer is known to occur in cases wherein the donor and acceptor are covalently bound as well as ones where the two components are non-covalently bound. Both binding modes have been explored for their potential use in artificial photosynthetic systems.[6,8-10] To study the dynamics of ET, transient absorption (TA) spectroscopy is usually employed. This technique allows for energy migration within the complex to be studied as well as the formation of new chromophoric chemical species, such as charge separated (CS) species.[11] To do this, laser flash photolysis is used and the absorbance of the excited state is recorded with initial measurements occurring as soon as 100 femtoseconds following the photoexcitation.[11] In TA spectroscopy, molecules are promoted to an electronically excited state by a light "pump" which enters

the sample at an angle to the detector, so the light of excitation is not detected by the instrument. At a varying time delays, a white light "probe" is sent through the sample. The absorbance of the species is then recorded at varying times post excitation. The instrument displays the data as ΔAbsorbance versus wavelength of light. A depiction of the instrumentation set up for TA spectroscopy can be seen in Scheme 1.1.[11]

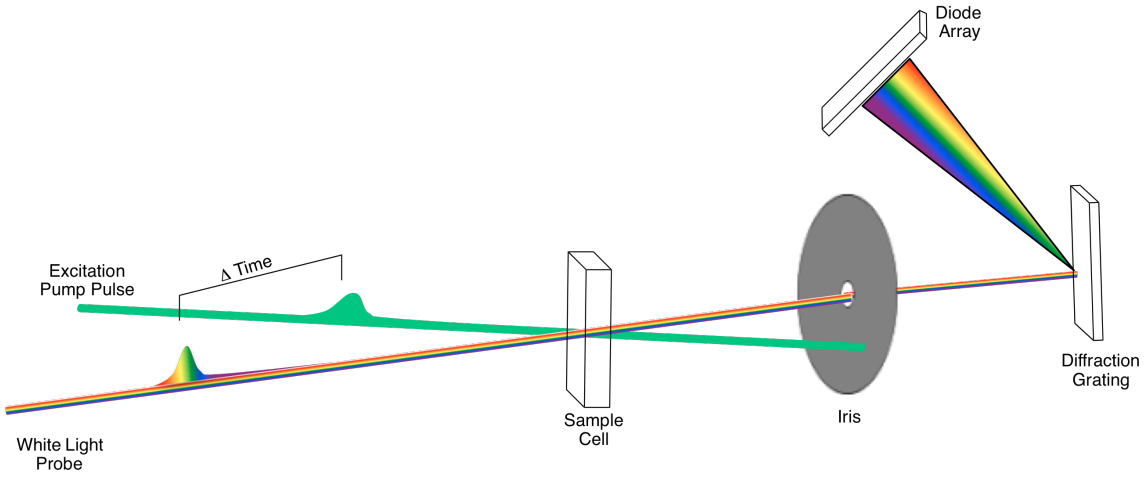

Scheme 1.1 Instrumental set up for transient absorption spectroscopy. The excitation pump pulse excites the sample and is angled as to not enter the detector through the iris. The white light probe then follows the pump after a certain time delay, which is varied, to determine the absorption of the photoexcited sample. The non-absorbed light continues through the iris to the diode array detector via diffraction grating.[11]

1.1.2.1 PET within Covalently Bound Donor-Acceptor Moieties

There are two main types of photoinduced ET complexes: Those with covalently bound and those with noncovalently bound donor (D) and acceptor (A) moieties. This first section will discuss various types of covalently bound systems and approaches that

have been pursued in an effort to increase the lifetime of the charge separated (CS) state within these complexes.

The steps involved in the conversion of light energy to chemical energy include the creation of an exciton upon photon absorption, separation and diffusion of the exciton into an electron and hole, transport of the electron and the hole to their respective electrodes, and collection of the charges.[9,12-14] In order to achieve efficient charge separation, the rate of forward electron transfer must be rapid while the back electron transfer event needs to be slow. Such kinetics allows the charges to separate fully and diffuse to their respective electrodes before charge recombination can occur.[2,5,6,12]

Two relatively simple ways that have been used to increase the lifetime of CS states within covalently bound D-A assemblies both involve manipulating the reorganization energy (λ) of the system. Marcus Theory states that the more exergonic an ET reaction is, the slower the rates of both forward and backward ET. However, if the driving force for back ET becomes larger than the reorganization energy associated with this ET event, the back electron transfer process becomes slowed. This slowing can occur while a relatively fast forward ET rate is still mainatained.[15] The first approach to manipulating the reorganization energy is to use a non-polar solvent. This minimizes the λ value and allows for the driving force of back ET to be larger than λ. A drawback of this technique, however, is that non-polar solvents can increase the energy level of the CS state making the forward ET process less favored. This results in a smaller quantum yield of ET and a reduced ability to do photo-chemical work.[16] The other common approach used in covalently bound systems is to employ a short linker between the donor and the acceptor moieties.[16] This allows for the back electron transfer process to be well within the Marcus inverted region due to a small reorganization energy.[16] Typically, the use of a short linker entity causes the rate of electron transfer to decrease due to a corresponding

increase in driving force. This, in turn, allows for the CS lifetime to be reasonably long, for example 310 μs at 278 K for dyad **1.1**[15] and 230 μs at 298 K for dyad **1.2**[17] as reported by the Fukuzumi and coworkers.

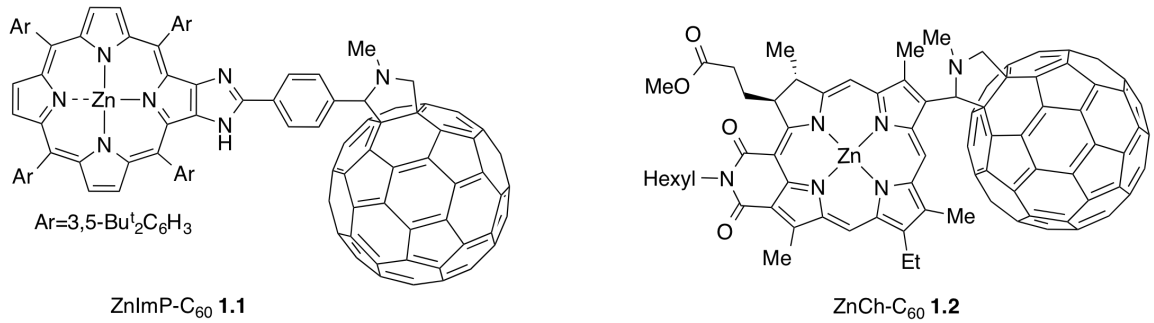

Figure 1.6 Structures for donor-acceptor dyads with relatively long charge separated state lifetimes, a zinc imidazolporphyrin-C_{60} dyad (ZnImP-C_{60}, **1.1**)[15] and a zinc chlorin-C_{60} dyad (ZnCh-C_{60}, **1.2**).[17]

When a stronger electron donor, ferrocene, was incorporated into dyad **1.1** to create **1.3** (Figure 1.7), the photoinduced CS state was extended from 310 μs to 630 μs.[18] This longer lived state was achieved through a secondary interaction of the ferrocene with the porphyrin donor. Upon excitation, the porphyrin donated an electron to the fullerene moiety, as seen in **1.1**; however, after ET evidence of a hole transfer step from the porphyrin moiety to the ferrocene was seen. The long-lived CS state was ascribed, in part, to the smaller λ value achieved through the shorter linkers between D and A, as well as the orbital delocalization and increased electronic coupling value V, resulting in the charge recombination (CR) process being slowed.[16]

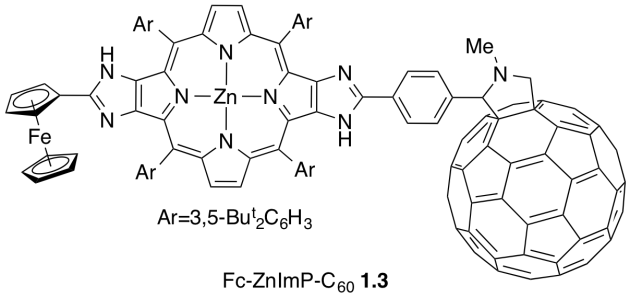

Figure 1.7 Structure for the ferrocene zinc imidazolporphyrin-C_{60} triad (ZnImP-C_{60}, **1.3**).[18]

Switching the bridge moiety between the ferrocene (Fc) unit and the fullerene (C_{60}) from a porphyrin to a naphthalenediimide (NDI) resulted in an even longer CS lifetime of 935 ps, as reported by Fukuzumi et al. in 2011.[19] This triad (**1.4**), seen in Figure 1.8, was shown to undergo stepwise ET. Density functional theory (DFT) calculations revealed that the highest occupied molecular orbital (HOMO) of the complex is located on the ferrocene moiety, while the lowest unoccupied molecular orbital (LUMO) is located on the fullerene. The LUMO+1 (i.e., second lowest unoccupied molecular orbital) was located on the NDI moiety. Upon photoirradiation of the NDI, initial CS occurs between the NDI and ferrocene subunits to form Fc^+–$NDI^{\bullet-}$–C_{60}. This CT is then followed by an ET event from NDI to fullerene resulting in the formation of Fc^+–NDI–$C_{60}^{\bullet-}$.

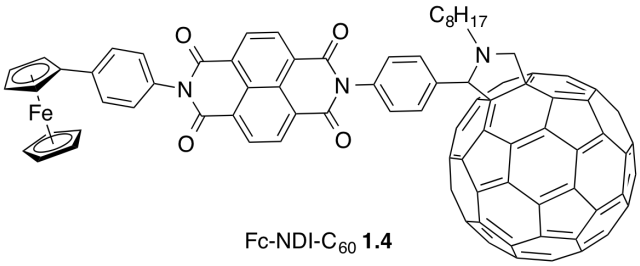

Figure 1.8 Structure of the ferrocene-naphthalenediimide-fullerene triad that undergoes photoinduced ET to create a CS state with a lifetime of 931 ps, as reported by Fukuzumi in 2011.[19]

To get around the restraint of using short linkers between D and A moieties, Ghiggino and Paddon-Row employed of a long, rigid linker, which allowed for efficient forward ET and produced a relatively long-lived CS state.[20] The specific dyad these researchers employed consisted of a porphyrin-tetraazaanthracene donor with either a benzoquinone (BQ) or tetracyanonaphthoquinidodimethane (TCQ) acceptor (**1.5** and **1.6**, respectively) with the D and A covalently linked through a six σ-bond polynorbornane bridge. In fact, a 7.32 Å distance was inferred between D and A (Figure 1.9). The lifetime of the CS state produced upon photoirradiation of the porphyrin subunit in this system reached up to 56 ns for **1.6** in *iso*-pentane.

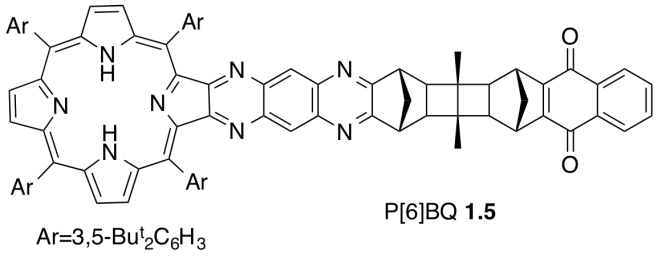

P[6]BQ **1.5**

Ar=3,5-$Bu^t_2C_6H_3$

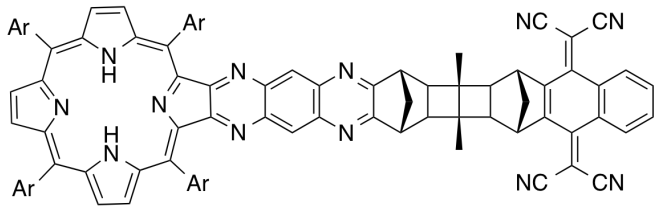

Ar=3,5-$Bu^t_2C_6H_3$ P[6]TCQ **1.6**

Figure 1.9 Porphyrin-tetraazaanthracene with either a benzoquinone (P[6]BQ) (**1.5**) or a tetracyanonaphthoquinidodimethane (P[6]TCQ) (**1.6**) covalently linked through a six σ-bond polynorbornane bridge.[20]

One of the longest known CS lifetimes, albeit at low temperature, was reported by Fukuzumi, Imahori, and Ito in 2004. It was produced upon photoexciting the ferrocene – *meso,meso*-linked porphyrin trimer – fullerene pentad (**1.7**) shown in Figure 1.10.[21] The

lifetime of the CS state was 0.52 seconds in dimethylformamide at 163 K and, although the linker length between the D and A subunits was 46.9 Å, the quantum yield of the CS (0.83) was high. These favorable features were ascribed in part to the stepwise ET from D to A through the three porphyrin bridge units. The long-lived intramolecular CS state produced using this system was considered comparable to that produced by the photosynthetic reaction center, a complex supramolecular ensemble consisting of a bateriochlorophyll dimer radical cation and a secondary quinone radical anion (~1 sec). Thus, this report represented a rather important step forward in the field of photoinduced ET.

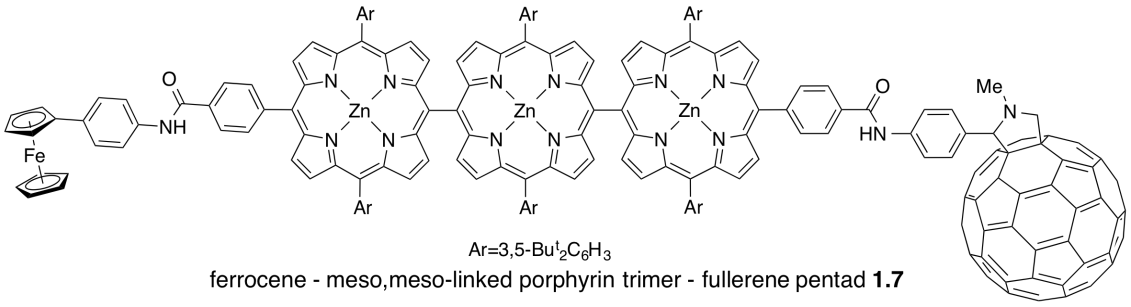

Figure 1.10 The ferrocene – *meso,meso*-linked porphyrin trimer – fullerene pentad (**1.7**) reported by Fukuzumi, Imahori, and Ito in 2004.[21]

As one might suspect, the synthesis of these covalently bound D-A complexes can be rather tedious depending on the complex. Due to these difficulties, efforts have increasingly turned towards the generation of artificial photosynthetic systems that produce long-lived CS states and which assemble using supramolecular means. In the next section we review some features of representative noncovalently bound D-A assemblies.

1.1.2.2 PET within Non-Covalently Bound Donor-Acceptor Moieties

Developing a two-component dyad that undergoes rapid forward electron transfer while maintaining a slow back electron transfer rate would be of great significance in the search for efficient artificial photosynthetic devices. However, the synthetic difficulties and low yields of the complex dyads described in the previous section makes this challenge a difficult one to over come. While there has been tremendous progress towards such a dyad,[9,22-25] there still has not been a simple and efficient cost effective device discovered. Using supramolecular interactions to construct electron transfer donor-acceptor dyads is of inherent interest due to the synthetic convenience of synthesizing each moiety individually and the ability to tune the electronics of each component separately.[12,26-43] By utilizing interactions, such as anion or hydrogen binding, the donor and acceptor can be brought close together in solution to form the D-A assembly. If the system is appropriately designed, the complex will then remain intact throughout forward and backward electron/charge transfer reactions.[26]

One of the first examples of a noncovalently linked D-A assembly was reported in 1992 by Harriman, Kubo, and Sessler.[44] In this system, Watson-Crick base-pairing interactions were employed to bring a porphyrin donor and a benzoquinone acceptor together with an association constant of around 3,100 M^{-1}. This system, shown in Figure 1.11 as **1.8** was further improved in 1993 by Sessler, Wang, and Harriman[42] by rigidifying the linker between the donor and acceptor and their respective DNA bases (**1.9**). The decreased flexibility in **1.9** allowed for the ET to occur via a through-bond process wherein the hydrogen bonding played a major role.[42] In the original system **1.8**, the authors believed that the conformational freedom in the system allowed ET to occur through the hydrogen bonding units as well as via diffusional (through space) encounters between the D and A.[44]

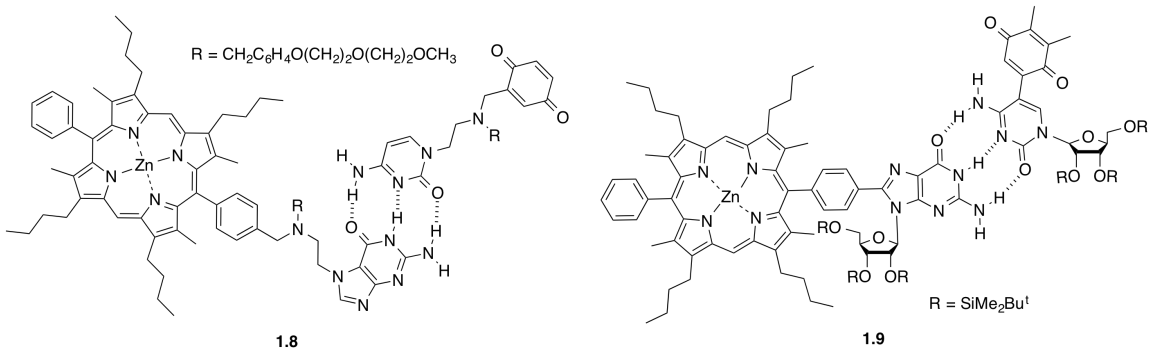

Figure 1.11 Photoinduced electron transfer dyads consisting of a porphyrin donor and a benzoquinone acceptor linked via Watson-Crick base pairing reported by Sessler et al. in 1992[44] (**1.8**) and 1993[42] (**1.9**).

In 2006, D'Souza and coworkers utilized noncovalent supramolecular interactions to construct a zinc N-confused porphyrin that allowed axial coordination of an imidazole-functionalized fullerene to produce complex **1.10**.[45] The binding constant for the fullerene moiety to the zinc N-confused porphyrin in a 1:1 stoichiometry was reported to be $2.8 \times 10^4\ M^{-1}$ based on UV-Vis spectral titrations in which the imidazole-appended fullerene (C_{60}Im) was titrated into a solution containing either a pyridine coordinated zinc N-confused porphyrin or a zinc N-confused porphyrin dimer (Figures 1.12a and 1.12b, respectively). Without the axial coordination of pyridine to zinc, the zinc N-confused porphyrin dimerized wherein the nitrogen lone-pair of the N-confused pyrrole ring coordinated to the zinc of a second N-confused porphyrin to create a "slip-stacked" type dimer.

The complexation of the imidazole-fullerene moiety to the zinc shifted the LUMO from the N-confused porphyrin, as seen in the uncomplexed compound, to the fullerene. On this basis it was suggested that electron movement should occur from the porphyrin derivative to the imidazole-fullerene (Figure 1.13). Based on DFT studies, the distance between the zinc to the coordinated nitrogen of the imidazole-fullerene was calculated to

be 2.01 Å. Charge separation was found to be rather efficient with a quantum yield of 0.97 and a forward ET rate of 1.1×10^{10} sec^{-1} as judged from fluorescence quenching studies of the singlet excited state of the dyad.

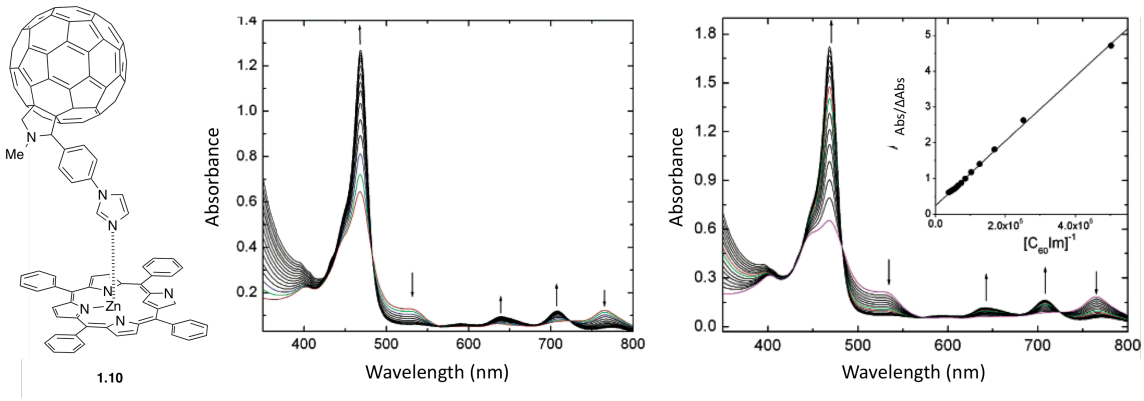

Figure 1.12 Structure of the dyad (**1.10**) formed from a zinc N-confused tetraphenylporphyrin and an imidazole substituted fullerene dyad (left). Spectral changes observed during the titration of the constituent imidazole-appended fullerene C_{60}Im (2.0 μL each addition) to *o*-dichlorobenzene solution containing (a) pyridine coordinated zinc N-confused porphyrin (3.3 mM) and (b) zinc N-confused porphyrin dimer (3.4 mM). The inset to figure b shows a Bensei-Hildebrand plot from which the binding constant was derived. Figures reprinted with permission from *Inorg. Chem.* **2006,** *45,* 5057-5065. Copyright 2006 American Chemical Society.

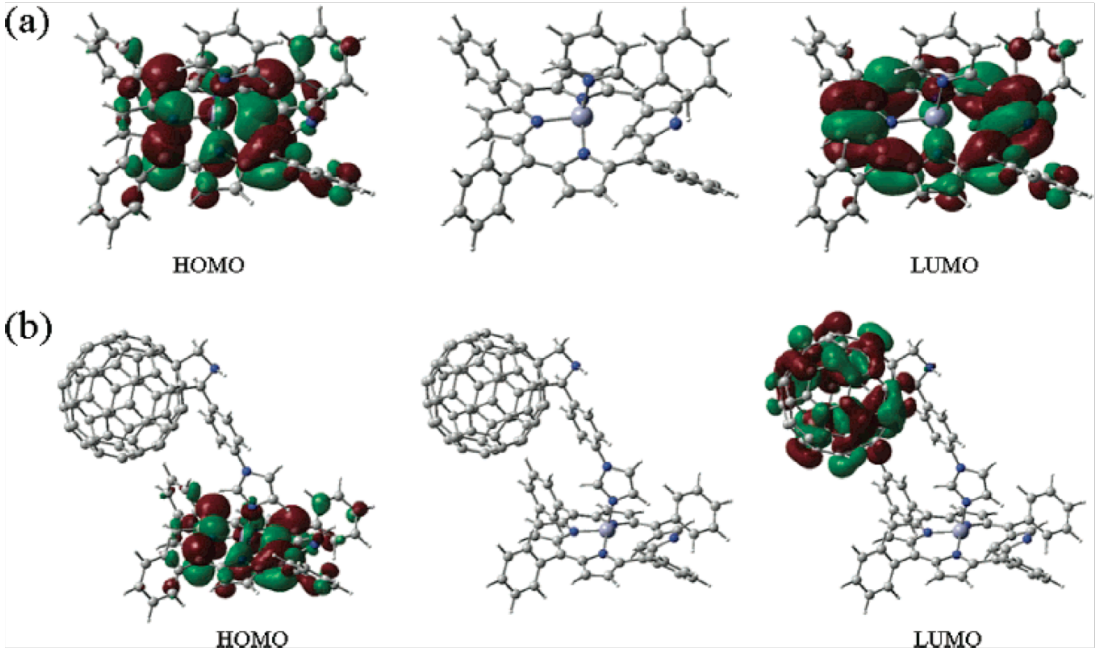

Figure 1.13 B3LYP/3-21G(*) optimized structures of (a) the zinc N-confused porphyrin and (b) the dyad formed by axial coordination of an imidazole appended fullerene to the zinc center of this N-confused porphyrin. The frontier HOMO and LUMO are shown on the left and right sides of each optimized structure, respectively. Figure reprinted with permission from *Inorg. Chem.* **2006,** *45,* 5057-5065. Copyright 2006 American Chemical Society.

By exploiting axial coordination to produce noncovalent D-A ensembles, Fukuzumi et al. were able to construct two silicon phthalocyanine-naphthalenediimide-fullerene complexes (**1.11** and **1.12**). These displayed CS state lifetimes of ca. 1000 and 250 ps for **1.11** and **1.12**, respectively (Figure 1.14).[46] Studies of these two complexes revealed that the use of fullerenes as the final electron acceptors, as in **1.11**, led to a more stable charge separated state as compared to the corresponding naphthalenediimide system (**1.12**). However, in both systems the CS lifetime was rather long leading the authors to suggest that either complex could be employed as a light-harvesting system.

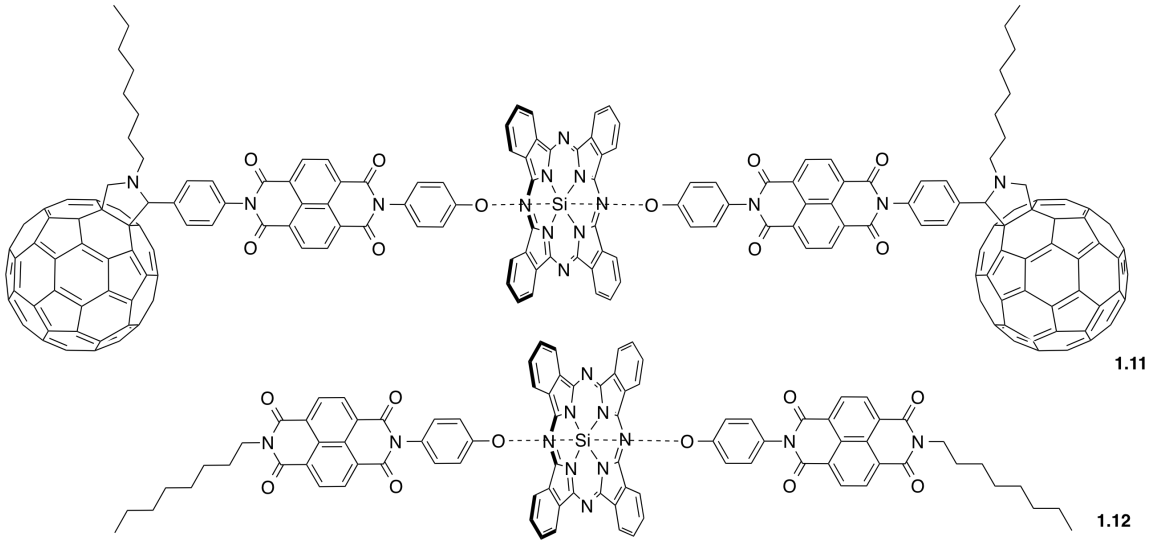

Figure 1.14 Structures for the silicon phthalocyanine-naphthalenediimide-fullerene complexes **1.11** and **1.12** reported by Fukuzumi et al. Figure reprinted with permission from *Chem. Eur. J.* **2009**, *15*, 5301-5310. Copyright 2009 John Wiley and Sons.

In collaborative work between Fukuzumi, Kim, and D'Souza,[47] it was demonstrated that supramolecular composites of porphyrins and fullerenes within organized polypeptide structures could be employed as photovoltaic devices characterized by power conversion efficiencies of 1.6% with photon-to-photocurrent efficiency values as high as 56% (Figure 1.15). The assemblies were composed of three-dimensional arrays of the porphyrin-peptide oligomers and fullerenes on nanostructured tin-oxide films. The relatively high efficiency of this system was ascribed in part to the use of porphyrins and fullerenes as light collecting moieties, since this allowed a large portion of the visible and infrared spectra to be harvested. These researchers also determined that as the number of porphyrins contained within a polypeptide increased, the ET properties improved as inferred from femtosecond transient absorption and fluorescence measurements involving composite films.

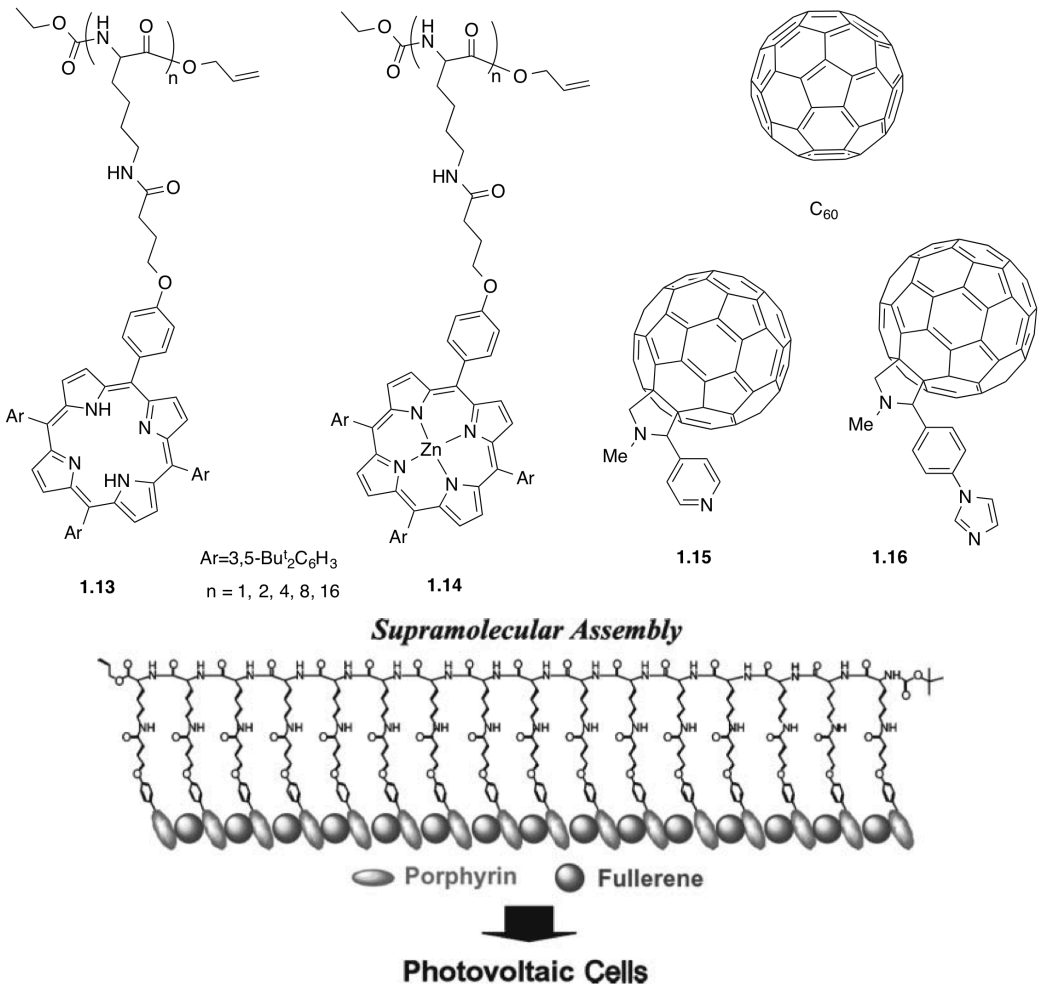

Figure 1.15 Porphyrin-peptide oligomers and fullerene derivatives of freebase (**1.13**) and zinc metalated (**1.14**) porphyrin peptides. Also shown are fullerene C_{60}, fullerene modified with pyridine (**1.15**), and fullerene modified with imidazole (**1.16**) (top). The proposed supramolecular organization between the porphyrins and fullerenes within the polypeptide framework is shown at the bottom of the figure. Taken from a report by Fukuzumi, Kim, and D'Souza (bottom).[47] Figures reprinted with permission from *J. Mater. Chem.* **2007**, *17*, 4160-4170. Copyright 2007 Royal Society of Chemistry.

Using lithium encapsulated fullerene ($Li^+@C_{60}$), an acceptor that is more electron deficient than fullerene itself, in conjugation with the sulfonated tetraphenylporphyrins $ZnTPPS^{4-}$ (**1.17**) and H_2TPPS^{4-} (**1.18**) shown in Figure 1.16a, the Fukuzumi group was

able to attain 300 and 310 ps CS lifetimes, respectively, in benzonitrile at room temperature.[48] Based on nanosecond transient absorption studies, they were able to identify the radical cation $[H_2TPPS^{4-}]^{\bullet+}$ at λ_{max} = 670 nm as well as the radical anion $(Li^+@C_{60})^{\bullet-}$ at λ_{max} = 1030 nm following photoirradiation of the porphyrin moiety (Figure 1.16b). The decay of the radical species was first order leading the authors to conclude that intramolecular back ET was occurring with little or no appreciable intermolecular back ET. Though the quantum yield of the CS state was only on the order of 0.39, the CS lifetimes were found to be the longest ever observed in solution for porphyrin/fullerene ensembles constructed via a noncovalent approach.

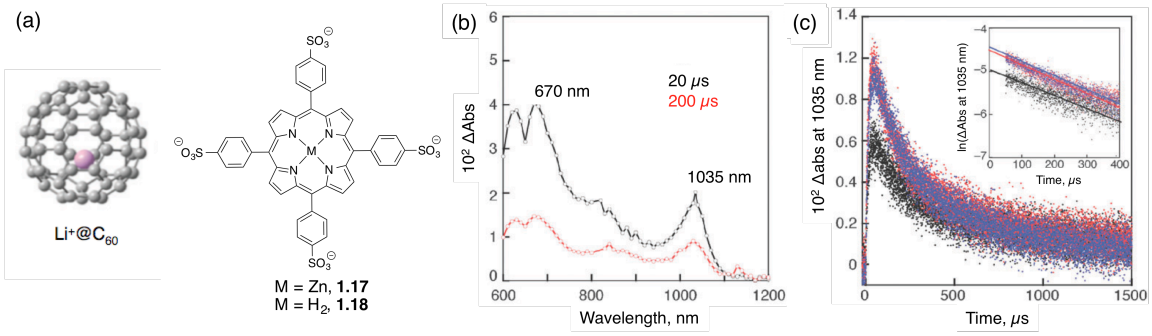

Figure 1.16 (a) Structures of $Li^+@C_{60}$ and sulfonated porphyrins **1.17** and **1.18**. (b) Transient absorption spectra of H_2TPPS^{4-} (2.5×10^{-5} M) recorded 20 and 200 μs after nanosecond laser excitation at 520 nm in the presence of $Li^+@C_{60}$ (5.0×10^{-5} M) in deaerated benzonitrile at 298 K. (c) Decay time profile at 1035 nm with different laser intensities (1, 3, 6 mJ pulse). Figures reprinted with permission from *Chem. Comm.* **2012**, *48*, 4314–4316. Copyright 2013 Royal Society of Chemistry.

In 2013, Hasobe and Fukuzmi further elaborated on this $Li^+@C_{60}$/anionic-porphyrin-based construct approach to formation by constraining the sulphonated *meso*-tetraphenylporphyrin and $Li^+@C_{60}$ in supramolecular nanoclusters. This allowed them to produce a working photoelectrochemical solar cell in 2013.[49] A depiction of the

photoelectrochemical cell, which consists of an optical transparent electrode (OTE) covered with nanostructured tin-oxide (SnO_2) is shown in Figure 1.17. Also shown are the TEM images of these nanoclusters.

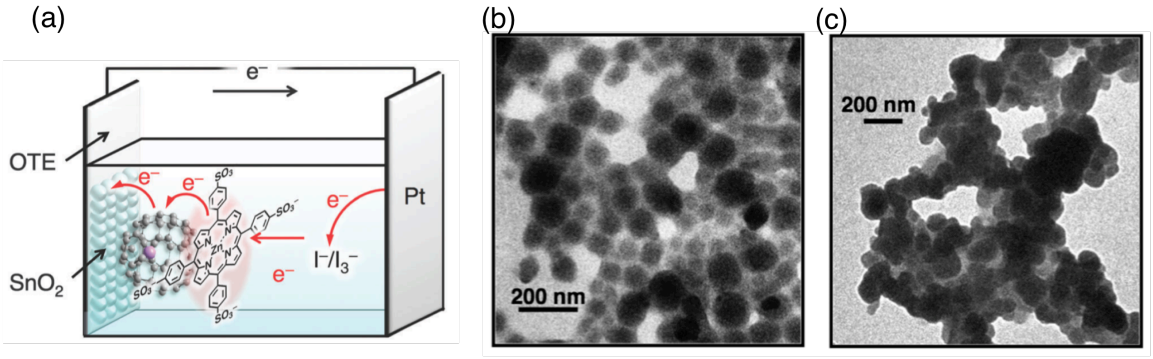

Figure 1.17 (a) Schematic representation of a photoelectrochemical cell consisting of an optical transparent electrode (OTE) of nanostructured tin-oxide (SnO_2) and nanoclusters of **1.17** and $Li^+@C_{60}$. (b) TEM images of $Li^+@C_{60}$-**1.17** and (c) $C^+@C_{60}$-**1.18**. Figures reprinted with permission from *Chem. Comm.* **2013**, *49*, 4474-4476. Copyright 2013 Royal Society of Chemistry.

For the complex of **1.17** and $Li^+@C_{60}$, the CS lifetime was found to be sufficiently long-lived (220 μs) that an electron from the radical anion $Li^+@C_{60}^{\bullet-}$ could be injected into the tin-oxide electrode prior to charge recombination. The use of **1.18** instead of **1.17** did not afford a long enough lifetime and thereby led to a much smaller photocurrent when employed in the photoelectrochemical cell.

Most recently, a collaboration between the Sessler, Kim, and Fukuzumi groups has led to the discovery of complex **1.20**, which exhibits an extremely long CS lifetime of 83 ms in benzonitrile at room temperature.[50] This CS state comes from photoinduced electron transfer in the triplet excited state. Complex **1.20** is composed of one tetra-anionic porphyrin (**1.17**) and two dicationic porphyrins (**Zn1.19**) as shown in Figure 1.18. The formation constant for complex **1.20** was determined via isothermal titration

calorimetry (ITC) as well as fluorescence spectroscopy titrations and found to be 6.3 × 10^{11} M^{-2} (Figure 1.19 a, b, and c). The use of electrostatic interactions to bring donor and acceptors together in solution to create a supramolecular complex represented a new noncovalent approach towards producing an extremely long-lived CS state.

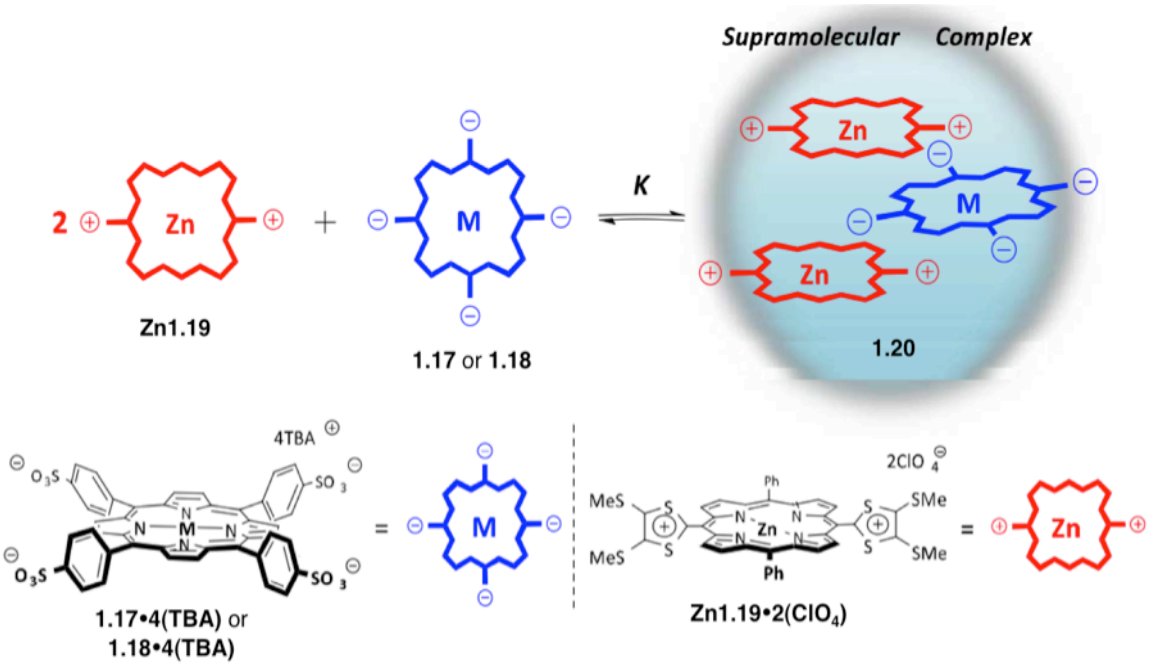

Figure 1.18 Structures of complex **1.20** and porphyrins **1.17** (M = Zn), **1.18** (M = H_2), and **Zn1.19**. Figures reprinted with permission from Bill, N. B.; Ishida, M.; Kawashima, Y.; Ohkubo, K.; Sung, Y. M.; Lynch, V. M.; Lim, J. M.; Kim, D.; Sessler, J. L.; Fukuzumi, S. *Chem. Sci.* **2014**, *5*, 3888-3896. Copyright 2013 Royal Society of Chemistry.

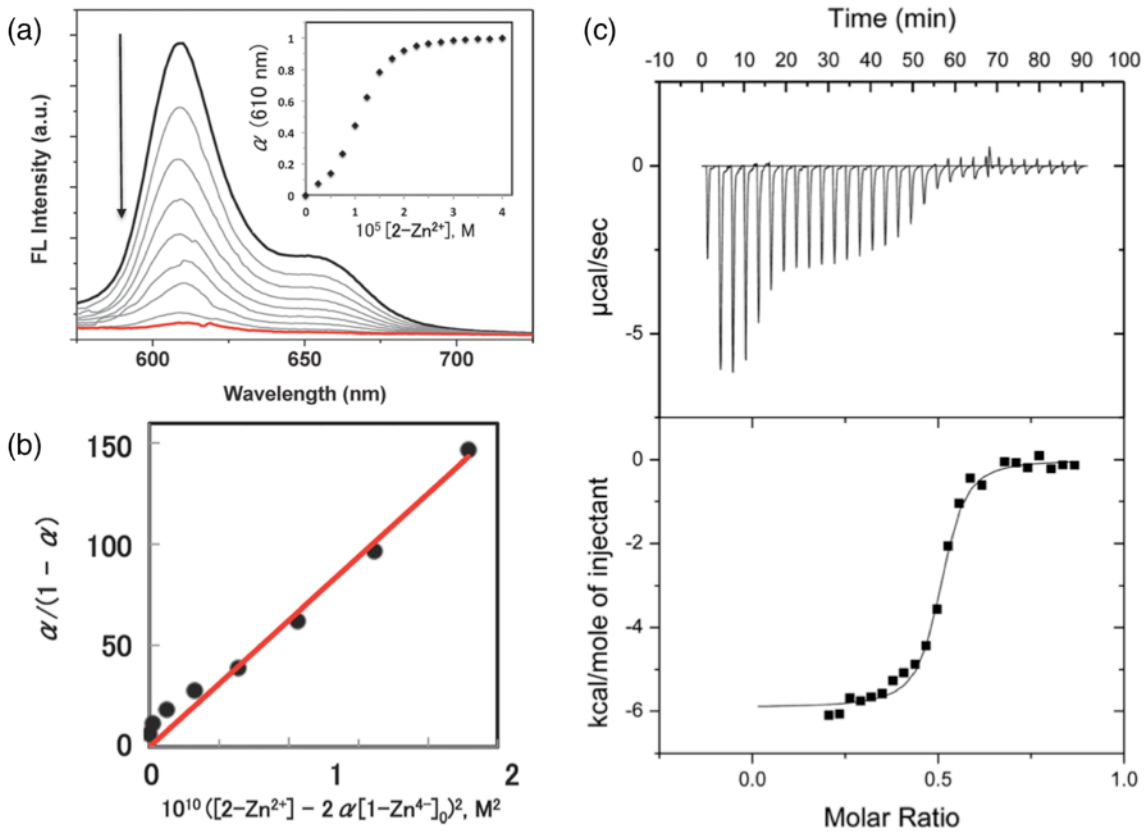

Figure 1.19 (a) Fluorescence spectral changes observed upon the treatment of a PhCN solution of **1.17** (10 mM) with **Zn1.19** at 298 K. Excitation was effected at 430 nm. The inset shows a plot of the ratio of the complex (a) vs the concentration of **Zn1.19.** (b) Plot of $\alpha/(1-\alpha)$ vs $\mathbf{[Zn1.19]_0} - 2\alpha\mathbf{[1.17]_0}$, which was used to determine the association constant, *K*, based on the equation $\alpha/(1-\alpha) = K[(\mathbf{Zn1.19})_0 - 2\alpha[(\mathbf{1.17})_0]$ wherein $\alpha = (I_0-I)/I_0$. (c) Results of an isothermal titration calorimetric study showing the titration of **1.18** into a PhCN solution of **Zn1.19**. Figures reprinted with permission from Bill, N. B.; Ishida, M.; Kawashima, Y.; Ohkubo, K.; Sung, Y. M.; Lynch, V. M.; Lim, J. M.; Kim, D.; Sessler, J. L.; Fukuzumi, S. *Chem. Sci.* **2014**, *5*, 3888-3896. Copyright 2013 Royal Society of Chemistry.

1.1.3 Thermal Electron Transfer

Thermal electron transfer, as opposed to photoinduced ET, occurs without the excitation of either the donor or acceptor species. A recent and excellent example of a thermal electron transfer process within a supramolecular ensemble comes from a collaboration involving the Sessler, Fukuzumi, Jeppesen, and Kim research groups. The newly synthesized π-extended porphyrin **$H_2$1.19** was shown to undergo redox control by metal cation complexation as well as anion binding.[51] This porphyrin is fused with strongly electron-donating 1,3-dithiol-2-ylidene moieties, the signature group of tetrathiafulvalenes which will be discussed in the next section of this chapter. Porphyrin **$H_2$1.19** was shown to exist in three distinct oxidations states (Figure 1.20a). The neutral complex is non-aromatic due to cross conjugation within the porphyrin core relative to the 1,3-dithiol-2-ylidene moieties. Upon one-electron oxidation with tris(4-bromophenyl)aminium hexachloridoantimonate ("magic blue"), the radical cation **$H_2$1.19$^{\bullet+}$** is produced. This radical was shown to be relatively stable as the hexachloridoantimonate ($SbCl_6^-$) salt. The radical cation was characterized via EPR, as well as though UV-Vis-NIR spectroscopies (Figure 1.20b). The potential of the one electron oxidation was shown to be dependent upon the coordinated metal cation, with Cu, Ni, Zn, and the free-base form being studied (Figure 1.20c). After a second one-electron oxidation, the porphyrin core became fully aromatic. This aromaticity induced a conformational change within the porphyrin structure from the "saddle-shape" seen in the neutral species to planar structure as seen in the solid state via X-ray crystallography (Figure 1.21).

Sessler et al. found that axial coordination of halide anions, especially chloride, to **Zn1.19**, serves to enhance the strong electron donor ability further. While **Zn1.19** showed no interaction with $Li^+@C_{60}$ in benzonitrile at 298 K even upon the addition of

tetrabutylammonium perchlorate, an oxidizing agent. However, when chloride anion is added to the solution in the form of tetrabutylammonium chloride, spectral features ascribable to **Zn1.19**$^{\bullet+}$ and $Li^{+}@C_{60}^{\bullet-}$ were seen via UV-Vis-NIR and EPR spectroscopy; this was taken as evidence that thermal ET was occurring. The axial coordination of a chloride anion to **Zn1.19** caused a negative shift in the two-electron oxidation potential from 0.21 V to 0.13 V vs SCE.

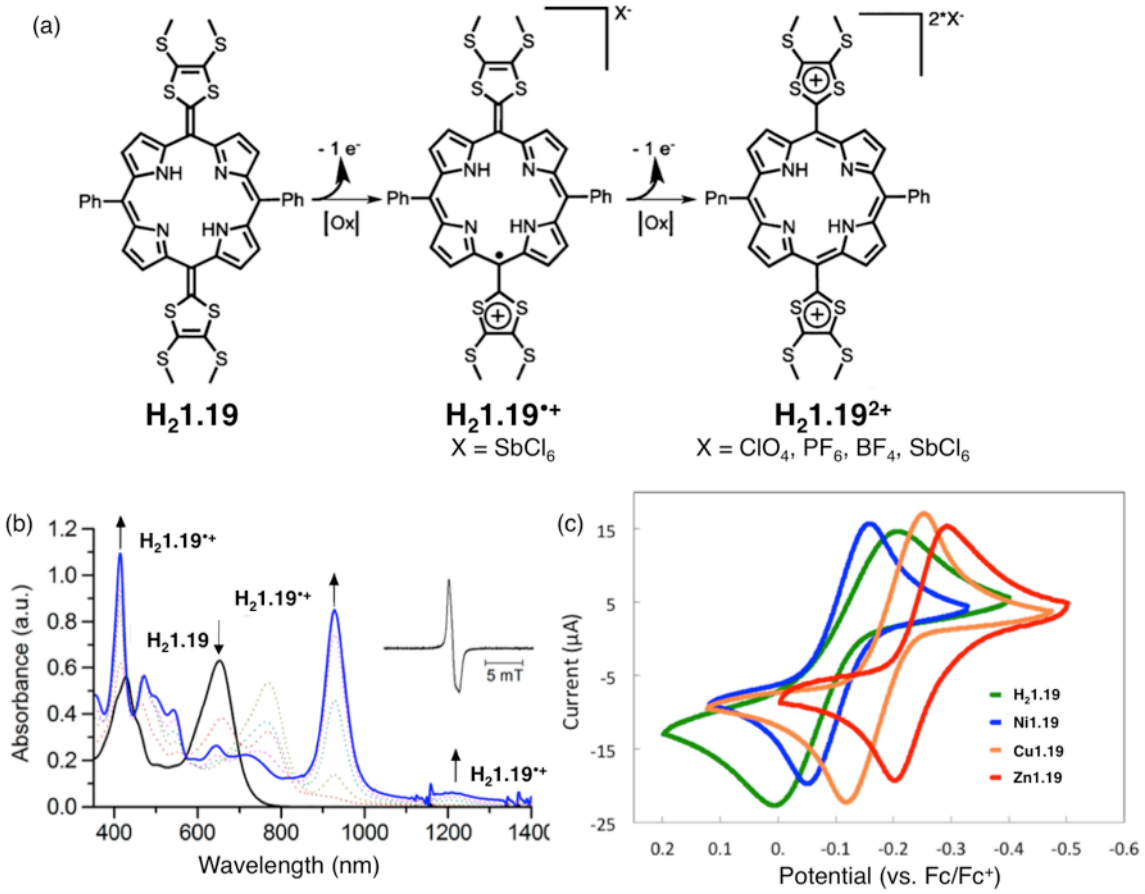

Figure 1.20 (a) Structures of π-extended porphyrin **$H_2$1.19** and the species produced upon one- and two-electron oxidation. (b) UV-Vis-NIR absorption spectra of **$H_2$1.19** recorded in dichloromethane at 298 K in the presence of increasing quantities of magic blue up to one molar equivalent; [**$H_2$1.19**] = 10 µM. Inset is the EPR spectrum of **$H_2$1.19$^{•+}$** as the hexachloridoantimonate salt prepared via the addition of 1 equivalent of magic blue. (c) Cyclic voltammograms (CVs) of **1.19** in its free base form and as the nickel, copper, and zinc complexes ($E_{1/2}$ = –0.097, –0.105, –0.186, and –0.245 versus ferrocene/ferrocenium couple, respectively). All CVs were recorded in dichloromethane at room temperature under identical conditions: 50 mV/sec scan rate, 1 mM solution of the compound under study, 100 mM tetrabutylammonium hexafluorophosphate as the counter electrolyte. Figures reprinted with permission *J. Am. Chem. Soc.* **2013**, *135*, 10852-10862. Copyright 2013 American Chemical Society.

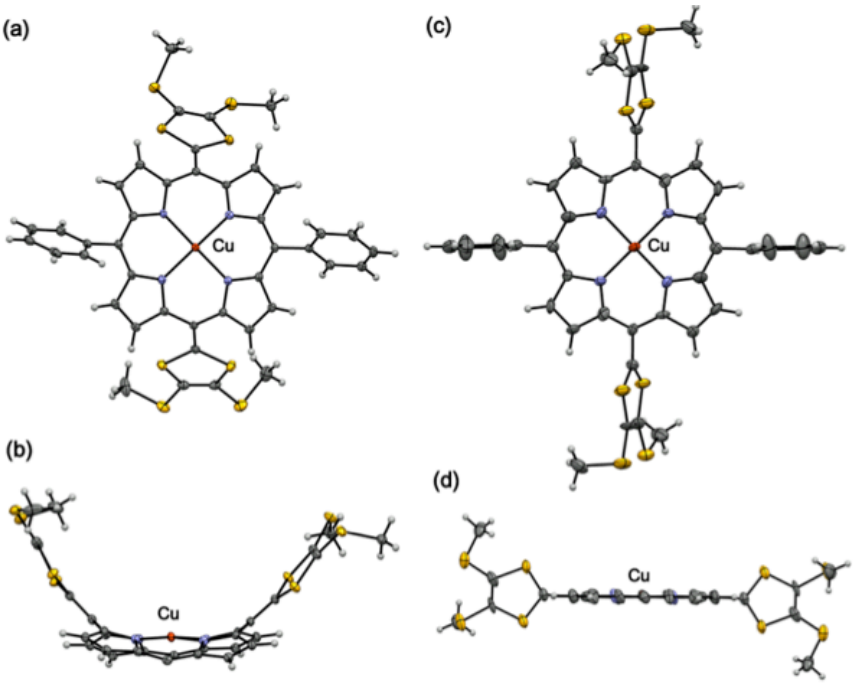

Figure 1.21 Crystal structures of **Cu1.19** (a, front view; b, side view) and Cu**1.19**•2OTf (c, front view; d, side view). Thermal ellipsoids represent 50% probability. Triflate counter anions of **Cu1.19**•2OTf and *meso*-phenyl groups (in side views) are omitted for clarity. Figure reprinted with permission *J. Am. Chem. Soc.* **2013**, *135*, 10852-10862. Copyright 2013 American Chemical Society.

The ability for $\mathbf{H_2}$**1.19** to form stable one- and two-electron oxidation products is a characteristic of tetrathiafulvalene (TTF) derivatives in general. Due to the high stability of these oxidized conjugates, TTF moieties have been extensively studied in electron transfer chemistry. The next sections are dedicated to a summary of TTF and TTF substituted calix[4]pyrroles that are able to undergo reversible charge and electron transfer via ion regulation.

1.2 TETRATHIAFULVALENE

The first report of tetrathiafulvalene (TTF), 2,2'-bi(1,3-dithiolylidene), dates back to the mid 1920's when Hurtley and Smiles reported the benzo-annulated TTF moiety.[52] However, unsubstituted, pristine TTF was not reported until 1970 by Wudl,[53] who was later followed by Coffen[54] and Hünig[55], independently, in 1971. In his initial paper, Wudl indicated that TTF has the ability to react with the electron deficient olefins as well as undergo stepwise one-electron oxidations to the radical cation ($TTF^{\bullet+}$) and dication (TTF^{2+}) upon oxidation (Figure 1.22). The radical cation proved to be relatively stable with half-lives of 6 and 48 hours for aqueous and ethanolic solutions, respectively, at room temperature and atmospheric conditions. This unusual stability comes from the formation of 6-π electron aromatic rings upon the oxidation of the non-aromatic 14-π electron system, as well as the ability of the polarizable sulfur atoms to reduce the energy of the oxidized species.

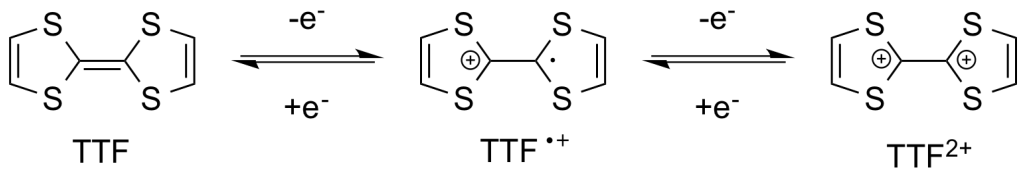

Figure 1.22 Stepwise one-electron oxidation of tetrathiafulvalene ($TTF^{\bullet+}$) to the radical cation (TTF) and dication (TTF^{2+}).

In 1973, Ferraris reported a charge-transfer (CT) complex consisting of crystallized stacks of TTF and tetracyano-*p*-quinodimethane (TCNQ) with metallic behavior.[56] Seven years later, a superconducting material composed of a selenium derivative of TTF and hexafluorophosphate was reported by Bechgaard and Jérome.[57,58] Since this time, considerable effort has been devoted to synthesizing TTF derivatives and

studying their properties as electron donors. This interest reflects in the many desirable attributes of the TTF core itself:[59]

1. The 14-π system is a strong electron-donor
2. One-electron oxidations to the radical cation and subsequently the dication are stepwise and reversible and can be carried out electrochemically or chemically
3. The potential of these oxidations can be easily tuned through substitution at the C-H positions of the 1,3-dithiolydine rings with either electron withdrawing or electron donating moieties.
4. TTF derivatives are capable of forming charge transfer complexes and are able to undergo thermal and photoinduced electron transfer
5. The electron transfer capabilities of TTFs may be turned on or off through redox manipulation

Over the past few decades, the sophistication of the macromolecular complexes containing TTF or its derivatives has increased.[12,60] For example, TTF derivatives, when paired with suitable electron acceptors, have been employed in nonlinear optical arrays,[61] environmentally responsive devices,[62] light harvesting complexes,[63] as well as in controlled self-assembled nanostructures.[64] Scheme 1.1 below depicts a variety of other uses for TTF derivatives.[65] The majority of the work in this dissertation revolves around a set of non-aromatic porphyrin analogues known as calix[4]pyrroles that have been synthetically elaborated with TTF or TTF derivatives.

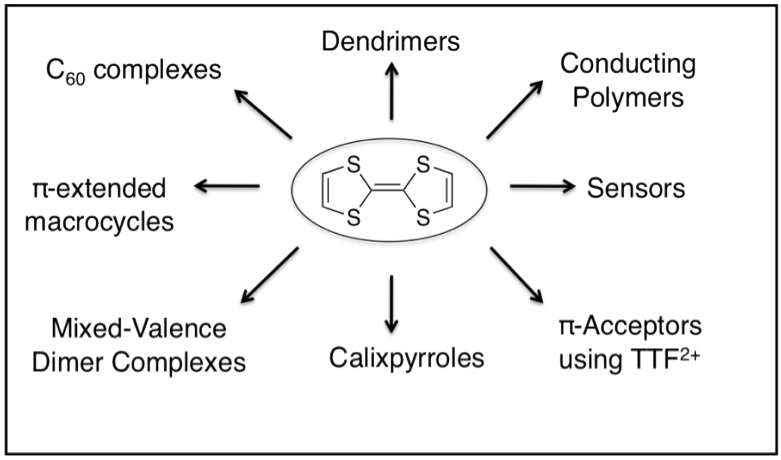

Scheme 1.2 Known applications of tetrathiafulvalene and tetrathiafulvalene derivatives.

1.3 TETRATHIAFULVALENE CALIX[4]PYRROLES AND ELECTRON/CHARGE TRANSFER REACTIONS

Calix[4]pyrroles (C4Ps) (Figure 1.23), first synthesized by Baeyer in 1886,[66] are similar to porphyrinogens in that they are composed of four pyrrole rings linked together by an sp^3-hybridized carbon at the α-position of the pyrrole ring.[67-69] However, calixpyrroles are fully substituted at this *meso*-carbon whereas porphyrinogens typically have hydrogen atoms causing them to be rather unstable and easily oxidized to the porphyrin.[67,68,69]

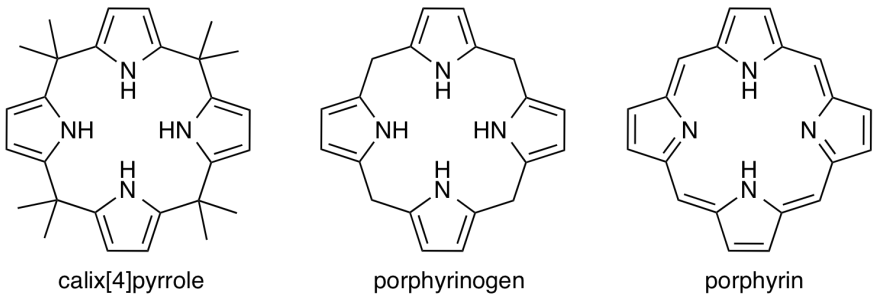

Figure 1.23 Structures for *octa*-methyl calix[4]pyrrole, porphyrinogen, and porphyrin.

In 1996, C4Ps were shown to be efficient anion binding agents in relatively apolar organic solvents. Recognition was driven by NH-anion hydrogen bond interactions in the case of tetrabutylammonium (TBA) halide salts.[67,69] This anion binding induces a conformational change from the thermodynamically stable 1,3-alternate conformer to the cone conformation, wherein all the NH protons are facing the same side of the macrocycle (Figure 1.24). The stability constants for halide binding depend upon the size of the halide used and the solvent. In dichloromethane, the largest binding affinity, 17,170 M^{-1}, is observed for the TBA salt of fluoride, with chloride having an affinity of 350 M^{-1}, bromide having an affinity of 10 M^{-1}, and iodide, the largest halide studied, having the smallest binding affinity at <10 M^{-1}.[67] Typically anion binding induces a signature downfield shift of the NH proton resonances in the ^{1}H NMR spectrum due to their proximity to the electronegative anion.

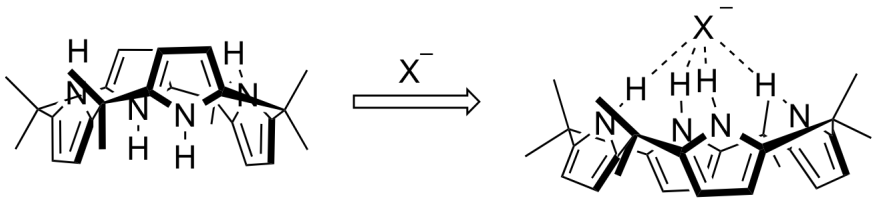

Figure 1.24 Conformational changes in the calix[4]pyrrole skeleton, from the 1,3-alternate conformation to the cone conformation, induced upon anion (X-) binding.

In 2004, the first tetra-tetrathiafulvalene calix[4]pyrrole (TTF-C4P) **1.20** was synthesized. It was developed as a rationally designed receptor for electron-deficient guests (Figure 1.25).[70] TTF-C4P predominately exists in the thermodynamically stable 1,3-alternate conformation in solution (halogenated solvents). However, upon addition of anions, such as chloride, TTF-C4P undergoes the usual conformational change seen with calix[4]pyrroles upon addition of an anion, namely the corresponding conversion to the

cone conformer. In accord with design expectations, this substituted C4P proved capable of efficiently binding neutral small, flat electron-deficient guests, such as 1,3,5-trinitrobenzene,[70] tetrachloro-*p*-benzoquinone, tetrafluoro-*p*-benzoquinone, and methyl 2,5,6-trinitrofluorenone-4-carboxylate in the 1,3-alternate conformation, a recognition feat not easily obtained with other TTF-containing hosts.[70-71] Two of the flat, electron efficient guests are able to bind per TTF-C4P, one in each set of TTF "arms." This leads to the production of 1:2 (receptor:analyte) charge transfer (CT) complexes. Complex formation is reflected in the appearance of a new absorption band at 677 nm as seen in UV-Vis-NIR spectral titrations involving addition of an electron deficient guest compound to receptor **1.20**.[70] Upon addition of an anion, however, the TTF-C4P undergoes a conformational change to the cone conformer, thus destroying the CT complexes (Figure 1.25).

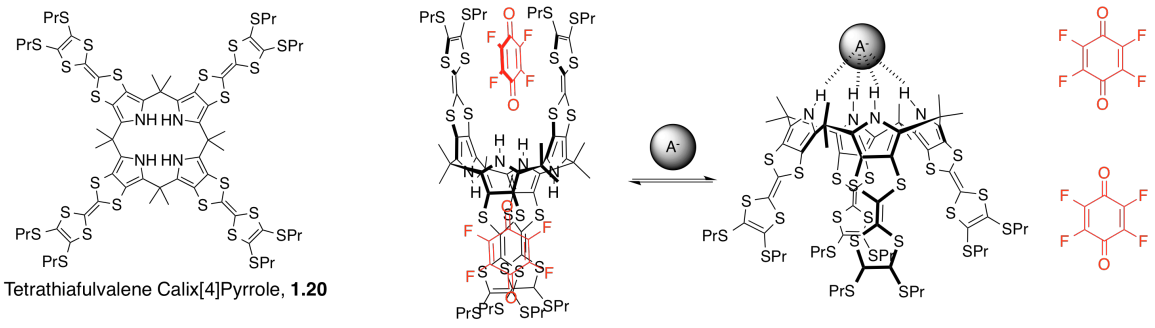

Figure 1.25 Structure of tetra-tetrathiafulvalene calix[4]pyrrole **1.20** and the conformational change seen upon anion (X^-) binding. Also shown are structures of electron deficient guests.

The deep bowl-shaped cavity of the anion-bound TTF-C4P led the Sessler and Jeppesen research groups to employ larger electron deficient moieties, such as fullerene C_{60}, with the TTF-C4P cone conformer to achieve a two-step molecular recognition process.[72] The first recognition event in this process involved treatment of the TTF-C4P

moiety with an anion to induce the conformational change shown in Figure 1.25. This is followed by the complexation of C_{60} into the TTF-C4P cavity. The recognition processes were followed by UV-Vis-NIR spectral titrations. By itself, TTF-C4P in a solution of dichloromethane appears yellow. However, upon addition of fullerene followed by encapsulation, the solution turns green. Presumably this is due to the formation of a CT complex between TTF-C4P and C_{60}. This CT assembly and its dissociation was the first approach to complex formation that allows anion-binding triggered structural manipulation.

It was discovered by Sessler and coworkers that when a large, highly electron deficient moieties, such as bisimidazolium quinone (BIQ^{2+}), were used as guests for the cone conformer of **1.20**, thermal electron transfer took place.[73] The 2:1 host-guest complex that resulted was characterized in the solid state by both X-ray diffraction analysis and EPR spectroscopy. It was fond to contain one reduced $BIQ^{\bullet+}$, one oxidized TTF-C4P$^{\bullet+}$, and one unreacted BIQ^{2+} in an overall capsule arrangement. In solution, TTF-C4P appears yellow while BIQ^{2+} is clear and colorless. Upon adding BIQ^{2+} in dichloromethane to TTF-C4P in the absence of anions, little appreciable change in the solution color is observed. However, upon addition of an anion (X^-) such as chloride, bromide, or methylsulfate, the TTF-C4P is converted into its corresponding cone conformation and the solution turns green with new absorption bands being observed in the UV-Vis-NIR spectrum at 751 nm and 2000 nm. This was taken as evidence of the formation of $BIQ^{+}\cdot X^-$ and TTF-C4P$^{\bullet+}$, respectively (Figure 1.26a). The formation of the radicals was also seen via EPR spectroscopy wherein upon the addition of anion to solution the intensity of the EPR signal attributed to $BIQ^{+}X^-$ and TTF-C4P$^{\bullet+}$ increased (Figure 1.26a inset).

Since tetraethylammonium (TEA^+) is known to bind within the cavity of the calix[4]pyrrole in its cone conformeration,[74,75] Sessler et al. added TEACl to the presumed 2:1 TTF-C4P:BIQ^{2+} complex to see if TEA^+ could act as a competitive guest for the TTF-C4P cavity.[73] To the extent it did it would displace the BIQ^{2+} (or prevent its binding) and turn off the thermal ET process. Upon the addition of TEACl, the color of the solution changed from green to yellow indicating the dissolution of the radical species and a turning off of the electron transfer to process (i.e. regeneration of BIQ^{2+} and TTF-C4P) (Figure 1.26b). This back electron transfer process could also be followed via EPR spectroscopy by monitoring the decrease in the signal intensity of the radical species that is seen upon increasing the relative concentration of TEACl (Figure 1.26b inset). Ion-mediated electron transfer within a supramolecular donor-acceptor ensemble, such as that occurring in this instance (cf. Scheme 1.3), represented a first in the field of ET. It thus represents an important step forward in the understanding of how allosteric regulation might be modulating ET reactions within natural systems.[73]

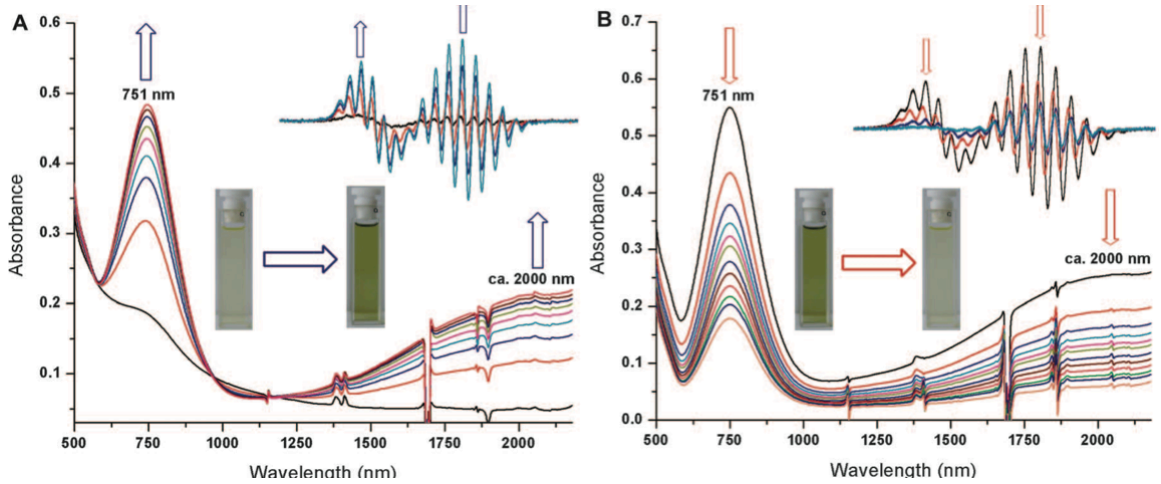

Figure 1.26 (A) Spectroscopic changes observed when **1.20** (30 μM in chloroform) is treated first with 1 molar equiv of $BIQ^{2+}PF_6$ and then with increasing quantities of tetrahexylammonium chloride (THACl) in chloroform (up to 10 equivalents). (Inset) The EPR spectra of the 1:1 mixture of **1.20** and $BIQ^{2+}PF_6$ (1.1×10^{-4} M each) in chloroform at room temperature recorded upon the addition of THACl. (B) Cation-induced reverse electron transfer seen upon the addition of up to 15 equivalents tetraethylammonium chloride (TEACl) to a 1:1 solution of **1.20** and $BIQ^{2+}2Cl^-$ in chloroform (30 μM each). (Inset) EPR spectra of a 1:1 mixture of **1.20** and $BIQ^{2+}2Cl^-$ (1.1×10^{-4} M each) in chloroform at room temperature recorded upon the addition of up to 5 molar equivalents of TEACl. Figure reprinted with permission *Science* **2010**, *329*, 1324-1327. Copyright 2010 American Association for the Advancement of Science.

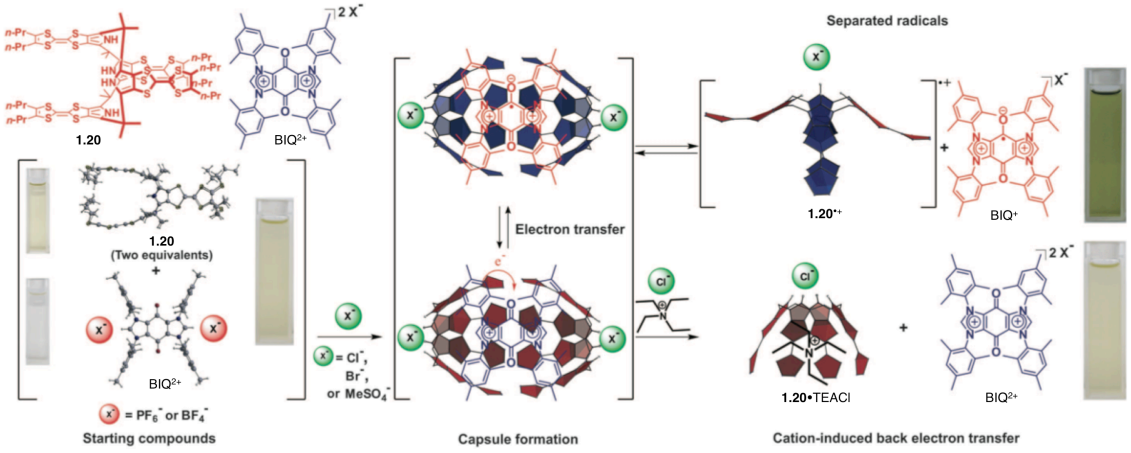

Scheme 1.3 Chemical structures of **1.20** and BIQ^{2+} salts and their proposed ion-mediated electron transfer reactions. Figure reprinted with permission *Science* **2010**, *329*, 1324-1327. Copyright 2010 American Association for the Advancement of Science.

One of the next major developments in the area of supramolecular electron transfer came from the use of $Li^+@C_{60}$ in conjunction with **1.20** to produce another ensemble that displayed ion-controlled on-off switching of a thermal ET process.[76] In most cases the use of C_{60} as an electron acceptor results in formation of CT complexes rather than full ET unless photoirradiation is used.[76] This is due to the fact that fullerene is not a adequately strong electron acceptor in the ground-state except when very strong electron donors are employed.[76-78] However, $Li^+@C_{60}$ is a stronger electron acceptor than C_{60} (by 0.57 V).[76] Thus, when donor TTF-C4P **1.20** is mixed with $Li^+@C_{60}$ in benzonitrile (PhCN) full ET is seen, presumably via formation of a supramolecular complex.[76] The actual ET product was, as above, characterized in the solid state via a single crystal X-ray diffraction analysis as well as in solution via EPR spectroscopy. Again, THACl was used to turn "on" the ET while TEACl was used to turn it "off" through the competitive binding of TEA^+ into the cavity of TTF-C4P as seen previously.[73] The ion-controlled ET from a TTF moiety of **1.20** to $Li^+@C_{60}$ is depicted in Scheme 1.4 below.

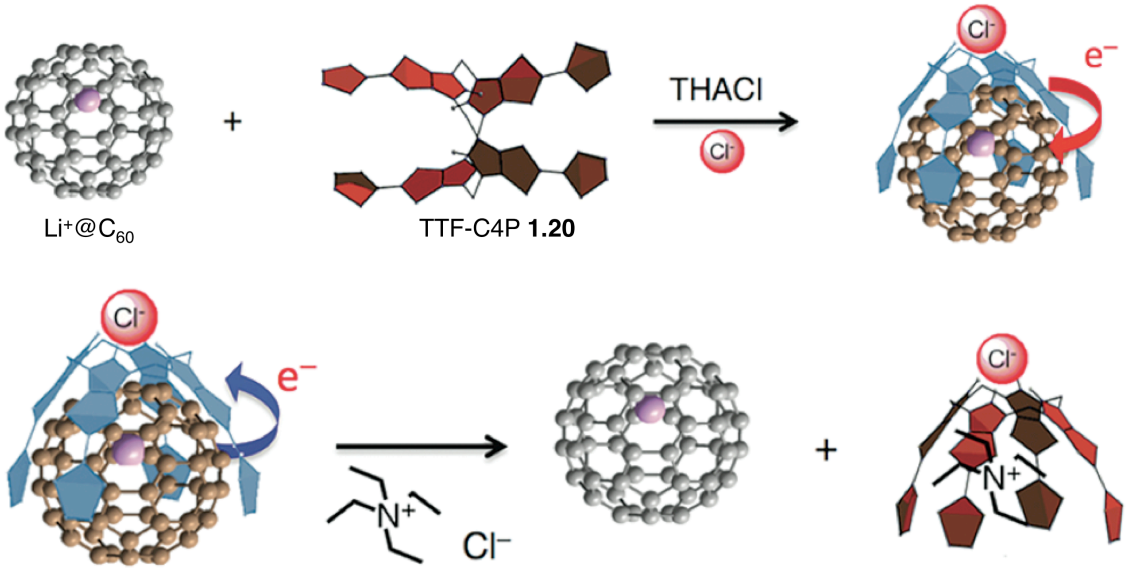

Scheme 1.4 Formation of the supramolecular electron transfer (ET) complex between TTF-C4P **1.20** and $Li^+@C_{60}$ that occurs upon the addition of tetrahexylammonium chloride (THACl). The complex undergoes disassociation upon the subsequent addition of tetraethylammonium chloride (TEACl), which acts as an inhibitor for fullerene binding, thereby turning "off" the ET. Figure reprinted with permission *J. Am. Chem. Soc* **2011**, *133*, 15938-15941. Copyright 2011 American Chemical Society.

1.4 Summary and Outline

As detailed throughout this chapter, forming a long-lived charge separated state upon electron transfer, and more specifically photoinduced electron transfer, has become increasingly important for efforts directed towards the creation of artificial photosynthetic devices. Supramolecular assemblies that allow for long-lived CS states have become of increasing interest due to the ease of synthesis as compared to covalently bound ensembles. This dissertation will focus on work involving tetrathiafulvalene calix[4]pyrroles as electron donors in photoinduced ET assemblies.

Chapter 2 details a supramolecular charge transfer ensemble consisting of a benzo-annulated tetrathiafulvalene calix[4]pyrrole used as a donor and fullerene C_{60} as an acceptor. The allosteric regulation of fullerene binding was examined using both anions and cations as regulating agents. As will be detailed in this chapter, the anions induced a conformational change in the calix[4]pyrrole to the active binding conformer whereas small cations acted as inhibitors for fullerene binding. The majority of the work within this chapter was published in the *Journal of the American Chemistry Society* in 2014. The work was in collaboration with the research groups of Prof. Dongho Kim of Yonsei University, Prof. Kent Nielsen and Prof. Jan Jeppesen of University of Sothern Denmark, and Prof. Jung Su Park of Sookmyung Woman's University. The candidate is a co-first author of this paper and was responsible for synthesis, NMR spectral studies, and various UV-Vis spectral titration studies.

Chapter 3 details an electron transfer process wherein a benzo-annulated tetrathiafulvalene calix[4]pyrrole acts as a donor and a free-base porphyrin carboxylate acts as an acceptor within a supramolecular ensemble upon conditions of photoirradiation. The work was done in collaboration with the research groups of Prof. Shunichi Fukuzumi of Osaka University and Prof. Dongho Kim of Yonsei University.

The majority of the work was published in the *Journal of Physical Chemistry C* with the candidate as first author. The candidate was responsible for the synthesis of the supramolecular assembly components as well as the UV-Vis-NIR, fluorescence, and phosphorescence spectroscopic studies and cyclic voltammetry. She also carried out EPR and transient absorption spectroscopic studies in conjunction with other coauthors from the Fukuzumi group while visiting Osaka University.

Chapter 4 describes studies of electron transfer involving tetrathiafulvalene derivatives, namely a tetrathiafulvalene modified Schiff-base calix[4]pyrrole and a π-extended tetrathiafulvalene BODIPY. The studies described within this chapter were published in *Organic Letters* and *Chemical Communications* with the candidate as second and third author, respectively. The candidate was responsible for EPR studies involving the TTF modified Schiff-base and UV-Vis-NIR and fluorescence spectroscopic analysis of the π-extended TTF-BODIPY.

1.5 CHAPTER 1 REFERENCES

1. Anslyn, E. V.; Dougherty, D. A. *Modern Physical Organic Chemistry*. University Science Books: USA, 2006.
2. Marcus, R. A.; Sutin, N. *Biochim. Biophys. Acta*. **1985**, *811*, 265-322.
3. Berg, J. M.; Tymoczko, J. L.; Stryer, L. *Biochemistry*. 6th ed.; W. H. Freeman and Company: USA, 2007.
4. Marcus, R. A. *J. Chem. Phys* **1956**, *24*, 966-978.
5. Marcus, R. A. *Angew. Chem. Int. Ed*. **1993**, *32*, 1111-1121.
6. Fukuzumi, S. *Phys. Chem. Chem. Phys*. **2008**, *10*, 2283-2297.
7. Kavarnos, G. J. *Fundamentals of Photoinduced Electron Transfer*. VCH Publishers, Inc.: USA, 1993.
8. Fukuzumi, S. *Bull. Chem. Soc. Jpn*. **2006**, *79*, 177-195.
9. Fukuzumi, S.; Ohkubo, K. *Dalton Trans*. **2013,** *42*, 15846-15858.
10. Wasielewski, M. R. *Chem. Rev*. **1992**, *92*, 435-461.
11. Berera, R.; Grondelle, R.; Kennis, J. T. M. *Photosynth. Res*. **2009**, *101*, 105-118.
12. Davis, C. M.; Kawashima, Y.; Ohkubo, K.; Lim, J. M.; Kim, D.; Fukuzumi, S.; Sessler, J. L. *J. Phys. Chem. C*. **2014**, DOI: 10.1021/jp504087b.
13. Günes, S.; Neugebauer, H.; Sariciftci, N. S. *Chem. Rev*. **2007**, *107*, 1324-1338.
14. Nunzi, J.-M. *C. R. Physique* **2002**, *3*, 523-542.
15. Kashiwagi, Y.; Ohkubo, K.; McDonald, J. A.; Blake, I. M.; Crossley, M. J.; Araki, Y.; Ito, O.; Imahori, H.; Fukuzumi, S. *Org. Lett*. **2003**, *5*, 2719-2721.
16. Fukuzumi, S.; Kojima, T. *J. Mater. Chem*. **2007**, *18*, 1427-1439.
17. Ohkubo, K.; Kotani, H.; Shao, J.; Ou, Z.; Kadish, K. M.; Li, G.; Pandey, R. K.; Fujitsuka, M.; Ito, O.; Imahori, H.; Fukuzumi, S. *Angew. Chem. Int. Ed*. **2004**, *43*, 853-856.
18. Curiel, D.; Ohkubo, K.; Reimers, J. R.; Fukuzumi, S.; Crossley, M. J. *Phys. Chem. Chem. Phys*. **2007**, *9*, 5260-5266.
19. Supur, M.; El-Khouly, M. E.; Seok, J. H.; Kay, K.-Y.; Fukuzumi, S. *J. Phys. Chem. A*. **2011**, *115*, 14430-14437.
20. Hutchison, J. A.; Bell, T. D. M.; Ganguly, T.; Ghiggino, K. P.; Langford, S. J.; Lokan, N. R.; Paddon-Row, M. N. *J. Photochem. Photobiol., A* **2008**, *197*, 220-225.
21. Imahori, H.; Sekiguchi, Y.; Kashiwagi, Y.; Sato, T.; Araki, Y.; Ito, O.; Yamada, H.; Fukuzumi, S. *Chem. Eur. J*. **2004**, *10*, 3184-3196.
22. Fukuzumi, S. *Pure Appl. Chem*. **2007**, *79*, 981-991.
23. Fukuzumi, S. Electron Transfer of π-Functional Systems and Applications. In *Functional Organic Materials*, Wiley-VCH: Weinheim: 2007; pp 465-510.
24. Durrant, J. R.; Haque, S. A.; Palomares, E. *Chem. Comm*. **2006**, 3279-3289.
25. Ohkubo, K.; Fukuzumi, S. *Bull. Chem. Soc. Jpn*. **2009**, 3279-3289.
26. Fukuzumi, S.; Ohkubo, K.; D'Souza, F.; Sessler, J. L. *Chem. Comm*. **2012**, *48*, 9801-9815.

27. Martín, N.; Sánchez, L.; Herranz, M. a. Á.; Illescas, B.; Guldi, D. M. *Acc. Chem. Res.* **2007**, *40*, 1015-1024.
28. Wasielewski, M. R. *Acc. Chem. Res.* **2009**, *42*, 1910-1921.
29. Fukuzumi, S.; Ohkubo, K. *J. Mater. Chem.* **2012**, *22*, 4575.
30. Fukuzumi, S.; Saito, K.; Ohkubo, K.; Khoury, T.; Kashiwagi, Y.; Absalom, M. A.; Gadde, S.; D'Souza, F.; Araki, Y.; Ito, O.; Crossley, M. J. *Chem. Comm.* **2011**, *47*, 7980-7982.
31. de la Escosura, A.; Martínez-Díaz, M. V.; Guldi, D. M.; Torres, T. *J. Am. Chem. Soc.* **2006**, *128*, 4112-4118.
32. Ballardini, R.; Balzani, V.; Clemente-León, M.; Credi, A.; Gandolfi, M. T.; Ishow, E.; Perkins, J.; Stoddart, J. F.; Tseng, H.-R.; Wenger, S. *J. Am. Chem. Soc.* **2002**, *124*, 12786-12795.
33. Wessendorf, F.; Grimm, B.; Guldi, D. M.; Hirsch, A. *J. Am. Chem. Soc.* **2010**, *132*, 10786-10795.
34. Wessendorf, F.; Gnichwitz, J.-F.; Sarova, G. H.; Hager, K.; Hartnagel, U.; Guldi, D. M.; Hirsch, A. *J. Am. Chem. Soc.* **2007**, *129*, 16057-16071.
35. D'Souza, F.; Amin, A. N.; El-Khouly, M. E.; Subbaiyan, N. K.; Zandler, M. E.; Fukuzumi, S. *J. Am. Chem. Soc.* **2011**, *134*, 654-664.
36. Molina-Ontoria, A.; Fernández, G.; Wielopolski, M.; Atienza, C.; Sánchez, L.; Gouloumis, A.; Clark, T.; Martín, N.; Guldi, D. M. *J. Am. Chem. Soc.* **2009**, *131*, 12218-12229.
37. D'Souza, F.; Maligaspe, E.; Ohkubo, K.; Zandler, M. E.; Subbaiyan, N. K.; Fukuzumi, S. *J. Am. Chem. Soc.* **2009**, *131*, 8787-8797.
38. Bandi, V.; El-Khouly, M. E.; Nesterov, V. N.; Karr, P. A.; Fukuzumi, S.; D'Souza, F. *J. Phys. Chem. C.* **2013**, *117*, 5638-5649.
39. Bandi, V.; El-Khouly, M. E.; Ohkubo, K.; Nesterov, V. N.; Zandler, M. E.; Fukuzumi, S.; D'Souza, F. *J. Phys. Chem. C.* **2014**, *118*, 2321-2332.
40. Kawashima, Y.; Ohkubo, K.; Kentaro, M.; Fukuzumi, S. *J. Phys. Chem. C.* **2013**, *117*, 21166-21177.
41. Guldi, D. M.; Costa, R. D. *J. Phys. Chem. Lett.* **2013**, *4*, 1489-1501.
42. Sessler, J. L.; Wang, B.; Harriman, A. *J. Am. Chem. Soc.* **1993**, *115*, 10418-10419.
43. Sessler, J. L.; Jayawickramarajah, J. *Chem. Comm.* **2005**, 1939-1949.
44. Harriman, A.; Kubo, Y.; Sessler, J. L. *J. Am. Chem. Soc* **1992**, *114*, 388-390.
45. D'Souza, F.; Smith, P. M.; Rogers, L.; Zandler, M. E.; Islam, S. D.-M.; Araki, Y.; Ito, O. *Inorg. Chem.* **2006**, *45*, 5057-5065.
46. El-Khouly, M. E.; Kim, J. H.; Kay, K.-Y.; Choi, C. S.; Ito, O.; Fukuzumi, S. *Chem. Eur. J.* **2009**, *15*, 5301-5310.
47. Hasobe, T.; Saito, K.; Kamat, P. V.; Troiani, V.; Qui, H.; Solladié, N.; Kim, K. S.; Park, J. K.; Kim, D.; D'Souza, F.; Fukuzumi, S. *J. Mater. Chem.* **2007**, *17*, 4160-4170.
48. Ohkubo, K.; Kawashima, Y.; Fukuzumi, S. *Chem. Comm.* **2012**, *48*, 4314-4316.

49. Ohkubo, K.; Kawashima, Y.; Sakai, H.; Hasobe, T.; Fukuzumi, S. *Chem. Comm.* **2013**, *49*, 4474-4476.
50. Bill, N. L.; Ishida, M.; Kawashima, Y.; Ohkubo, K.; Sung, Y. M.; Lynch, V. M.; Lim, J. M.; Kim, D.; Sessler, J. L.; Fukuzumi, S. *Chem. Sci.* **2014**, *Just Accepted*, DOI: 10.1039/C4SC00803K.
51. Bill, N. L.; Ishida, M.; Bähring, S.; Lim, J. M.; Lee, S.; Davis, C. M.; Lynch, V. M.; Nielsen, K. a.; Jeppesen, J. O.; Ohkubo, K.; Fukuzumi, S.; Kim, D.; Sessler, J. L. *J. Am. Chem. Soc.* **2013**, *135*, 10852-1085262.
52. Hurtley, W. R. H.; Smiles, S. *J. Chem. Soc.* **1926**, 2263-2270.
53. Wudl, F.; Smight, G. M.; Hufnagel, E. J. *Chem. Comm.* **1970**, 1453-1454.
54. Coffen, D. L.; Q., C. J.; Williams, D. R.; Garret, P. E.; Canfield, N. D. J. *J. Am. Chem. Soc* **1971**, *93*, 2258-2268.
55. Zahradnik, R.; Carsky, P.; Hünig, S.; Kiesslich, G.; Scheutzow, D. *Int. J. Sulfur. Chem. Part C.* **1971**, *6*, 109-122.
56. Ferraris, J.; Cowan, D. O.; Walatka, V.; Peristein, J. H. *J. Am. Chem. Soc* **1973**, *95*, 948-949.
57. Jérome, D.; Mazaud, A.; Ribault, M.; Bechaard, K. *J. Physique. Lett.* **1980**, *41*, 95-98.
58. Bechgaard, K.; Jérome, D. *Sci. Am.* **1982**, *247*, 50.
59. Canevet, D.; Sallé, M.; Zhang, G.; Zhang, D.; Zhu, D.-B. *Chem. Comm.* **2009**, 2245-2269.
60. Simonsen, K. B.; Becher, J. *Synlett* **1997**, 1211-1220.
61. Matsuo, Y.; Maruyama, M.; Gayathri, S. S.; Uchida, T.; Guldi, D. M.; Kishida, H.; Nakamura, A.; Nakamura, E. *J. Am. Chem. Soc.* **2009**, *131*, 12643-12649.
62. Nielsen, K. A.; Sarova, G. H.; Martín-Gomez, L.; Fernandez-Lazaro, F.; Stein, P. C.; Sanguinet, L.; Levillain, E.; Sessler, J. L.; Guldi, D. M.; Sastre-Santos, Á.; Jeppesen, J. O. *J. Am. Chem. Soc.* **2008**, *130*, 460-462.
63. Romero-Nieto, C.; Medina, A.; Molina-Ontoria, A.; Claessens, C. G.; Echegoyen, L.; Martín, N.; Torres, T.; Guldi, D. M. *Chem. Comm.* **2012**, *48*, 4953-4955.
64. Brunetti, F. G.; Romero-Nieto, C.; López-Andarias, J.; Atienza, C.; López, J. L.; Guldi, D. M.; Martín, N. *Angew. Chem. Int. Ed.* **2013**, *52*, 2180-2184.
65. Becher, J.; Li, Z.-T.; Blanchard, P.; Svenstrup, N.; Lau, J.; Nielsen, K. A.; Leriche, P. *Pure Appl. Chem.* **1997**, *69*, 465-470.
66. Baeyer, A. *Ber. Dtsch. Chem. Ges* **1886**, *19*.
67. Gale, P. A.; Sessler, J. L.; Král, V.; Lynch, V. *J Am Chem Soc* **1996**, *118*, 5140-5141.
68. Gale, P. A.; Sessler, J. L.; Kral, V. *Chem. Comm.* **1998**, *1*, 1-8.
69. Gale, P. A.; Anzenbacher, P.; Sessler, J. L. *Coord. Chem. Rev.* **2001**, *222*, 57-102.
70. Nielsen, K. A.; Cho, W.-S.; Jeppesen, J. O.; Lynch, V. M.; Becher, J.; Sessler, J. L. *J. Am. Chem. Soc.* **2004**, *126*, 16296-16297.
71. Nielsen, K. A.; Martín-Gomez, L.; Sarova, G. H.; Sanguinet, L.; Gross, D. E.; Fernández-Lázaro, F.; Stein, P. C.; Levillain, E.; Sessler, J. L.; Guldi, D. M.; Sastre-Santos, Á.; Jeppesen, J. O. *Tetrahedron* **2008**, *64*, 8449-8463.

72. Nielsen, K. A.; Cho, W.-S.; Sarova, G. H.; Petersen, B. M.; Bond, A. D.; Becher, J.; Jensen, F.; Guldi, D. M.; Sessler, J. L.; Jeppesen, J. O. *Angew. Chem. Int. Ed.* **2006**, *45*, 6848-6853.
73. Park, J. S.; Karnas, E.; Ohkubo, K.; Chen, P.; Kadish, K. M.; Fukuzumi, S.; Bielawski, C. W.; Hudnall, T. W.; Lynch, V. M.; Sessler, J. L. *Science* **2010**, *329*, 1324-1327.
74. Custelcean, R.; Delmau, L. H.; Moyer, B. A.; Sessler, J. L.; Cho, W.-S.; Gross, D. E.; Bates, G. W.; Brooks, S. J.; Light, M. E.; Gale, P. A. *Angew. Chem. Int. Ed.* **2005**, *44*, 2537-2542.
75. Sessler, J. L.; Gross, D. E.; Cho, W.-S.; Lynch, V. M.; Schmidtchen, F. P.; Bates, G. W.; Light, M. E.; Gale, P. A. *J. Am. Chem. Soc.* **2006**, *128*, 12281-12288.
76. Fukuzumi, S.; Ohkubo, K.; Kawashima, Y.; Kim, D. S.; Park, J. S.; Jana, A.; Lynch, V. M.; Kim, D.; Sessler, J. L. *J. Am. Chem. Soc.* **2011**, *133*, 15938-15941.
77. Konarev, D. V.; Khasanov, S. S.; Otsuka, A.; Maesato, M.; G., S.; Lyubovskaya, R. M. *Angew. Chem. Int. Ed.* **2010**, *49*, 4829-4832.
78. Konarev, D. V.; Kuzmin, A. V.; Simonov, S. V.; Khasanov, S. S.; Yudanova, E. I.; Lyubovskaya, R. M. *Dalton Trans.* **2011**, *40*, 4453-4458

Chapter 2

Ion Regulated Allosteric Binding of Fullerenes by Tetrathiafulvalene Calix[4]Pyrroles

2.1 INTRODUCTION*

Allosteric regulation by co-factors, especially by positively or negatively charged species, plays an essential role in modulating a wide range of enzymatic and other biological processes.[1-3] Therefore, considerable scientific effort has been devoted towards understanding and interpreting the effects that various cofactors have on the control of cooperative binding events.[3,4] Cations and anions, for example, can bind to enzymes to influence the sites of biological activity and either enhance or hinder subsequent binding events thereby promoting or reducing the reactivity of said host.[3,5] Consequently, the design and study of artificial systems that display allosteric binding behavior regulated by small charged species is of inherent interest.[6-19] Not only can such systems help provide a better fundamental understanding of molecular recognition processes, but they might also serve as a basis for preparing functional materials whose properties can be tuned to control the cooperative binding interactions.

---

* Parts of this chapter were taken with permission from Davis, C. M.; Lim, J. M.; Larsen, K. R.; Kim, D. S.; Sung, Y. M.; Lyons, D. M.; Lynch, V. M.; Nielsen, K. A.; Jeppesen, J. O.; Kim, D.; Park, J. S.; Sessler, J. L. *J. Am. Chem. Soc.* **2014**, *136*, 10410-10417. Copyright 2014 American Chemical Society. Synthesis was done by CMD, KRL, and JSP. Crystal structures, grown by JSP and DSK, were solved by VML. UV-Vis studies were done by CMD, KRL, and JSP. NMR spectral studies were carried out by CMD. Job plot analyses were done by JSP and KRL. Photophysical studies were performed by JML and YMS. DFT calculations were done by JML. The final editing was by JLS. The initial draft was written by CMD and JSP.

Recently, we reported reversible electron transfer (ET) within a supramolecular assembly composed of tetrathiafulvalene (TTF) calix[4]pyrrole (**2.1)** and dicationic bisimidazoliumquinone (BIQ^{2+}) salts (e.g. **2.3**) (Figure 1).[20] We showed that the ET events within the complex could be controlled via external addition of tetraalkylammonium-anion pairs. Coordinating anions, such as chloride (Cl^-), bromide (Br^-), or methylsulfonate ($MeSO_4^-$), were found to promote the forward ET from **2.1** to **2.3** due to their ability to stabilize the supramolecular capsule-like ensemble [**2.1**$_2$·**2.3**]·2X^- (wherein X = Cl^-, Br^-, or $MeSO_4^-$) that acted as an intermediate to the ET event. The smaller tetraalkylammonium counter cations, such as tetraethylammonium and tetrabutylammonium, were found to compete with **2.3** for the cavity of the cone conformer of TTF-calix[4]pyrrole **2.1**. Upon binding with **2.1**, these tetraalkylammonium cations promoted the backward ET event by displacing BIQ^{2+}. In later studies, the electron deficient lithium encapsulated in fullerene ($[Li@C_{60}]^+$) was employed as the electron acceptor and the electronics were such that the complex was able to undergo ion-controlled "on" – "off" thermal ET processes.[21]

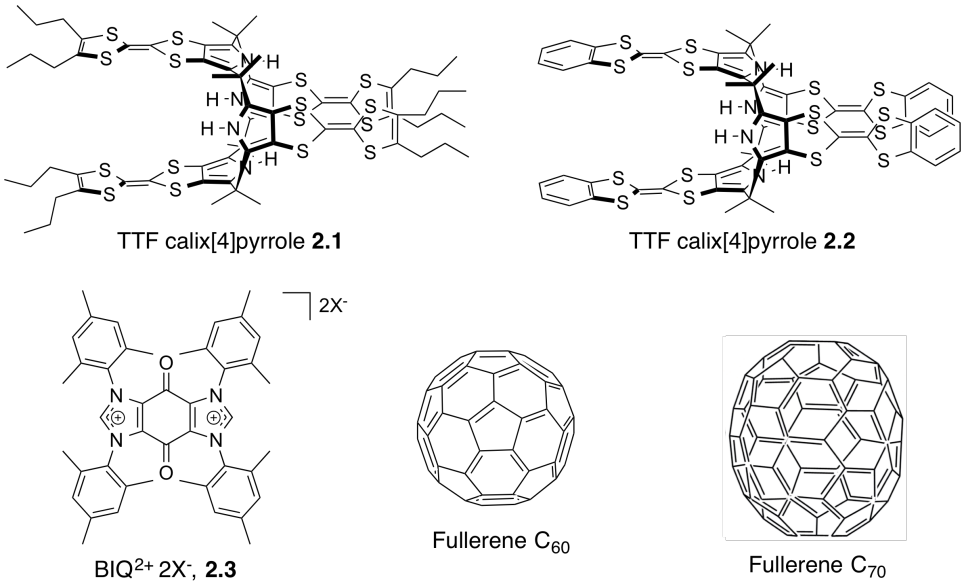

Figure 2.1 Structures of the tetrathiafulvalene calix[4]pyrroles **2.1** and **2.2**, bisimidazoliumquinone **2.3**, and fullerenes C_{60} and C_{70}.

To elucidate the function certain coordinating anions and cations have on the supramolecular thermal ET processes involving TTF-calix[4]pyrroles, specifically **2.1** and its recently prepared benzo-annulated derivative **2.2**,[22] the studies detailed in this chapter were carried out. Most specifically, the effect halide anions (F^-, Cl^-, and Br^-) and tetraalkylammonium cations (tetraethylammonium (TEA^+), tetrabutylammonium (TBA^+), and tetrahexylammonium (THA^+)) have on the ability of said calix[4]pyrroles to bind fullerene guests (C_{60} and C_{70}) were investigated. Because receptor **2.2** has not previously been studied, most emphasis will be placed on this receptor as opposed to **2.1**. Receptor **2.2** was synthesized as depicted in Scheme 2.1 below.

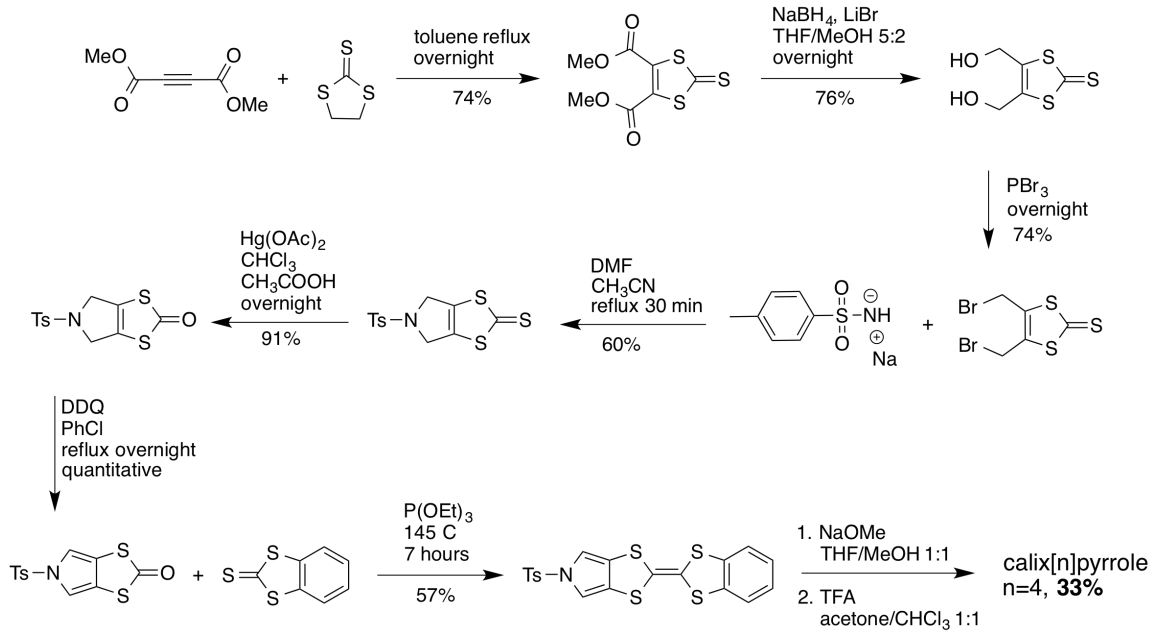

Scheme 2.1 Synthesis of tetrathiafulvalene calix[4]pyrrole **2.2**.

This chapter describes the intrinsic binding affinity of receptors **2.1** and **2.2** towards fullerenes C_{60} and C_{70}. As detailed below, it was found that the binding interactions can be modulated through the use of coordinating anion. The halide anions used, F^-, Cl^-, and Br^-, all bind to the TTF-calix[4]pyrroles to induce a conformational change from the thermodynamically stable 1,3-alternate to the cone conformation. This latter form provides a bowl-like cavity into which the fullerenes C_{60} and C_{70} can fit. Thus, all three anions act as positive heterotropic allosteric regulators for the binding of both C_{60} and C_{70} by the **2.1** and **2.2**. The selectivity of the calix[4]pyrrole cavity for a specific fullerene can be modulated by varying the halide anion. In fact, the use of a specific anion has a strong effect on the thermodynamic stability of the resulting anion-calix[4]pyrrole-fullerene assembly. In addition, in analogy to what was seen in the case of **2.1** and **2.3**,[20] the tetraalkylammonium cation acts as a negative allosteric regulator in that smaller derivatives, such as TEA^+, can compete with the fullerene for the cavity of

the calix[4]pyrrole. The net result of varying the halide anions and tetraalkylammonium cations in the context of calix[4]pyrrole fullerene recognition is a level of control not generally available for simple artificial fullerene receptors.

In addition to these studies, the stoichiometry for the binding between calix[4]pyrrole and fullerene was investigated. In earlier studies involving fullerene C_{60} and calix[4]pyrrole **2.1**, a 2:1 stoichiometry between the receptor and guest was proposed.[23,24] However, in the later studies with $[Li@C_{60}]^+$, a 1:1 binding stoichiometry was inferred. As the result of studies presented in this chapter, the conflict between the two proposed binding stoichiometries has been resolved. The 1:1 stoichiometry prevails.

2.1 Effects of Tetraalkylammonium Cations on Solid-State Structures

In our previous studies on the anion-triggered binding of C_{60} by **2.1**, TBACl was used as the source of anion to induce the conformational change in the calix[4]pyrrole to the cone conformer. As mentioned above, such a conformational rearrangement was a necessary prerequisite to binding.[23] Although we expected the fullerene would sit inside of the bowl-shaped cavity of **2.1**, an X-ray crystallographic analysis of single crystals obtained from a mixture of TBACl, receptor **2.1**, and C_{60} in toluene revealed the complex existed in the solid state as a multi-component host-guest ensemble $(TBA)_6[(\mathbf{2.1}\cdot Cl)_6(C_{60})_8(toluene)_5]$ in which TBA^+ was bound within the calix[4]pyrrole cavity (Figure 2.2a). In addition, the stoichiometry between **2.1** and C_{60} within the complex was 3:4. Due to the unexpected complexation of TBA^+ by **2.1**, we studied the binding of the cation with **2.1** and found that TBA^+ binds within the bowl of the calix[4]pyrrole in the complex **2.1**·Cl in a 1:1 fashion.[24] The stoichiometry of the original crystal structure, however, still perplexed us. After our studies of **2.1** with both **2.3** and

$[Li@C_{60}]^+$, we realized that smaller electron-deficient substrates, including small tetraalkylammonium cations, could compete with fullerene and BIQ^{2+} for the bowl-like cavity present in the cone-like conformers of the TTF-calix[4]pyrrole receptors. Such competitive binding might explain why in the crystal structure noted above the fullerene was not found within the cavity of **2.1**. The TBA^+ cation simply occupies the site.

In order to test this hypothesis, co-crystallization experiments were conducted with **2.1** and C_{60} in the presence of tetraoctylammonium chloride (TOACl). Crystals were grown via pentane diffusion into a dichloromethane solution containing an equimolar mixture of the three components. Since the TOA^+ cation is larger than TBA^+, it was expected that the host cavity would be left vacant. This would lead to a situation in which the fullerene C_{60} could occupy the calix[4]pyrrole cavity. The resulting structure shown in Figure 2b revealed that the fullerene was bound within the receptor **2.1**·Cl with a 1:1:1 stoichiometry between the three components. The TOA^+ cation was found bound to the outer surface of **2.1**. Based on the structural parameters, electronic donor-acceptor interactions between the electron rich TTF moieties of **2.1** and the electron deficient C_{60} surface were inferred.

To confirm further the 1:1:1:1 relationship between the four components of the complex, multiple co-crystallizations were carried out using various combinations of TTF-calix[4]pyrroles **2.1** and **2.2** with C_{60} and C_{70} in the presence of various tetraalkylammonium salts of chloride, fluoride, and bromide. Three diffraction-quality single crystals were collected, namely (TBA)[C_{60}⊂**2.1**·F], (TOA)[C_{70}⊂**2.1**·Cl], and (THA)[C_{70}⊂**2.2**·Cl]. The resulting structures are shown in Figure 2.2. It is important to note that when TBAF was cocrystallized with C_{60} and **2.2**, the TBA^+ counter cation is located outside of the cavity of **2.2** while C_{60} is encapsulated within, as seen in Figure 2.2c. This is in direct contrast with what was seen previously with **2.1**.[23] We propose that

the difference between these solid-state structures lies in the fact that the benzo-annulated TTF moieties of **2.2** have a larger electron rich area, thereby allowing it to embrace better the spherical fullerene substrate as compared to the TBA^+ cation.

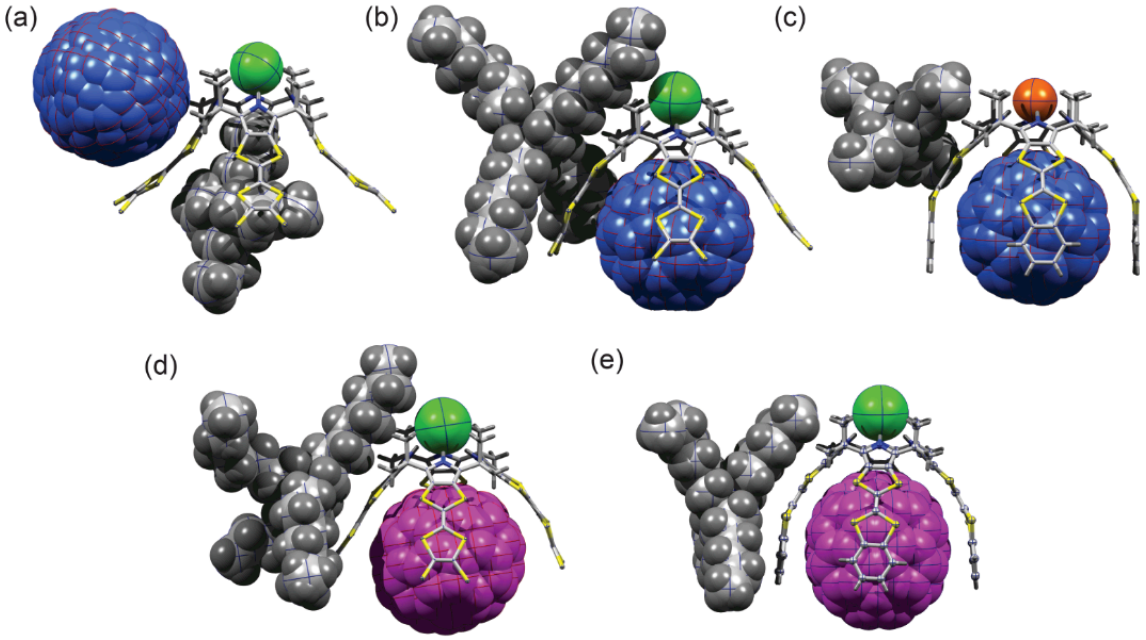

Figure 2.2 X-ray crystallographic analyses of (a) $(TBA)_6[(\mathbf{2.1}\cdot Cl)_6(C_{60})_8(toluene)_5]$[23], (b) $(TOA)[C_{60}\subset(\mathbf{2.1}\cdot Cl)]$, (c) $(TBA)[C_{60}\subset(\mathbf{2.2}\cdot F)]$, (d) $(TOA)[C_{70}\subset(\mathbf{2.1}\cdot Cl)]$, and (e) $(THA)[C_{70}\subset(\mathbf{2.2}\cdot Cl)]$. For clarity, C_{60} and C_{70} are depicted as blue and purple space filling models, respectively.

The use of C_{70} instead of C_{60} for crystallization experiments resulted in the identification of additional differences between the solid-state cavities of receptors **2.1** and **2.2**. Fullerene C_{70} is larger and has an ellipsoidal shape as compared to the spherical C_{60}. In the case of **2.1**, the egg-shaped C_{70} binds in a 1:1 fashion with a side-on conformation with respect to the imaginary C_4 axis of the cone shaped calix[4]pyrrole cavity (Figure 2.2d). However, when receptor **2.2** was used, a solid-state structural analysis revealed that C_{70} is bound in an end-on orientation (Figure 2.2e). These

differences in C_{70} orientation are thought to reflect the specific nature of the size, shape, and inherent flexibility of the concave π-surfaces present in **2.1** and **2.2**. However, crystal-packing effects cannot be completely discounted.

These solid-state analyses lead to the conclusion that a 1:1 encapsulation of fullerene within the TTF receptor cavity is favored under most crystallization conditions involving tetraalkylammonium halides. Although it is appreciated that the most stable solid-state structure may not correlate to the dominant species in solution, this finding lead us to reevaluate the 2:1 (**2.1**:C_{60}) solution-state stoichiometry proposed previously.[23]

2.2 Solution-State Stoichiometry Determinations via Continuous Variation Analysis

The 2:1 calix[4]pyrrole:fullerene stoichiometry proposed previously was based on continuous variation analysis, also known as Job plots.[23] For a well-behaved equilibrium between two species, this form of analyses can be an informative tool for determination of stoichiometry of host-guest binding. However, in the case of mixtures containing TTF calix[4]pyrroles, fullerenes, and TBA^+ salts, there are multiple equilibria at play. For example, **2.1**·Cl can bind with either TBA^+ or fullerene when all three components are in solution. The originally reported Job plot analyses were done by mixing two solutions of dichloromethane, one containing C_{60} and the other [**2.1** + TBACl], in different ratios while keeping the total concentration of [**2.1** + C_{60}] constant. These conditions lead to a Job plot with a maximum of 0.35, suggesting a 2:1 stiochiometry.[25] However, by not holding the concentration of TBACl constant, this approach did not account for the multiple equilibria that could occur and overlooked the potential competing nature of TBA^+ for the TTF-calix[4]pyrrole cavity.

To carry out a more accurate Job plot analysis, we felt it best to allow only one set of species to vary under the titration conditions. Therefore, the Job analyses were repeated while maintaining a constant concentration of TBACl throughout the titration. Under these conditions, the intensity of the charge transfer (CT) absorbance band associated with fullerene encapsulation within the TTF-calix[4]pyrrole cavity[23] reached a maxima when the molar fraction of $[C_{60}]/[\mathbf{2.1} + C_{60}]$ was close to 0.5, indicating a 1:1 stoichiometry (Figure 2.3a). The Job plot analysis of **2.2** with C_{60} and C_{70} under analogous conditions also resulted in maxima CT absorbance at a molar ratio of 0.5 (Figures 2.3b and 2.3c, respectively), further indicating a 1:1 stoichiometry. These observations are in agreement with the solid-state data, suggesting a 1:1 stoichiometry as the more accurate representation of fullerene binding into the cavity of TTF-calix[4]pyrrole receptors under these solutions phase conditions.

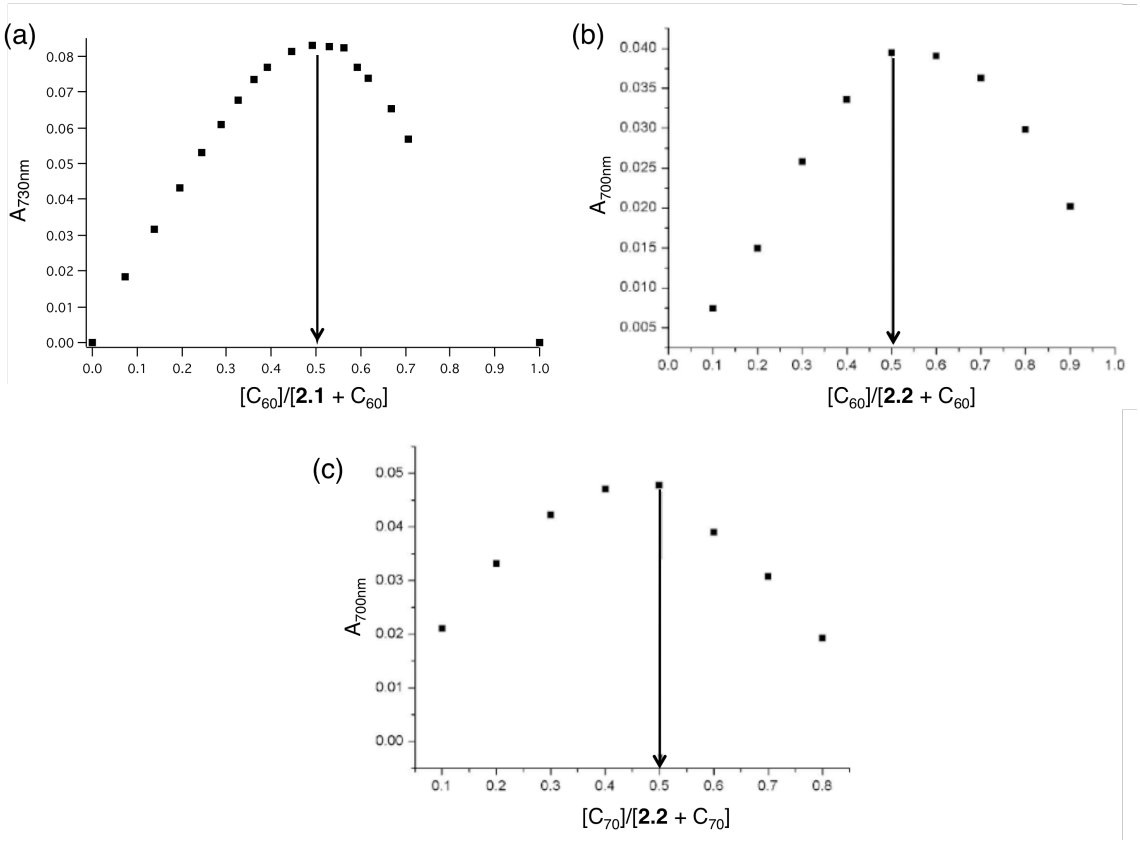

Figure 2.3 Continuous variation plots for the mixtures of (a) **2.1** and C_{60} ([**2.1** + C_{60} = 100 μM) in the presence of TBACl (500 μM) (b) **2.2** and C_{60} ([**2.2** + C_{60}] = 50 μM) in the presence TBACl (250 μM) and (c) **2.2** and C_{70} ([**2.2** + C_{70}] = 50 μM) in the presence TBACl (250 μM). Plots were constructed by plotting the absorbance of the CT band at (λ = 730 nm for **2.1** and λ = 700 nm for **2.2**) as a function of the mole-fraction of C_{60} or C_{70} as appropriate.[26]

The effect the ratio of TBACl to **2.1** had on the binding of C_{60} by **2.1** was also studied. To do this, the amount of TBACl was varied from 1 to 50 equivalents relative to the concentration of **2.1**. UV-Vis titrations and Job plot analyses were then carried out. As can be seen from an inspection of Figure 2.4, in all cases the maximal binding for **2.1** with C_{60} is seen at a molar ratio of 0.5, further confirming a 1:1 stoichiometry between **2.1** and C_{60}. The only effect the ratio of TBACl had throughout these studies was on the amount of CT complex formed. A maximum was seen at 5 equivalents. This latter

finding is interpreted in terms of at least 5 equivalents of Cl^- being needed to induce near-complete conversion of the calix[4]pyrrole to its cone conformation.

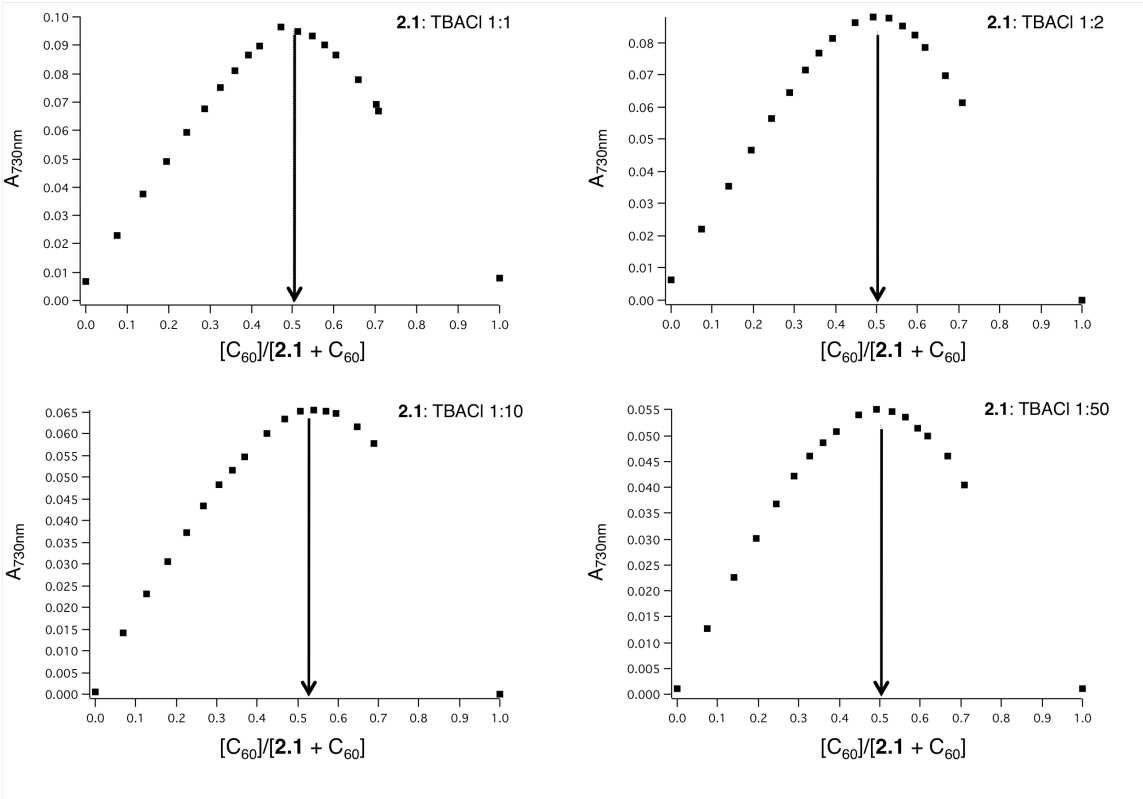

Figure 2.4 Continuous variation plots for [**2.1** + C_{60}] (0.1 mM) in the presence of 0.1-0.5 mM TBACl in dichloromethane at room temperature. Plots were constructed by plotting the absorbance of the CT band at 730 nm as a function of mole-fraction of C_{60}.

The disparity between the previous continuous variation titrations and the ones described above reflect two stark differences in the manner in which the experiments were carried out. Firstly, as discussed previously, the concentration of TBACl was kept constant throughout the spectroscopic analysis in the current study. The second difference has to do with how the data was plotted. Normally in Job plots, the x-axis is the *molar ratio of the species* and the y-axis is *Δabsorbance × [host]*.[25] This is how the original

spectroscopic data were plotted.[23] Since the host, receptor **2.1**, is involved in multiple equilibria, namely that with fullerene and TBA^+, multiplying the change in absorption of the CT band by the host concentration skews the data. This is not the case in conditions where the host is only involved in a single equilibrium. To circumvent this, the absorbance of the CT band was plotted directly against the molar ratio of $[C_{60}]/[$**2.1** + $C_{60}]$. Since the intensity of the CT band is directly correlated with formation of $[C_{60}\subset($**2.1**$\cdot Cl)]^-$, the absorbance itself is proportionate to the quantity of complex formation. These two changes in the analysis of the Job plot data allowed for a more accurate representation of the binding stoichiometry.

2.3 Effect of Halide Anions on the Fullerene-Binding Affinities of TTF-calix[4]pyrroles

To investigate if the coordinating halide anion plays a role in the regulation of the supramolecular interactions between the TTF-calix[4]pyrroles and fullerenes of this study (**2.1**, **2.2**, C_{60}, and C_{70}), a series of UV-Vis photometric titrations were carried out. The binding affinity (K_a) for the interactions between receptors **2.1** and **2.2** with C_{60} and C_{70} were determined in the presence of three halide anions, F^-, Cl^-, and Br^-. For these studies, the counter cation to all the halide anions was TBA^+. The binding affinities were determined using two separate titration conditions, "normal titrations" and "inverse titrations." In the normal titration method, a concentrated solution of the fullerene in question was titrated into a solution of either receptor **2.1** or **2.2** (receptor concentration at 10 μM) in the presence of 10 equivalents of TBAX (X = F^-, Cl^-, or Br^-). The inverse titrations were performed by titrating a concentrated solution of either receptor **2.1** or **2.2** into solutions of fullerenes (20 μM) containing 10 equivalents of TBAX.

These two titration methods were designed to evaluate different aspects of the competitive equilibrium. In the conditions of the normal titrations, the receptors are already in equilibrium with the TBA^+ salts before the addition of fullerene. Because of this, it is then expected that some TBA^+ would already be bound within the cavity of the calix[4]pyrrole cone conformer of either **2.1** or **2.2**. The fullerene, when added, must compete with the complexed TBA^+ cation. Early on in the titration the latter cation is in high excess relative to the added fullerene. Although this competition can complicated data analysis, this method allows for only one parameter to be changed, namely the ratio of fullerene to the TTF-calix[4]pyrrole receptor.

For the inverse titration, the calix[4]pyrrole in question is titrated into a solution of [TBACl + fullerene]. Upon the addition of the calix[4]pyrrole to this solution, the Cl^- anion binds to the calix[4]pyrrole to induce the cone conformation. After this takes place, either the fullerene or the TBA^+ cation can bind within the cavity. Upon subsequent additions of calix[4]pyrrole, the ratio of both receptor:fullerene and receptor:TBACl are changing concurrently. Since two parameters are changed in the inverse titrations, the calculated K_a values will vary depending on the method used to record them. The normal titration method better reflects the binding affinity since only one parameter is changed; however, in both cases a competition exists between the fullerene and the TBA^+ cation for the host cavity.

When fullerene is bound within the TTF-calix[4]pyrrole cavity, a CT band will appear in the UV-Vis spectroscopic region. This CT band directly reflects the formation of the complex $[\text{fullerene}\subset(\text{receptor})]^-$ and, therefore, the change in intensity can be monitored as a function of concentration of titrating component to give titration curves. These data were then analyzed using a standard 1:1 curve fitting[26] to give the binding affinities listed in Table 2.1.

Table 2.1 Effective binding constants (K_a, M^{-1}) corresponding to the interaction between **2.2** and C_{60} and C_{70} as determined in the presence of 10 molar equiv of the TBA salts of selected anions in dichloromethane.[a]

Compound		C_{60}	C_{70}
TBAF	Normal	2,500,000	210,000
	Inverse	8,100,000	830,000
TBACl	Normal	640,000	1,400,000
	Inverse	390,000	3,300,000
TBABr	Normal	450,000	17,000
	Inverse	28,000	17,000

[a]All K_a values were obtained from UV-Vis spectrophotometric titration experiments carried out at 296 K. The estimated errors are ≤15%.

Although all three halides used in the present study, namely F^-, Cl^-, and Br^-, bind to **2.1** and **2.2** and induce a conformational change from the 1,3-alternate to the cone conformer that is capable of encapsulating a fullerene, there are vast differences between the thermodynamic stabilities of the resulting supramolecular ensembles [fullerene⊂(**2.1**·X)]$^-$ and [fullerene⊂(**2.2**·X)]$^-$ that are directly related to the choice of coordinating halide anion. For **2.1**, the use of the fluoride anion (as its TBA^+ salt) gave rise to the highest binding affinity for C_{60} (K_a= 1.8 × 10^6 M^{-1}), followed by chloride (K_a= 1.1 × 10^5 M^{-1}) and bromide (K_a= 3.4 × 10^4 M^{-1}), as determined using the inverse titration method. These data follow the trend that the smaller, more basic anion (fluoride) is bound more strongly to **2.1** than the larger, less basic ones (bromide and chloride). This was also seen with **2.2** when studied with C_{60}. However, with C_{70}, the highest binding affinity was seen for chloride. Both fluoride and bromide gave rise to substantially lower binding affinities. Receptor **2.2**, therefore, binds C_{60} more strongly than C_{70} in the presence of fluoride or bromide. In contrast, it binds C_{70} preferentially in the presence of chloride. On this basis, we concluded that halide anions act as positive heterotropic allosteric effectors

for fullerene binding in that they are capable of modulating the binding affinity by altering the relative selectivity of receptor **2.2**. To the best of our knowledge, such switching has not been previously observed for artificial fullerene receptors.

The affinities of the halide anions for receptor **2.2** were analyzed in the absence of fullerene to better understand the above anion-dependent fullerene binding effects. Separate UV-Vis spectroscopic titrations carried out in the presence of TBAF, TBACl, and TBABr with receptor **2.2** to form (**2.2**·X^-). These studies served to confirm that fluoride binds with the highest affinity (K_a= 2.4 × 10^7 M^{-1}), followed by chloride (K_a= 1.6 × 10^6 M^{-1}) and bromide (K_a= 1.5 × 10^4 M^{-1}). This affinity order is in full agreement with what was previously observed for simple, unfunctionalized calix[4]pyrroles[27] as well as the three component assemblies [C_{60}⊂ (**2.1**·X)]$^-$ and [C_{60}⊂(**2.2**·X)]$^-$ but not [C_{70}⊂(**2.2**·X)]$^-$. Therefore, the change in binding association constants fullerene binding cannot be solely attributed to differences in the anion affinities.

We rationalized that the anion dependent change in fullerene binding behavior has a steric origin. The complexation of a halide anion with the NH protons of the calix[4]pyrrole affects the size and shape of the bowl-shaped cavity of receptor **2.2**. This change in the overall structure of the host depending on halide anion used dictates the subsequent fullerene binding events and the associated affinities. As seen in the X-ray structures for [C_{60}⊂(**2.2**·Cl^-)] and [C_{70}⊂(**2.2**·F^-)], the smaller fluoride anion is held above the calix[4]pyrrole cone at a shorter hydrogen bond distance than chloride (2.72 Å for N-H···F vs 3.25Å for N-H···Cl). Since the tightly bound fluoride allows for a wider bit angle in the cavity of receptor **2.2** (∠120° for NH···F···HN vs ∠94° for NH···Cl···HN) it is proposed that use of fluoride creates a more open calix[4]pyrrole cone that is a better suited anion for binding the larger, more spherical C_{60} over the ellipsoid-shaped C_{70}.

2.4. Effects of Tetraalkylammonium Cations on Fullerene-Binding Affinities of TTF-calix[4]pyrroles

After determining the role halide anions have on fullerene binding within the TTF-calix[4]pyrrole cavity, the next step was to study the competitive effect, if any, of tetraalkylammonium cations. Towards this end, we conducted UV-Vis spectroscopic titrations in dichloromethane solution using the chloride salts of the TEA^+, TBA^+, and THA^+ cations. This allowed us to determine the role charge density, as well as size, has on fullerene binding while keeping the anion constant.

Normal titrations were carried out in which aliquots of a concentrated solution of C_{60} (120 μM) were added to a dichloromethane solution of **2.2** (10 μM) in the presence of 10 molar equivalents of the tetraalkylammonium cation in question. During these titrations, the solution changed color form yellow to green. This is consistent with the CT complex $[C_{60}\subset(\mathbf{2.2}\cdot Cl)]^-$, a species that absorbs at 700 nm. However, at any given molar ratio, the quantity of CT complex, indicated by the absorbance intensity, differed depending on the tetraalkylammonium cation used. The greatest intensity and hence largest amount of the CT complex was formed when the relatively large THA^+ was used. Conversely, the use of the smaller, charge dense TEA^+ produced the smallest changes in the absorption intensity. Plotting the associated change in absorption intensity at 700 nm versus the fullerene concentration gave binding isotherms, whose K_a values are shown schematically in Figure 2.5.

The choice of tetraalkylammonium cation had a large effect on the binding of C_{60} by receptor **2.2**. Specifically, for the same receptor, anion, and solvent, the fullerene affinity is increased by over four orders of magnitude when the chloride counter cation was changed from TEA^+ to THA^+. Therefore, smaller more positively charged cationic species act as efficient inhibitors for fullerene complexation. This is fully consistent with

the solid-state data, in which there were stark differences between the structures of $(TBA)_6[(\mathbf{2.1}\cdot Cl)_6(C_{60})_8(toluene)_5]$ and both $(TOA)[C_{60}\subset\mathbf{2.1}\cdot Cl]$ and $(THA)[C_{60}\subset\mathbf{2.2}\cdot F]$. These results are taken as evidence that counter cations play a larger role in regulating anion and fullerene binding events than previously thought.

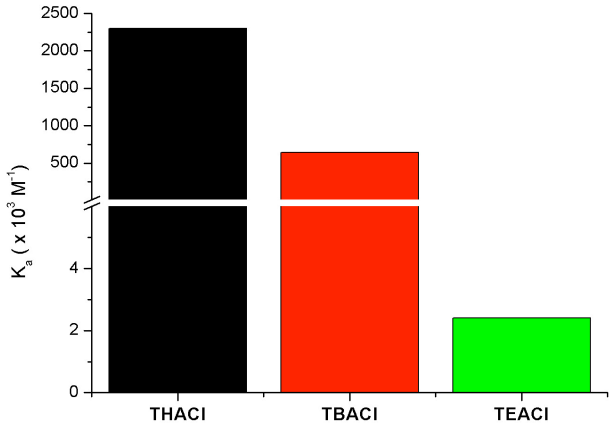

Figure 2.5 K_a values corresponding to the interaction of **2.2** and C_{60} as measured in dichloromethane solution in the presence of three different tetraalkylammonium (TAA^+) chloride salts, THACl, TBACl, and TEACl.

The efficiency of the binding inhibition by TEA^+ was further evaluated in fullerene displacement experiments. For these studies, both C_{60} and C_{70} were used in conjugation with **2.2** in dichloromethane. Specifically, aliquots of a concentrated solution of TEACl were added to the supramolecular ensembles $(THA)[C_{60}\subset(\mathbf{2.1}\cdot Cl)]$, $(THA)[C_{70}\subset\mathbf{2.1}\cdot Cl)]$, $(THA)[C_{60}\subset(\mathbf{2.2}\cdot Cl)]$, and $(THA)[C_{70}\subset(\mathbf{2.2}\cdot Cl)]$ in separate experiments. In all cases the addition of TEA^+ to the solution resulted in a color change from green to yellow. This is the opposite of what is observed during CT complex formation, and is thus consistent with displacement of the fullerene by TEA^+.

The TEA^+-induced displacement of fullerene was further characterized by ^1H NMR spectroscopy recorded in deuterated dichloromethane (400 MHz, room

temperature). The signal associated with the CH_2 protons of the ethyl groups of TEACl, usually centered around δ 3.42 ppm, was found to broaden and shift to δ 3.05 ppm when added to a solution containing the supramolecular ensemble, (THA)[C_{60}⊂(**2.2**·Cl)] (Figure 2.6). This broadening, associated with encapsulation of the TEA^+ into the cavity of (**2.2**·Cl)$^-$, was also seen upon addition of TEACl to a solution of **2.2** in the absence of fullerene (Figure 2.7). These spectral changes are analogous to what is seen in the case of TBA^+ complexation with **2.1** in the absence of a competitive guest and when the TEA^+ cation acts to displace **2.3** from **2.1**.[20,24] These results provide support for the conclusion that the TEA^+ cation is complexed within the cavity of (**2.2**·Cl)$^-$ in solution, rather than bound outside the receptor via nonspecific electrostatic interactions as seen in the crystal structure of $(TBA)_6[(\mathbf{2.1}\cdot Cl)_6(C_{60})_8(toluene)_5]$.

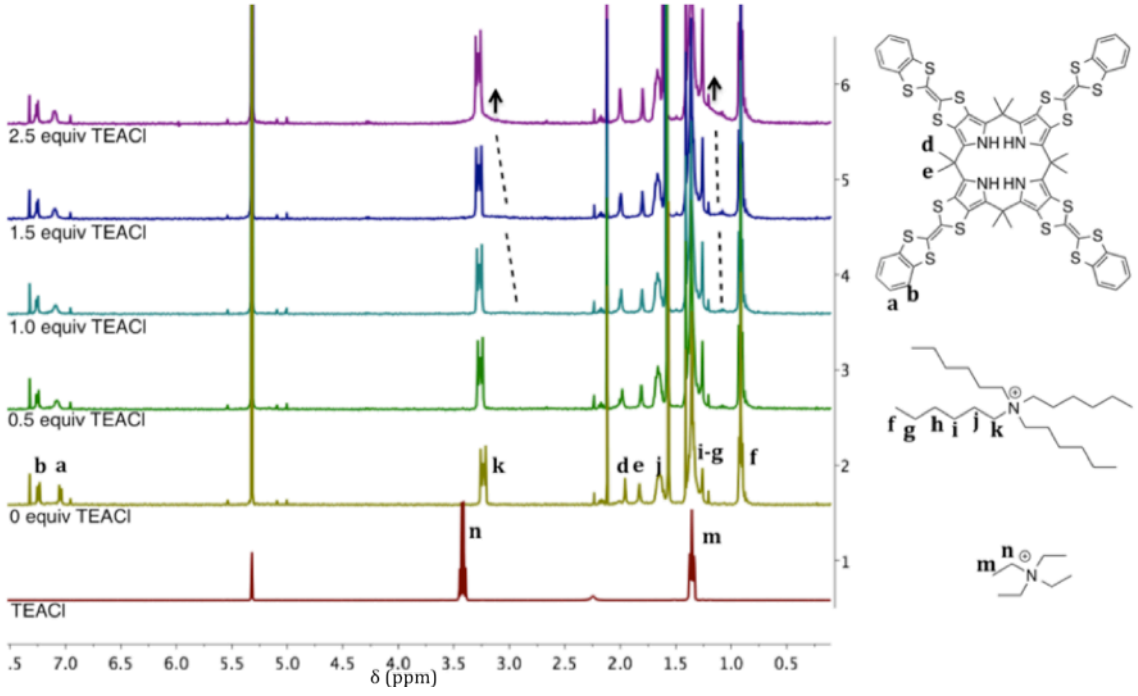

Figure 2.6 ^{1}H NMR spectral changes seen for a deuterated dichloromethane solution of **2.2** (0.5 mM), THACl (1.5 mM), and C_{60} (0.5 mM) upon titration with increasing amounts of TEACl. Residual chloroform and acetone signals are observed at δ 7.32 and 2.13 ppm, respectively.

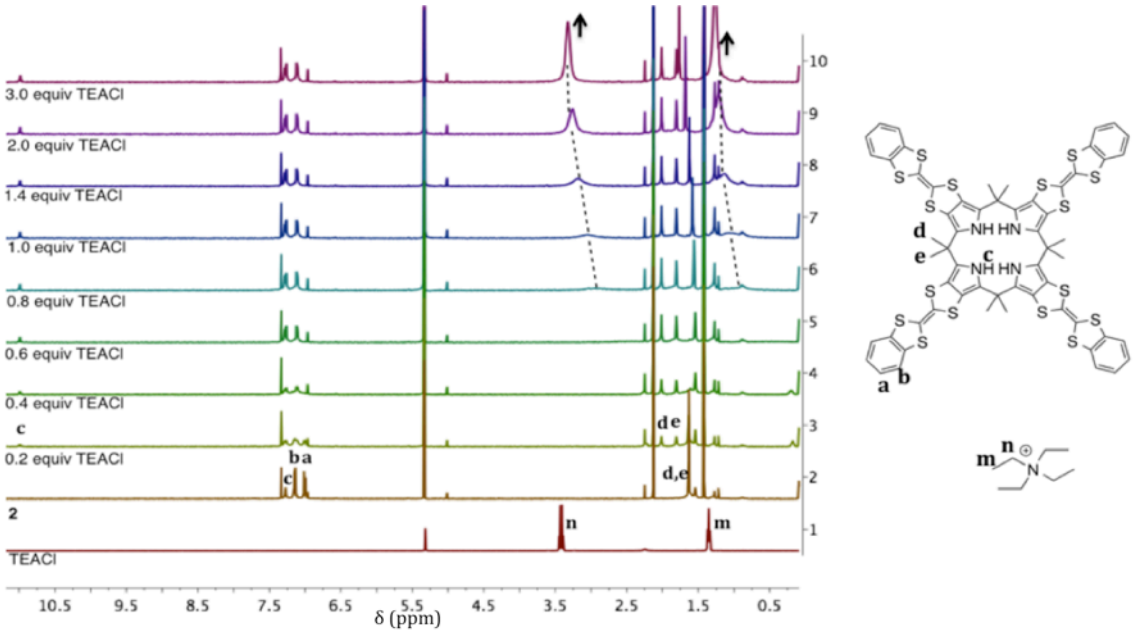

Figure 2.7 ^{1}H NMR spectral changes seen when TEACl was titrated into a deuterated dichloromethane solution of TTF-calix[4]pyrrole **2.2** (3 mM). Note: Some precipitation occurred over the course of the titration. Residual chloroform and acetone signals (reflecting impurities carried over from the synthesis) are observed at δ 7.32 and 2.13 ppm, respectively.

To determine the binding affinity of TEA^+ for the cavity of **2.2** in the presence of fullerenes C_{60} and C_{70}, the change in absorbance at 700 nm was plotted as a function of TEA^+ concentration. The titration curves produced upon this plotting were fitted using two binding models, a 1:1 binding model and a competitive interaction model.[26] The 1:1 binding model treats the TEA^+ cation and the complex [fullerene⊂(**2.2**·Cl)]$^-$ as the interacting species with the products of the interaction being [fullerene + TEA⊂(**2.2**·Cl)]. The titration were carried out such that aliquots of TEA^+ were added to dichloromethane solutions of either (THA)[C_{60}⊂(**2.2**·Cl)]$^-$ or (THA)[C_{70}⊂(**2.2**·Cl)]$^-$ consisting of 10 μM THACl, 10 μM of the specified fullerene, and 10 μM **2.2**. This revealed the binding constant for TEA^+ with [C_{60}⊂(**2.2**·Cl)]$^-$ as 6.9×10^4 M^{-1} and [C_{70}⊂(**2.2**·Cl)]$^-$ as 3.8×10^4 M^{-1}. The higher binding constant of TEA^+ with the C_{60} over C_{70} was taken as evidence

that C_{60} is not bound as tightly within host (**2.2**·Cl)$^-$ as C_{70}. This is consistent with what was inferred based on the direct analysis of [**2.2** + C_{60}] and [**2.2** + C_{70}] in the presence of TBA^+, a less competitive cation.

The use of the competitive binding model allowed for the binding of TEA^+ to (**2.2**·Cl)$^-$ to be calculated rather than the binding of TEA^+ to [fullerene⊂(**2.2**·Cl)]$^-$. The value calculated using this binding model was 4.2×10^5 M^{-1}. This value is on the same order of magnitude as the values obtained for the interaction of **2.2** with C_{60} in the presence of TBACl via both normal and inverse titrations. This concordance further supports the conclusion that small cations, such as TEA^+, can compete with larger guests, such as fullerenes, for the cavity of the calix[4]pyrrole. Failure to account for these competitive guests, as seen in our initial study,[23] can produce erroneous results.

2.5 Photophysical Properties of the Supramolecular Assemblies

To obtain direct evidence for the binding of fullerene into the cavity of **2.1** and **2.2** in solution, the excited-state dynamics of the supramolecular ensembles [C_{60}⊂(**2.1**·X)]$^-$ and [C_{60}⊂(**2.2**·X)]$^-$ were investigated using femtosecond transient absorption spectroscopy. Upon excitation of these ensembles at the CT band (800 nm), the transient spectra of each complex revealed broad excited-state absorption (ESA) features in the visible and NIR spectral regions (Figure 2.8a and 2.8b). These features were also seen upon excitation of [C_{70}⊂(**2.2**·X)]$^-$ (Figure 2.9b). Most notably, upon excitation, a prominent peak around 1080 nm was observed. This feature is attributed to the one-electron reduced C_{60} radical anion.[23,28] The formation of the C_{60} radical anion in solution upon excitation indicates that photoinduced electron transfer occurs within the ensemble, giving rise to a CT state. The absorption of the fullerene radical anion is seen

instantaneously (within instrumental resolution) upon photoexcitation. This is consistent with the charge separated (CS) state being formed via rapid electron transfer.

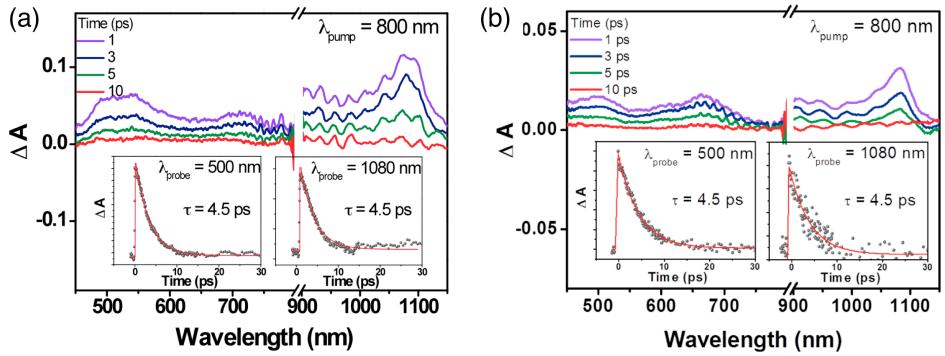

Figure 2.8 Femtosecond transient spectra of the supramolecular complexes formed between (a) $[C_{60}\subset(\mathbf{2.1}\cdot X)]^-$ and (b) $[C_{60}\subset(\mathbf{2.2}\cdot X)]^-$ in the presence of tetrabutylammonium chloride (TBACl) in dichloromethane at room temperature. The excitation wavelength was 800 nm. The insets show representative decay profiles at 500 and 1080 nm, respectively. The concentrations of **2.1**, **2.2**, C_{60}, and TBA^+ halides are ~100 μM.

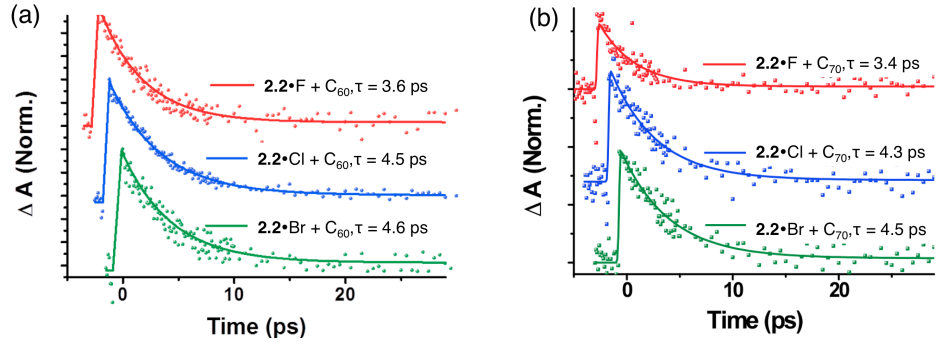

Figure 2.9 Representative decay profiles of (a) $[C_{60}\subset(\mathbf{2.2}\cdot X)]^-$ and (b) $[C_{70}\subset(\mathbf{2.2}\cdot X)]^-$ at 500 nm in the presence of tetrabutylammonium fluoride (TBAF, red), tetrabutylammonium chloride (TBACl, blue), and tetrabutylammonium bromide (TBABr. green), upon excitation at 800 nm recorded in dichloromethane at room temperature. The concentrations of **2.2**, C_{60} or C_{70}, and the TBA^+ halide salts are ~100 μM.

The photodynamic studies provide support for the suggestion that there are strong donor/acceptor interactions between the TTF moieties of the calix[4]pyrroles and the fullerene guests, as noted in the solid state (cf. Figure 2.2). The tight interaction between the TTF subunits and the fullerenes led us to predict that fast charge separation, as well as fast recombination, will occur upon photoirradiation. As seen in Table 2.2, a fast charge recombination (CR) is observed for all the [fullerene⊂(calix[4]pyrrole·X)]$^-$ ensembles in solution. This supports a model where the TTF-calix[4]pyrrole fullerene complexes are sustained via π-π donor-acceptor interactions between the TTF-subunits and the C_{60} or C_{70} moieties. Since the host-guest distances are relatively the same for all receptors-fullerene ensembles, the donor/acceptor interactions are expected to be similar, resulting in similarly fast photoinduced electron transfer dynamics. This is generally true; however, there seems to be a small discernable anion dependence. Specifically, the CR process increases for complexes of **2.1** and C_{60}. Also for **2.2** the CR with both C_{60} and C_{70} increases slightly as the anion is changed from fluoride (3.4-3.6 ps) to either chloride or bromide (4.3-4.6 ps) as seen by the half-lives of the absorption species at 500 nm (Table 2.2). We believe these lifetime differences reflect the halide anion-dependent inductive effects, which are fully consistent with the small anion-induced variations seen in the solid-state structures.

Table 2.2 Charge recombination dynamics of supramolecular CT complexes in dichloromethane. In all cases, the excitation wavelength was 800 nm. The probe wavelengths were 500 and 1080 nm for the C_{60} complexes and 500 nm for the C_{70} complexes, respectively. The concentrations of **2.1**, **2.2**, fullerenes, and tetrabutylammonium (TBA^+) halides were ~100 μM.

Receptor	Fullerene	TBA^+ Salt	Half Life, τ	Rate Constant, k_{CR}
		F^-	3.6 ps	2.78×10^8 sec^{-1}
2.1	C_{60}	Cl^-	4.5 ps	2.22×10^8 sec^{-1}
		Br^-	4.6 ps	2.17×10^8 sec^{-1}
		F^-	3.6 ps	2.78×10^8 sec^{-1}
2.2	C_{60}	Cl^-	4.5 ps	2.22×10^8 sec^{-1}
		Br^-	4.6 ps	2.17×10^8 sec^{-1}
		F^-	3.4 ps	2.94×10^8 sec^{-1}
2.2	C_{70}	Cl^-	4.3 ps	2.33×10^8 sec^{-1}
		Br^-	4.3 ps	2.22×10^8 sec^{-1}

2.6 MOLECULAR ORBITAL ANALYSES

Quantum mechanical calculations based on the X-ray crystal structures of receptors **2.1** and **2.2** with fullerenes C_{60} and C_{70} were carried out to determine the location of the highest occupied molecular orbital (HOMO) and lowest unoccupied molecular orbital (LUMO) within the complexes As can be seen from an inspection of Figure 2.10, the calculated molecular orbital structures have the HOMO electron density on the TTF units of calix[4]pyrroles **2.1** and **2.2** with the LUMO electron density on the fullerene guest moieties. These findings provide support for the notion that the photoinduced CT occurs from the TTF moieties of the calix[4]pyrrole receptors to the fullerene guests and that this CT process will be facile. The result will be a TTF cation radical and fullerene radical anion species, as observed by experiment.

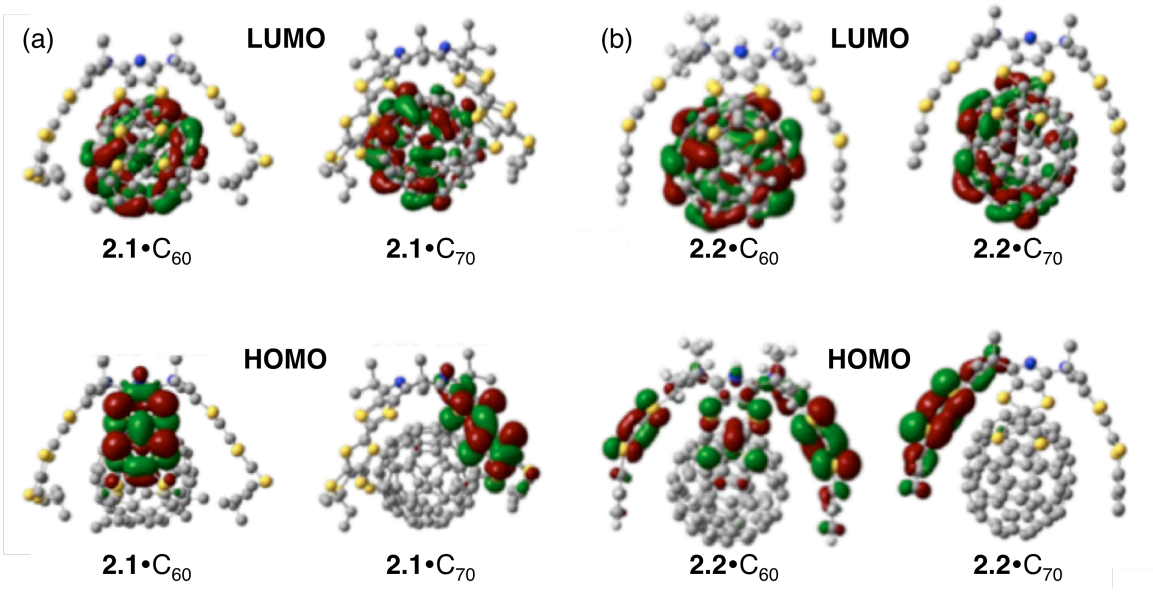

Figure 2.10 Frontier molecular orbitals of the supramolecular CT complexes formed between (a) **2.1** and fullerenes (C_{60} (left) and C_{70} (right)) and (b) **2.2** and fullerenes (C_{60} (left) and C_{70} (right))

2.7 CONCLUSIONS

In summary, we have codified the allosteric regulatory effects that tetraalkylammonium halide salts have on the binding of fullerenes to TTF-calix[4]pyrroles. These effects were thoroughly investigated via X-ray crystallographic and Job plot analyses, as well as K_a value determinations and transient absorption spectral studies. We conclude that the binding stoichiometry that best represents the interaction between TTF-calix[4]pyrroles, such as **2.1** and **2.2**, and fullerenes C_{60} and C_{70} is in fact 1:1, rather than the 2:1 host:guest stoichiometry proposed previously.[23]

In addition, we showed small tetraalkylammonium cations (such as TEA^+ and TBA^+) can act as inhibitors of fullerene binding in that they can compete with the larger electron deficient moieties for the cavity of the TTF calix[4]pyrroles. This study also

provides a cogent reminder that erroneous conclusions can be drawn from continuous variation plots unless the ratios of all species are kept constant, excluding the two interacting species under investigation. As the complexity of supramolecular ensembles increases, it becomes ever more important to pay close attention to the conditions of any given study, especially in the case of systems with multiple equilibria.

Although requiring an increased level of care for analysis, multicomponent supramolecular assemblies, such as the one detailed in this chapter, are deemed important to further our understanding of complex cooperative systems, both synthetic and natural. In the present case, the selectivity and sensitivity of receptors **2.1** and **2.2** for fullerenes C_{60} and C_{70} were turned via chose of anion, employed for activation of the binding event, and its corresponding counter cation. This work therefore sets the stage for even more elaborate studies wherein multicomponent allosteric binding effects are used to control recognition features of self-assembled materials, electron transfer ensembles, and species-selective chemosensor arrays.

2.8 EXPERIMENTAL METHODS

General chemicals of the best grade available were purchased from commercial suppliers and were used without further purification. Unless otherwise noted, benzonitrile (PhCN) was distilled over phosphorus pentoxide (P_2O_5) before use. Benzo-tetrathiafulvalene calix[4]pyrrole **3.1** was prepared using literature methods. Porphyrin **3.3**, prepared using a modification of literature procedures, was saponified using sodium hydroxide in aqueous tetrahydrofuran, followed by cation exchange using tetraethylammonium hydroxide to yield the porphyrin carboxylate salt **3.2**.

2.8.1 Instrumentation

UV-Vis spectrophotometric titrations were carried out at room temperature in dichloromethane. Those performed at UT Austin were measured using a Cary Varian 5000 UV-Vis-NIR spectrophotometer. ^{1}H NMR spectra were recorded on a Varian DirectDrive 400 MHz instrument at 400 MHz and ^{13}C NMR spectra were recorded on a Varian DirectDrive 600 MHz instrument at 151 MHz in deuterated dichloromethane at room temperature.

2.8.2 Laser Flash Photolysis Measurements

The femtosecond time-resolved transient absorption (TA) spectrometer consisted of NIR optical parametric amplifier (OPA) system (Quantronix, Pallitra) pumped by a Ti:sapphire regenerative amplifier system (Quantronix, Integra-C) operating at 1 kHz repetition rate and an optical detection system. The generated OPA output signals had a pulse width of ~ 100 fs in the range of 480-700 nm which were used as pump pulses. White light continuum (WLC) probe pulses were generated using a sapphire window (3 mm of thickness) by focusing of small portion of the fundamental 800 nm pulses. The time delay between pump and probe beams was carefully controlled by making the pump

beam travel along a variable optical delay (Newport, ILS250). The intensities of the spectrally dispersed WLC probe pulses were monitored using two miniature spectrographs (OceanOptics USB2000+). To obtain the time-resolved transient absorption difference signal (ΔA) at a specific time, the pump pulses were chopped at 25 Hz and absorption spectra intensities were saved alternately with or without pump pulse. Typically, 6000 pulses excite samples to obtain the TA spectra at a particular delay time. The polarization angle between pump and probe beam was set at the magic angle (54.7°) in order to prevent polarization-dependent signals. Cross-correlation fwhm in pump-probe experiments was less than 200 fs and chirp of WLC probe pulses was measured to be 800 fs in the 400–1200 nm region. To minimize chirp, non-reflection optics were used in the probe beam path and the cuvette was a 2 mm path length quartz cell. After the TA experiments, the absorption spectra of all compounds was carefully checked so as to control for artifacts arising from, e.g., photo-degradation or photo-oxidation of the samples in question. HPLC grade dichloromethane was used.

2.8.3 Quantum Mechanical Calculations

Quantum mechanical calculations were performed using the Gaussian09 program suite. All calculations were carried out using density functional theory (DFT) with the Becke's three-parameter hybrid exchange functional and the Lee-Yang-Parr correlation functional (B3LYP), employing a basis set of 6-31G(d,p) for all atoms.

2.8.4 X–ray Crystallographic Analyses

As noted in the main text, in order to characterize the solid-state conformational properties, binding modes, and stoichiometries resulting from the interaction between receptors **2.1** or **2.2** and fullerenes (C_{60} and C_{70}) in the presence of halide anions, an effort was made to obtain diffraction grade single crystals of representative supramolecular

ensembles. Towards this end, n-pentane was allowed to diffuse into equimolar mixtures of the TTF-C4Ps (**2.1** or **2.2**) and fullerenes (C_{60} or C_{70}) in dichloromethane containing 1 equiv of various tetraalkylammonium halide salts. In this way, dark blue, diffraction-quality single crystals were grown from the mixtures of [**2.1** + TOACl + C_{60}], [**2.2** + TBAF + C_{60}], [**2.2** + TOACl + C_{70}], and [**2.2** + THACl + C_{70}]. Subsequent single crystallographic X–ray diffraction analyses provided evidence for the formation of the supramolecular assemblies between the corresponding TTF-calix[4]pyrroles (**2.1** or **2.2**) and fullerenes (C60 or C70), and tetraalkylammonium halide salts (TBAF, THACl, or TOACl) in the solid state that are characterized by an overall 1:1:1 stoichiometry. The X-ray structures in question are displayed in Figures 2.11-2.14 below.

X–ray crystallographic data for (TOA)[$C_{60}\subset$(**2.1**·Cl)], (TOA)[($C_{70}\subset$(**2.1**·Cl)], and (THA)[$C_{70}\subset$(**2.2**·Cl)] were collected on a Rigaku AFC-12 diffractometer equipped with a Saturn CCD area detector and a graphite monochromatized MoK_{α} source ($\lambda = 0.71070$ Å). The data were collected at 100 K under a cold nitrogen stream. X–ray crystallographic data for (TBA)[$C_{60}\subset$(**2.2**·F)] were collected on a Rigaku SCX-Mini diffractometer equipped with a Mercury CCD area detector and a graphite monochromatized MoK_{α} source ($\lambda = 0.71075$ Å). The data were collected at 223 K. Data reduction for all these crystals was performed using the Rigaku Americas Corporation's Crystal Clear version 1.40.[29] Details of crystal data, data collections, and structure refinements of (TOA)[$C_{60}\subset$(**2.1**·Cl)], (TOA)[$C_{70}\subset$(**2.1**·Cl)], (THA)[$C_{70}\subset$(**2.2**·Cl)] and (TBA)[$C_{60}\subset$(**2**·F)] are listed in Table 2.3. The structures were solved by direct methods and refined by full-matrix least-squares on F^2 with anisotropic displacement parameters for the non-H atoms using SHELXL-97.[30] The hydrogen atoms were calculated in ideal positions with isotropic displacement parameters set to 1.2 × Ueq of the attached atom (1.5 × Ueq for methyl hydrogen atoms). All the calculations were carried out with the

SHELXTL program.[31] Further details of the individual structures can be obtained from the Cambridge Crystallographic Data Centre by quoting reference numbers CCDC 998440 for (TOA)[C_{60}⊂(**2.1**·Cl)], CCDC 998438 for (TBA)[C_{60}⊂(**2.2**·F)], CCDC 998441 for (TOA)[C_{70}⊂(**2.1**·Cl)], and CCDC 998439 for (THA)[C_{70}⊂(**2.2**·Cl)].

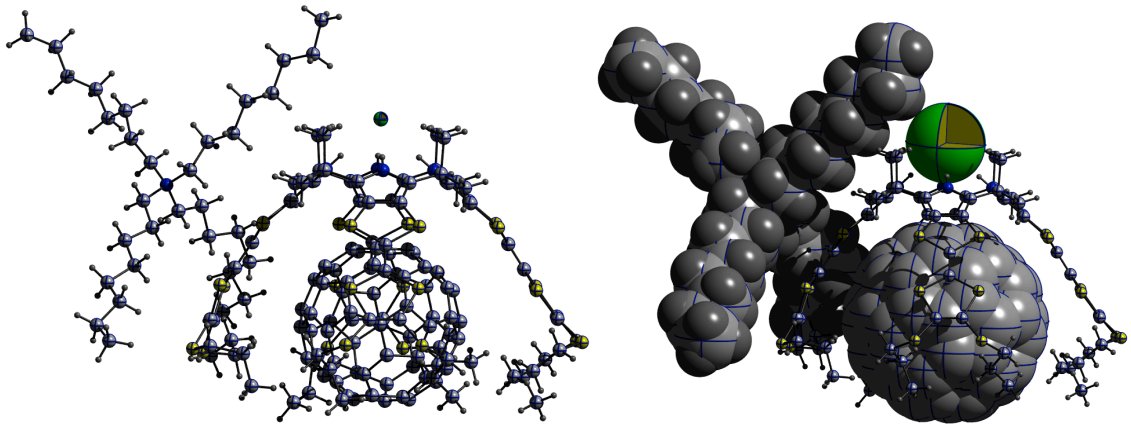

Figure 2.11 Single crystal X–ray diffraction structure of (TOA)[C_{60}⊂(**2.1**·Cl)].

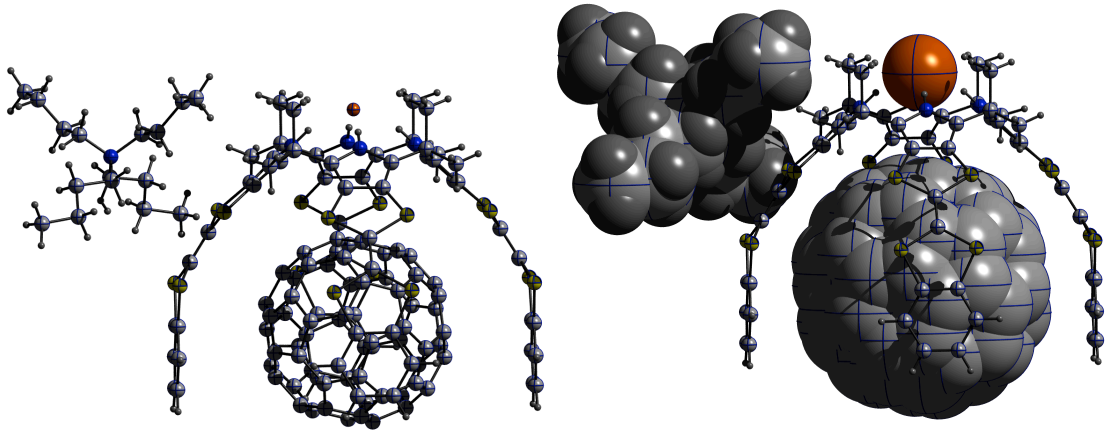

Figure 2.12 Single crystal X–ray diffraction structure of (TBAF)[C_{60}⊂(**2.2**·F)].

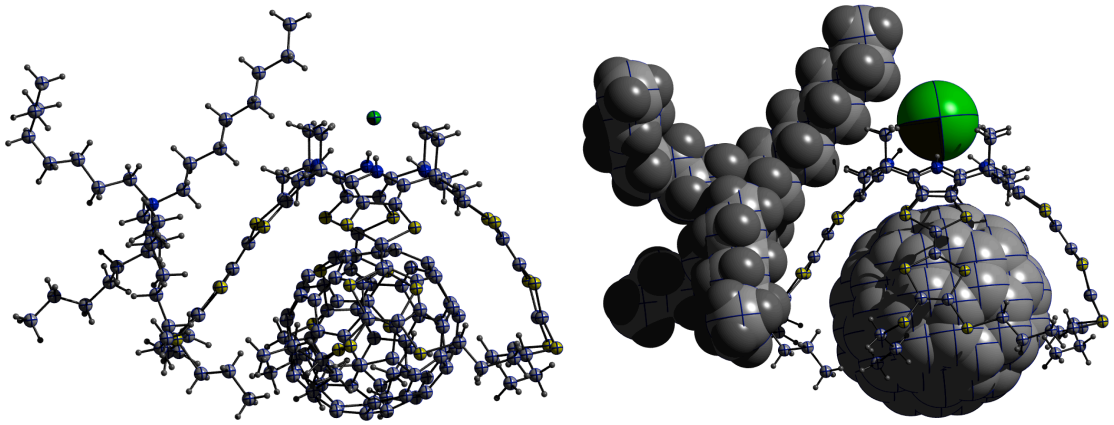

Figure 2.13 Single crystal X–ray diffraction structure of (TOA)[C_{70}⊂(**2.1**·Cl)].

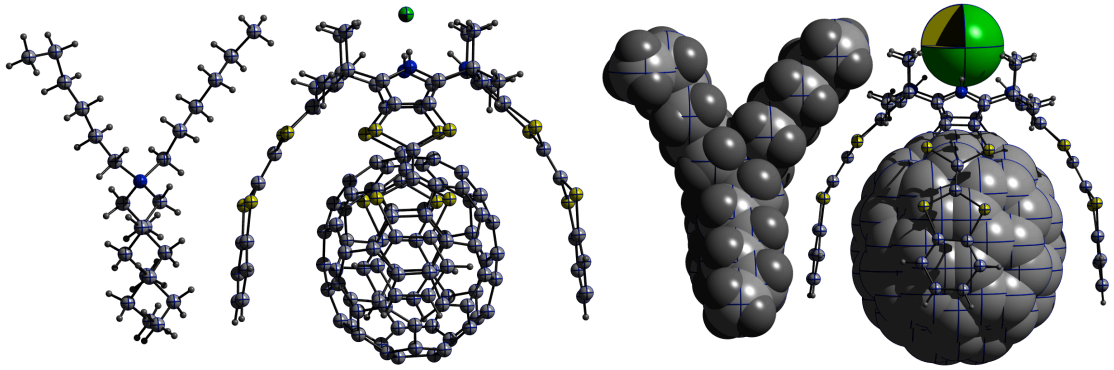

Figure 2.14 Single crystal X–ray diffraction structure of (THA)[C_{70}⊂(**2.2**·Cl)].

Table 2.3 Selected crystal data and refinement parameters.

	(TOA)[C_{60}⊂(2.1·Cl)]	**(TBAF)[C_{60}⊂(2.2·F)]**
Empirical formula	C_{160} H_{152} Cl N_5 S_{24}	C_{136} H_{80} F N_5 S_{16}
Temperature (K)	100(2)	233(2)
Crystal system	Monoclinic	Tetragonal
Space group	$P2_1/c$	P4/n
Crystal color	Dark Blue	Dark Blue
a (Å)	19.557(6)	18.7465(8)
b (Å)	19.323(6)	18.7465(8)
c (Å)	37.662(12)	14.7998(7)
α (deg)	90	90
β (deg)	98.973(6)	90
γ (deg)	90	90
Volume (Å^3)	14059(8)	5201.1(4)
Z	4	2
θ range (°)	1.19 to 25.00	3.07 to 25.00
Completeness to θ	99.0	99.8
Reflection collected/ Unique	111339 / 24512	34848 / 4583
Absorption correction	Semi-empirical from equiv.	Semi-empirical from equiv.
Data/restraints/parameters	24512 / 10881 / 1731	4583 / 9316 / 800
Goodness-of-fit on F^2	1.993	1.067
Final *R* indices [I>2δ(I)]	R_1 = 0.1930	R_1 = 0.1079
	wR_2 = 0.4031	*w*R_2 = 0.3074
R indices (all data)	R_1 = 0.2271	R_1 = 0.1287
	wR_2 = 0.4166	wR_2 = 0.3329
CCDC number	CCDC 998440	CCDC 998438

	(TOA)[C_{70}⊂(2.1·Cl)]	**(THA)[C_{70}⊂(2.2·Cl)]**
Empirical formula	$C_{172.60}H_{153.20}Cl_{6.20}N_5S_{24}$	C_{166} H_{124} Cl_5 N_5 S_{16}
Temperature (K)	100(2)	100(2)
Crystal system	Triclinic	Monoclinic
Space group	P-1	$P2_1/n$
Crystal color	Dark brown	Dark brown
a (Å)	19.601(11)	21.845(4)
b (Å)	20.274(11)	21.527(4)
c (Å)	20.336(10)	29.676(6)
α (deg)	74.425(16)	90
β (deg)	81.702(17)	106.20(3)
γ (deg)	86.891(19)	90
Volume (Å^3)	7702(7)	13401(5)
Z	2	4
θ range (°)	1.05 to 25.00	3.00 to 25.00
Completeness to θ	99.0 %	99.8 %
Reflection collected/ Unique	80910 / 26855	85772 / 23561
Absorption correction		

Table 2.3 continued.

Data/restraints/parameters Goodness-of-fit on F^2 Final *R* indices [I>2δ(I)] R indices (all data) **CCDC number**	Semi-empirical from equivalents 26855 / 7983 / 1952 2.259 R_1 = 0.1532 wR_2 = 0.3861 R_1 = 0.1762 *w*R2 = 0.4004 CCDC 998441	Semi-empirical from equivalents 23561 / 4849 / 1747 1.767 R_1 = 0.1064 wR_2 = 0.3227 R_1 = 0.1343 wR_2 = 0.3477 CCDC 998439

2.8.5 UV-Vis spectrophotometric titrations

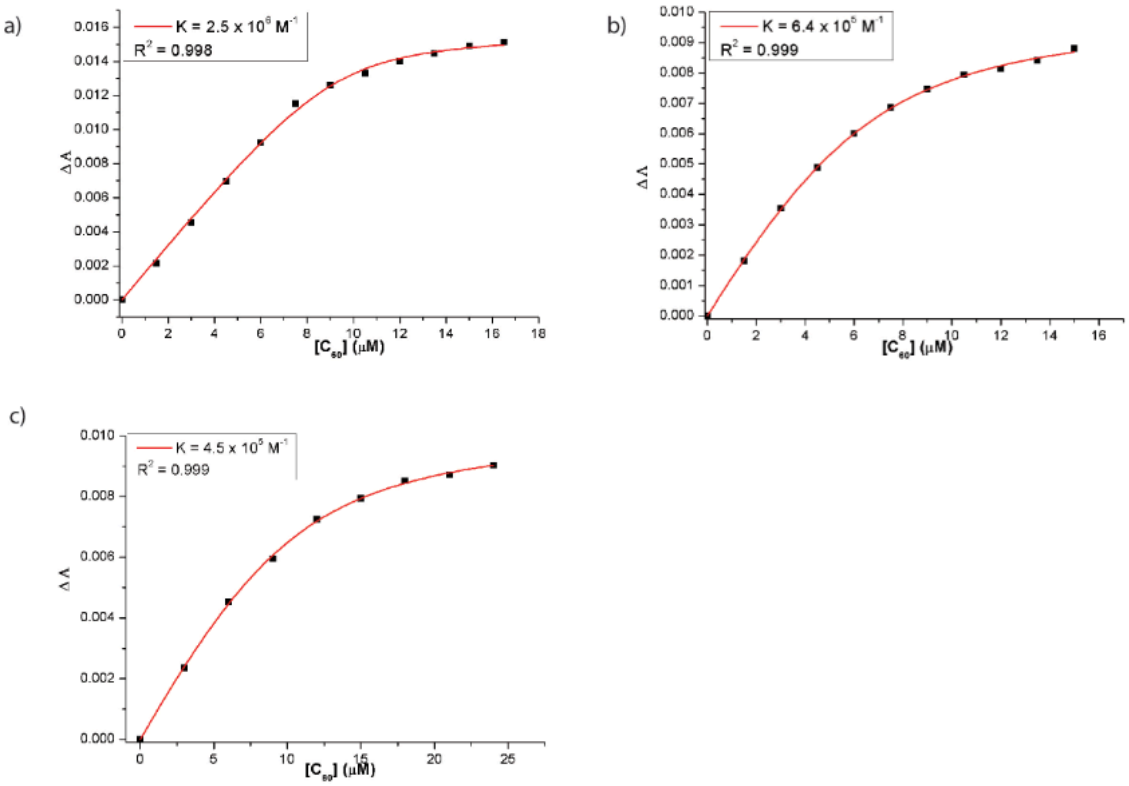

Figure 2.15 Binding data from "normal titrations" (see section 2.3 for definition) of **2.2** with C_{60} in the presence of 10 equiv of a) tetrabutylammonium fluoride (TBAF), b) tetrabutylammonium chloride (TBACl), and c) tetrabutylammonium bromide (TBABr). The studies were carried out in dichloromethane at 295 K.

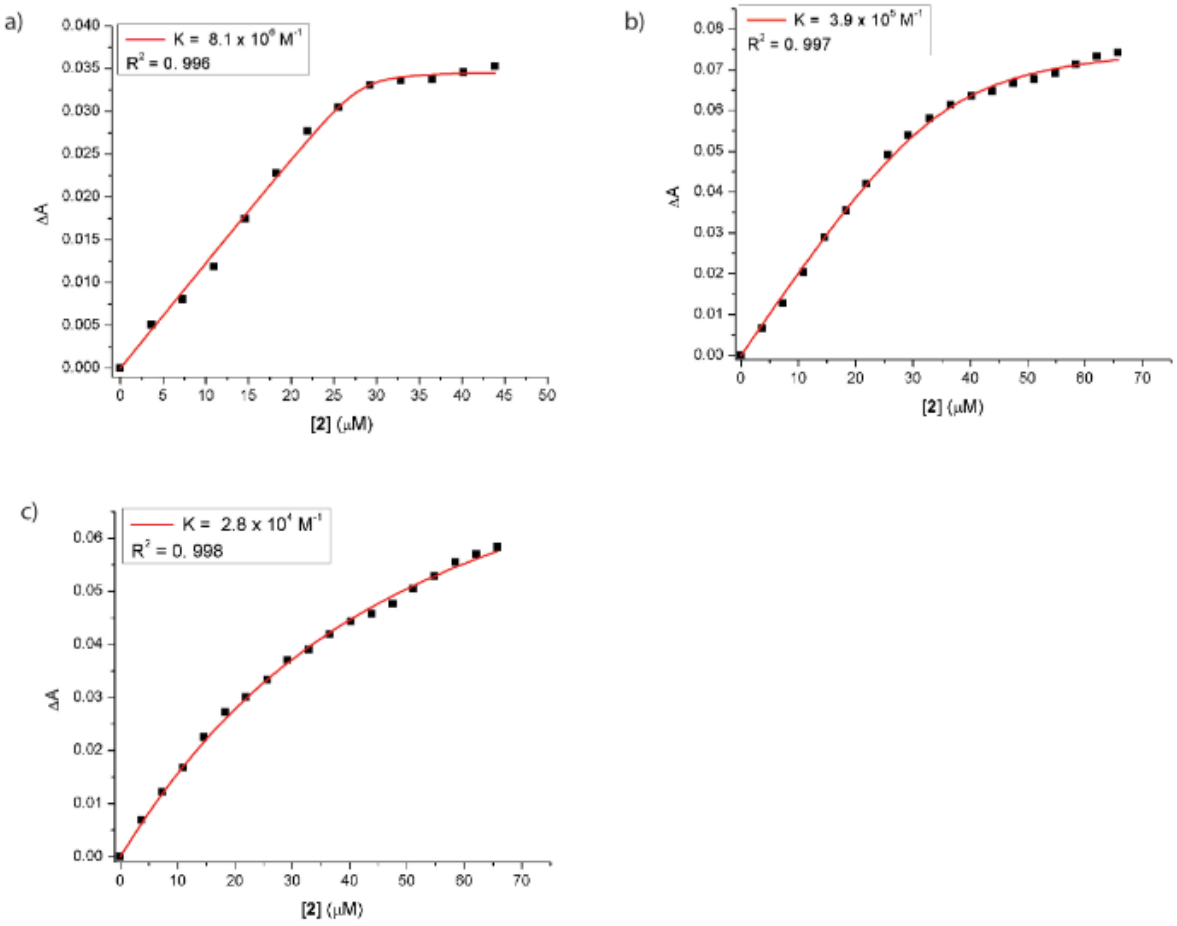

Figure 2.16 Binding data from "inverse titrations" (see section 2.3 for definition) of **2.2** with C_{60} in the presence of 10 equiv of a) tetrabutylammonium fluoride (TBAF), b) tetrabutylammonium chloride (TBACl), and c) tetrabutylammonium bromide (TBABr). The studies were carried out in dichloromethane at 295 K.

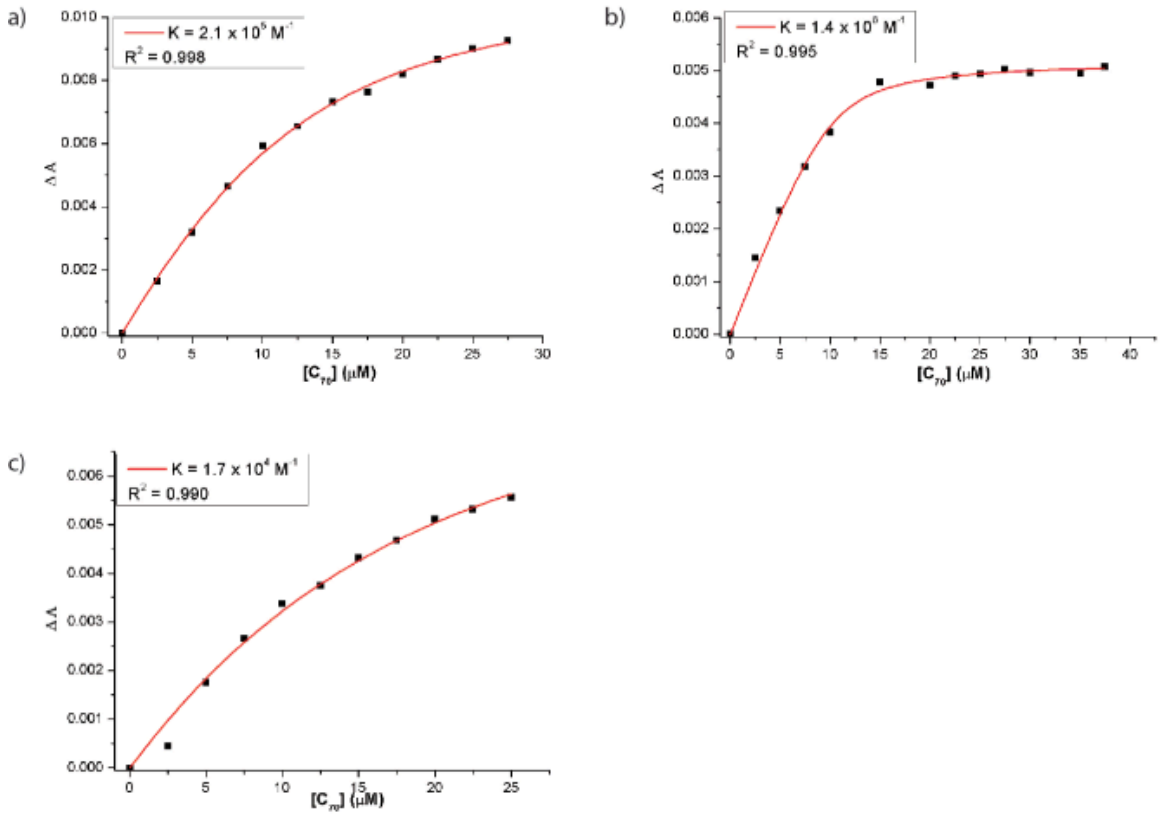

Figure 2.17 Binding data from "normal titrations" of **2.2** with C_{70} in the presence of 10 equiv of a) tetrabutylammonium fluoride (TBAF), b) tetrabutylammonium chloride (TBACl), and c) tetrabutylammonium bromide (TBABr). The studies were carried out in dichloromethane at 295 K.

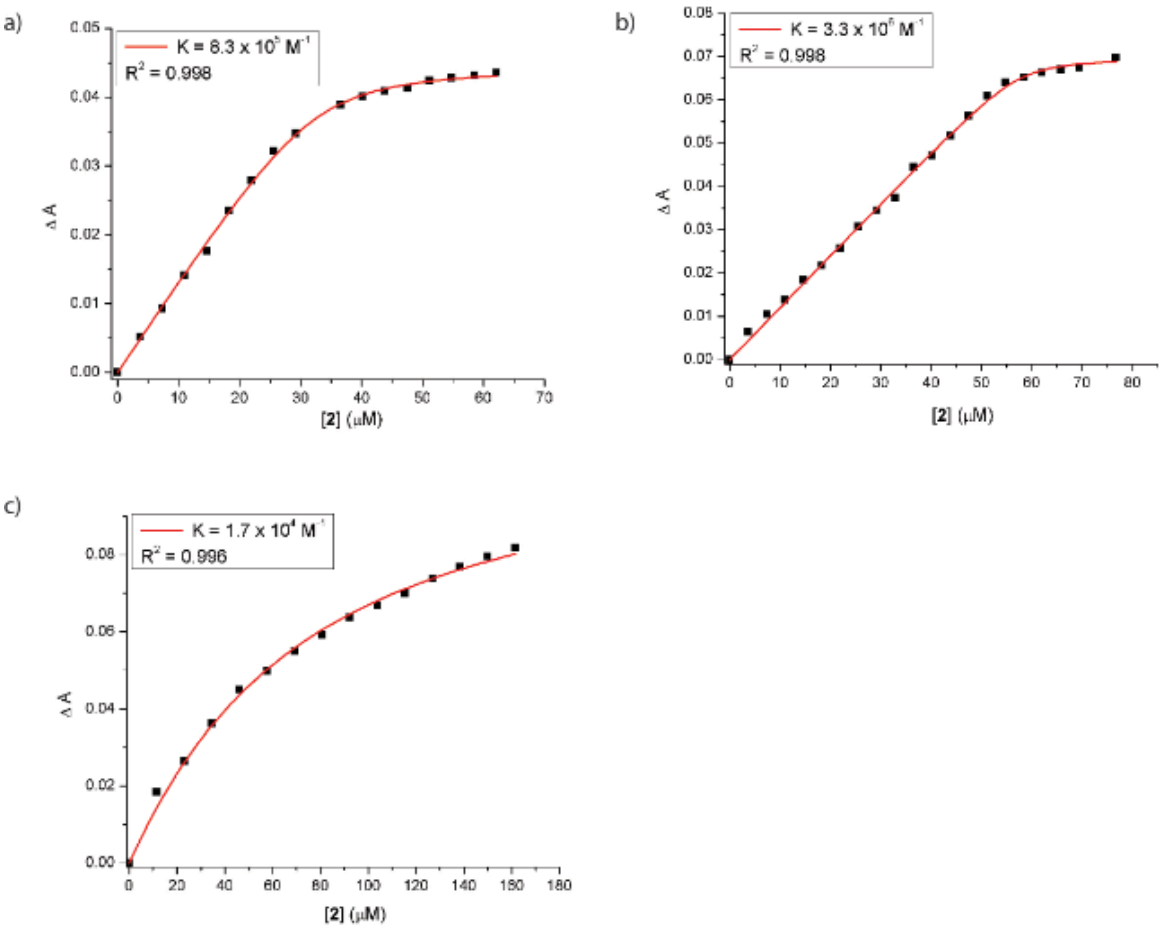

Figure 2.18 Binding data from "inverse titrations" of **2.2** with C_{70} in the presence of 10 equiv of a) tetrabutylammonium fluoride (TBAF), b) tetrabutylammonium chloride (TBACl), and c) tetrabutylammonium bromide (TBABr). The studies were carried out in dichloromethane at 295 K.

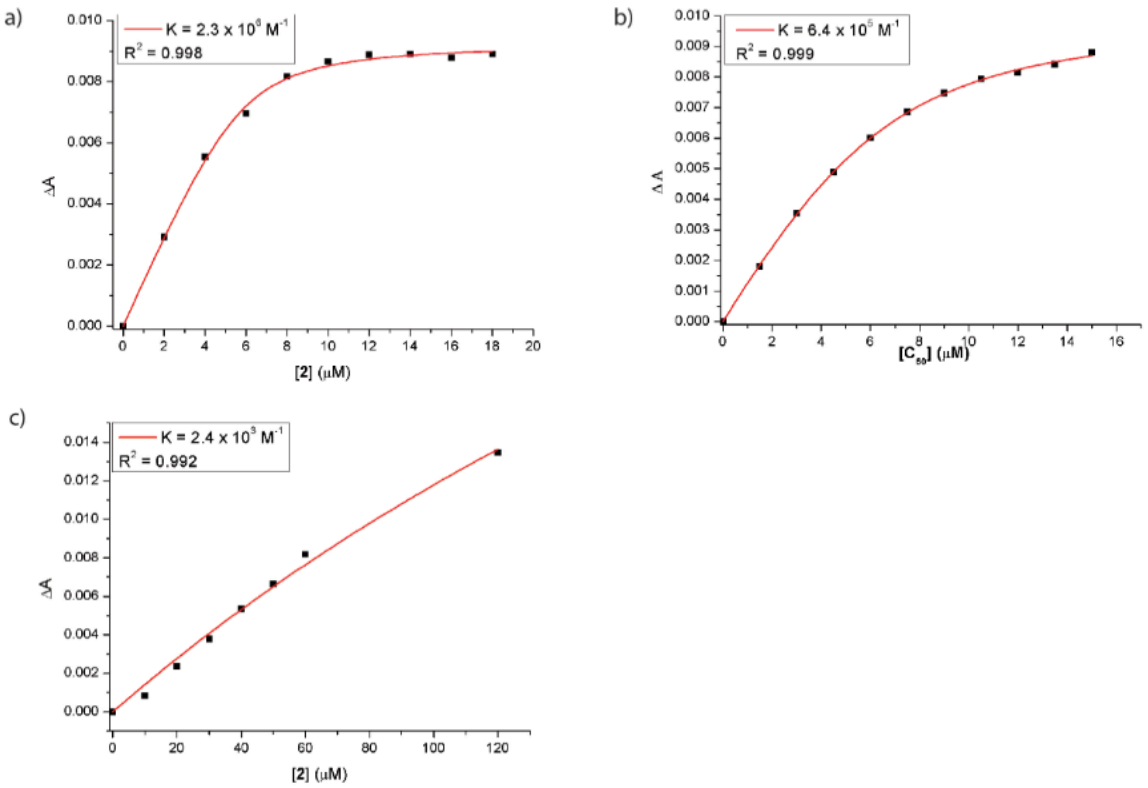

Figure 2.19 Binding data from "normal titrations" of **2.2** with C_{60} in the presence of 10 equiv of a) tetrahexylammonium chloride (THACl), b) tetrabutylammonium chloride (TBACl), and c) tetraethylammonium chloride (TEACl). The studies were carried out in dichloromethane at 295 K.

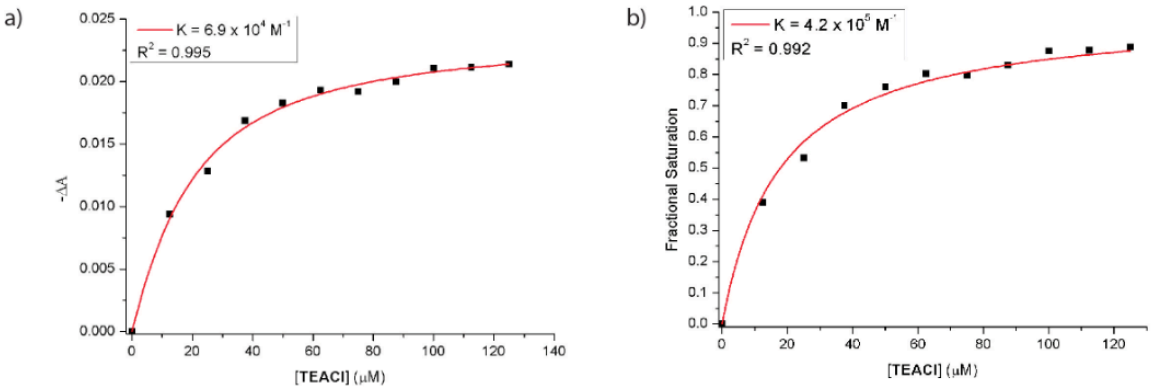

Figure 2.20 Binding isotherm analysis for "competitive titrations" (see section 2.4 for definitions) of $TBA^+[C_{60}\subset$**(2.2·Cl)**$]^-$ with TEACl using a) a standard 1:1 binding equation and b) a competitive binding equation. The underlying measurements were carried out in dichloromethane at 295 K.

2.8.6 ^{13}C NMR

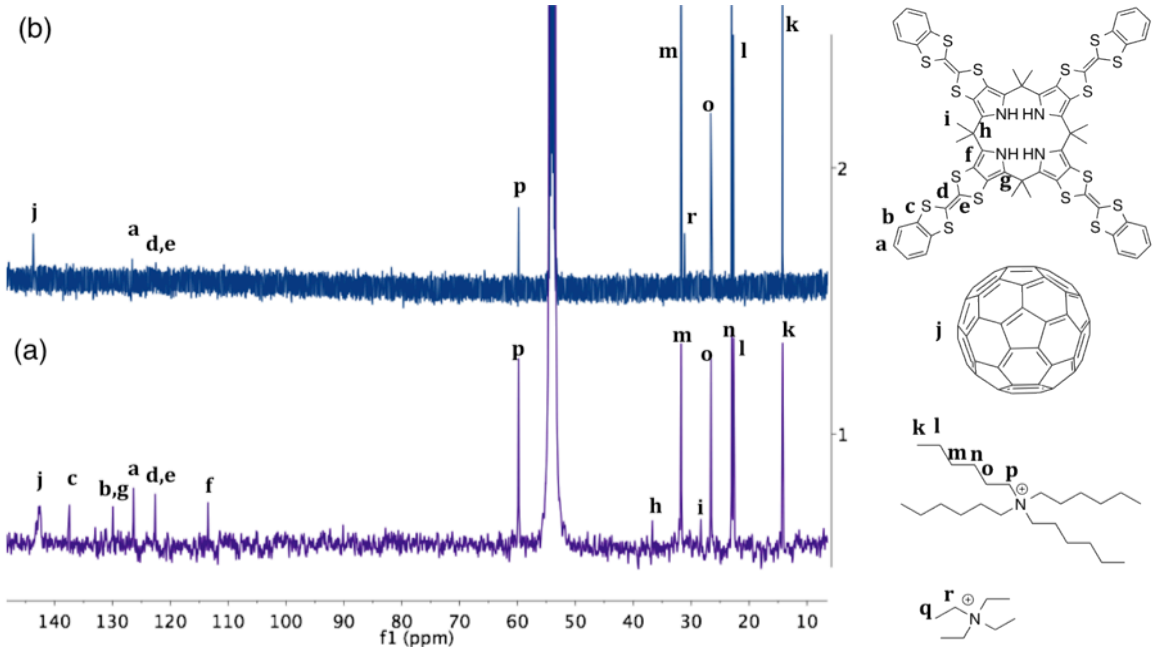

Figure 2.21 (a) ^{13}C NMR spectrum for a deuterated dichloromethane solution of **2.2** (0.5 mM), tetrahexylammonium chloride (THACl, 1.5 mM), and C_{60} (1.0 mM) recorded at room temperature. The signal for C_{60} is rather broad, presumably reflecting its being bound within the "bowl" present within the cone conformer of **2.2**. (b) ^{13}C NMR spectrum for a deuterated dichloromethane solution of **2.2** (0.5 mM), tetrahexylammonium chloride (THACl, 1.5 mM) and C_{60} (1.0 mM) recorded after the addition of a solution of tetraethylammonium chloride (TEACl, 1.0 mM) in deuterated dichloromethane at room temperature. The signals for **2.2** become less intense while those for C_{60} become sharper. These spectral changes are ascribed to the lowered solubility and precipitation of the TEA^+ complex of **2.2** and the concurrent release of C_{60} via competitive decomplexation from **2.2**.

2.9 CHAPTER 2 REFERENCES

1. Tsai, C.-J.; del Sol, A.; Nussinov, R. *J. Mol. Biol.* **2008**, *378*, 1-11.
2. Peracchi, A.; Mozzarelli, A. *Biochim. Biophys. Acta* **2011**, *1814*, 922-33.
3. Tompa, P. *Chem. Rev.* **2014**, *114*, 6715-6732.
4. Kremer, C.; Lützen, A. *Chem. Eur. J.* **2013**, *19*, 6162-6196.
5. Berg, J. M.; Tymoczko, J. L.; Stryer, L. *Biochemistry*. 6 ed.; W. H. Freeman and Company: USA, 2007.
6. Takeuchi, M.; Ikeda, M.; Sugasaki, A.; Shinkai, S. *Acc. Chem. Res.* **2001**, *34*, 865-873.
7. Fritsky, I. O.; Ott, R.; Krämer, R. *Angew. Chem. Int. Ed.* **2000**, *39* (18), 3255-3258.
8. Rebek, J.; Wattley, R. V. *J. Am. Chem. Soc.* **1980**, *102*, 4853-4854.
9. Rebek, J.; Costello, T.; Wattley, R. *J. Am. Chem. Soc.* **1985**, *107*, 7487-7493.
10. Traylor, T. G.; Mitchell, M. J.; Ciccone, J. P.; Nelson, S. *J. Am. Chem. Soc.* **1982**, *104*, 4986-4989.
11. Kubik, S. *J. Am. Chem. Soc.* **1999**, *121*, 5846-5855.
12. Nabeshima, T.; Hashiguchi, A.; Yazawa, S.; Haruyama, T.; Yano, Y. *J. Org. Chem.* **1998**, *63*, 2788-2789.
13. Wang, F.; Schwabacher, A. W. *J. Org. Chem.* **1999**, *64*, 8922-8928.
14. Beer, P. D.; Rothin, A. S. *J. Chem. Soc., Chem. Comm.* **1988**, 52-54.
15. Schneider, H.-J.; Werner, F. *J. Chem. Soc., Chem. Comm.* **1992**, 490-491.
16. Nabeshima, T. *Coord. Chem. Rev.* **1996**, *148*, 151-169.
17. Costero, A. M.; Rodriguez, S. *Tetrahedron* **1992**, *48*, 6265-6272.
18. Pierre, J.-L.; Gagnaire, G.; Chautemps, P. *Tetrahedron Lett.* **1992**, *33*, 217-220.
19. Kovbasyuk, L.; Krämer, R. *Chem. Rev.* **2004**, *104*, 3161-3188.
20. Park, J. S.; Karnas, E.; Ohkubo, K.; Chen, P.; Kadish, K. M.; Fukuzumi, S.; Bielawski, C. W.; Hudnall, T. W.; Lynch, V. M.; Sessler, J. L. *Science* **2010**, *329*, 1324-1327.
21. Fukuzumi, S.; Ohkubo, K.; Kawashima, Y.; Kim, D. S.; Park, J. S.; Jana, A.; Lynch, V. M.; Kim, D.; Sessler, J. L. *J. Am. Chem. Soc.* **2011**, *133*, 15938-15941.
22. Park, J. S.; Le Derf, F.; Bejger, C. M.; Lynch, V. M.; Sessler, J. L.; Nielsen, K. A.; Johnsen, C.; Jeppesen, J. O. *Chem. Eur. J.* **2010**, *16*, 848-854.
23. Nielsen, K. A.; Cho, W.-S.; Sarova, G. H.; Petersen, B. M.; Bond, A. D.; Becher, J.; Jensen, F.; Guldi, D. M.; Sessler, J. L.; Jeppesen, J. O. *Angew. Chem. Int. Ed.* **2006**, *45*, 6848-6853.
24. Nielsen, K. A.; Martín-Gomez, L.; Sarova, G. H.; Sanguinet, L.; Gross, D. E.; Fernández-Lázaro, F.; Stein, P. C.; Levillain, E.; Sessler, J. L.; Guldi, D. M.; Sastre-Santos, Á.; Jeppesen, J. O. *Tetrahedron* **2008**, *64*, 8449-8463.
25. Steed, J. W.; Atwood, J. L. *Supramolecular Chemistry, Second Edition*. John Wiley & Sons, Ltd.: 2009.

26. Connors, K. A. *Binding Constants: The Measurement of Molecular Complex Stability*. John Wiley & Sons, Inc.: 1987.
27. Gale, P. A.; Sessler, J. L.; Král, V.; Lynch, V. *J. Am. Chem. Soc.* **1996**, *118*, 5140-5141.
28. Guldi, D. M.; Prato, M. *Acc. Chem. Res.* **2000**, *33*, 695-703.
29. Crystal Clear 1.40, R. A. C., The Woodlands, Tx; 2008. DENZO-SMN. Otwinowski, Z.; Minor, W. Methods in Enzymology, 276: Macromolcular Crystallography, part A. 307-326, C. W. Carter, Jr. and R. M. Sweets, Editors, Academic Press; 1997.
30. Sheldrick, G. M. *SHELXL97. Program for the Refinement of Crystal Structures. University of Gottingen, Germany. 1994.*
31. Sheldrick, G. M. *SHELXTL/PC (Version 5.03). Siemens Analytical X-ray Insruments, Inc., Madison Wisconsin, USA; 1994.*

Chapter 3

Photoinduced Electron Transfer from a Tetrathiafulvalene Calix[4]pyrrole to a Porphyrin Carboxylate within a Supramolecular Ensemble

3.1 INTRODUCTION*

Over the last decade the need for clean renewable resources has become increasingly apparent. As green house levels continue to rise, there has been considerable scientific effort put towards developing artificial photosynthetic systems capable of converting light energy into chemical energy.[1-3] These systems are expected to release lower levels of greenhouse gasses, such as carbon dioxide, upon energy conversion than those that rely on fossil fuels.[1-3] Organic solar cells (OSCs) are artificial photosynthetic devices that convert solar energy to chemical energy by exploiting a potential difference created from electron transfer through a medium upon photon absoprtion.[3-5] The current shift towards using organic materials in solar cells is motivated by the increased structure flexibility allowed by organic compounds relative to over silicon based materials, as well as the lowered cost predicted for production.[6] OSCs are prepared through a technique that involves the use of active p-type (electron donor) and n-type (electron acceptor) materials layered between two electrodes.[3] Some of the most common OSC consist of substituted

* Parts of this chapter were taken with permission from Davis, C. M.; Kawashima, Y.; Ohkubo, K.; Lim, J. M.; Kim, D.; Fukuzumi, S.; Sessler, J. L. *J. Phys. Chem. C*. **2014**, *118*, 13503-13513. Copyright 2014 American Chemical Society. Photophysical studies were performed by YO, JML, and YK. ESR measurements were performed by CMD with the help of KO and YK. DFT calculations were done by KO and JML. All other data were collected by CMD. The first draft of this paper was written by CMD. The final polishing was performed by SF and JLS.

fullerenes as n-type moieties and conjugated polymers as p-type layers.[3] To date, the most efficient OSC, developed by Heliatek, has a 12% efficiency for energy conversion for a standard 1.1 cm^2 cell composed of oligomers and two patented absorbing materials.[7]

The steps involved in the conversion of solar energy to chemical energy include:

1. Formation of an exciton upon photon absorption
2. Separation and diffusion of the exciton to the interface between the donor and acceptor
3. Transport of the electron and hole to their respective electrodes
4. Collection of the charge

To increase further the energy conversion by OSCs, the efficiency of all of these steps must be improved. Our research has focused on ways to increase the lifetime of the charge-separated (CS) state produced upon photoirradiation by using systems that undergo electron transfer (ET) within noncovalently bound ensembles upon such photoirradiation. To mimic natural photosynthetic systems, the rate of forward ET, which leads to the production of chemical energy, must be faster than the rate of back ET (et. Chapter 1 of this dissertation).[2,8,9] However, controlling the rates of ET to create a long-lived CS state has proven difficult in artificial systems. Developing a simple two-component system, or molecular dyad, that undergoes rapid forward electron transfer and results in a long lifetime could represent an important step forward in the search for OSCs that enable efficient solar energy conversion.

In recent years there has been tremendous progress towards increasing the lifetime of CS states; however, this goal remains to be achieved in a simple and cost effective manner.[1,10-13] One approach that has particular promise is using self-assembled or noncovalent systems. In principle, the electronics of the system components can be

individually tuned. This would reduce the synthetic investment needed for obtaining a functioning charge-separating dyad.[14-31]

In the past few decades ET complexes that contain tetrathiafulvalene (TTF) moieties and their derivatives have received considerable attention due to the stability of the TTF radical cation and dication upon the first and second oxidation, respectively.[32] The first and second oxidation potentials of TTF can be fine-tuned by altering the substituents on the backbone.[32] As discussed in Chapter 1, TTF derivatives paired with suitable acceptors have been exploited for many purposes, including for the preparation of non-linear optical arrays,[33] controlled self-assembled nanostructures,[34] and light harvesting complexes.[35] Calix[4]pyrroles bearing TTF subunits, first reported in 2004,[36] have since been used as colorimetric chemosensors[37] as well as in switchable thermal ET systems.[38,39,40] Work by Sessler[41,42] and Jeppesen[43,44] resulted in the development of porphyrin derivatives with directly annulated TTF subunits. One such porphyrin has a 1,3-dithio-2-ylidene moiety across the core to produce what is known as a π-extended TTF.[45] This porphyrin has redox properties that are easily modulated through anion binding to the metalated core of the porphyrin. With the use of a proper anion, such as chloride, the TTF-fused porphyrin undergoes thermal electron transfer to electron deficient moieties such a Li^+ endofullerene ($Li^+ \subset C_{60}$).

These prior studies provided an incentive to investigate pairing TTF conjugates with porphyrins in systems that would undergo photoinduced ET rather than thermal ET. The first component of the system was chosen to be a TTF calix[4]pyrrole since the anion binding ability of these macrocycles in aprotic organic solvents are well recognized. For the second component of the dyad, a porphyrin bearing a carboxylate moiety was chosen since, based on previous results, it was expected to partake in anion binding to the calix[4]pyrrole.[46] For the counter cation, tetraethylammonium (TEA^+) was chosen as it is

known to bind inside the bowl-shaped cavity of the calix[4]pyrrole when in the cone conformation.[40,47,48] The dual binding of the TEA^+ and the carboxylate to the calix[4]pyrrole was employed to enhance the interaction between the two moieties of the dyad. By using a supramolecular assembly of this nature, the donor and acceptor components could be pre-organized in solution before photoirradiation. This preorganization, in turn, was expected to translate into facilitated photoinduced ET.

This Chapter describes the formation of a supramolecular complex (**3.4**) consisting of benzo-annulated TTF calix[4]pyrrole **3.1** as an electron donor with porphyrin **3.2** as an electron acceptor (Figure 3.1). This system is unique in that a porphyrin acts as the final electron acceptor. Though porphyrins have been demonstrated to act as efficient light absorption species and have been found to be efficient electron acceptors in a number of instance,[49-58] assemblies in which the final electron acceptor is a neutral, free-base porphyrin are essentially unknown.

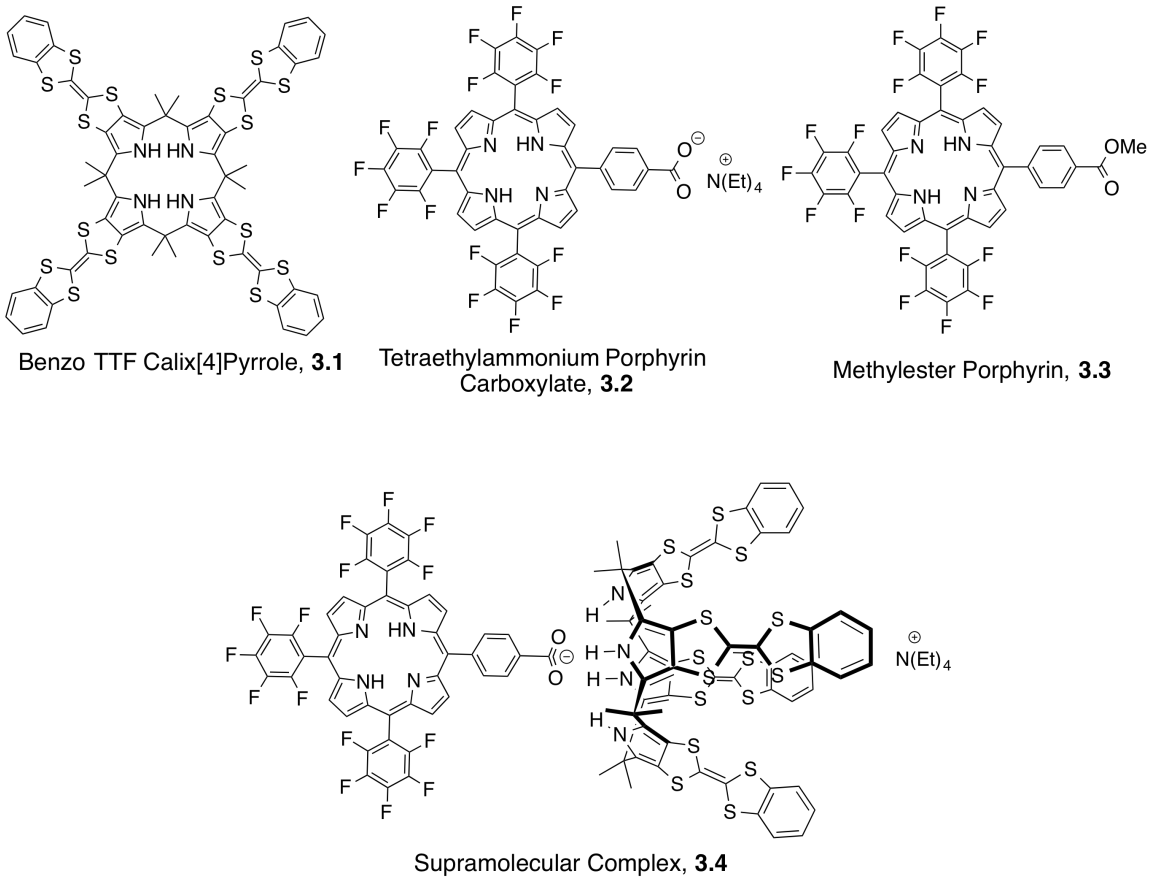

Figure 3.1 Structures of benzo-TTF-calix[4]pyrrole (**3.1**), tetraethylammonium porphyrin carboxylate (**3.2**), the methyl ester analogue (**3.3**), and the supramolecular ensemble produced between **3.1** and **3.2** (complex **3.4**).

The properties of complex **3.4** were studied using UV-Vis, fluorescence, phosphorescence, electron spin resonance (ESR), and ^{1}H NMR spectroscopy, as well as electrochemical analysis via cyclic voltammetry (CV) and differential pulse volatmmetry (DPV), density functional theory (DFT), isothermal titration calorimetry (ITC), and femto- and nanosecond laser flash photolysis. To the best of our knowledge, the CS state produced as the result of photoinduced ET has the longest lifetime yet reported for any noncovalently bound dyad analyzed in solution at 298 K. Support for this statement is given further on in this chapter.

3.2 UV-Vis-NIR Absorption Spectral Measurements and Binding Affinity Determination

The absorption spectra of the three species of interest, **3.1**, **3.2**, and **3.3** were recorded in benzonitrile (PhCN) at 298 K. Since the porphyrins **3.2** and **3.3** differ only in their carboxylate functionality, the absorption spectra are extremely similar. The Soret bands, an absorption feature arising from the allowed π–*to*–π* transition from the second highest occupied to the lowest unoccupied molecular orbital are essentially identical as seen in Figure 3.2.[59] The same is true for the Q-bands, an absorption originating in the forbidden π–π* transition from the highest occupied to the lowest unoccupied molecular orbital,[59]

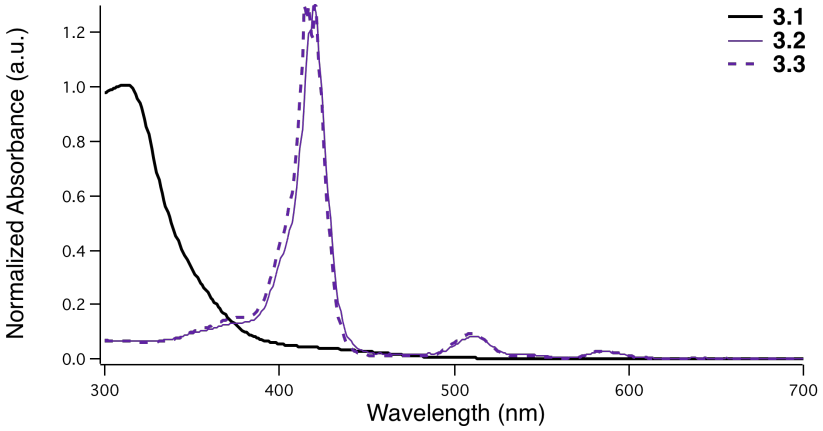

Figure 3.2 Normalized absorbance of **3.1** (black), **3.2** (purple solid), and **3.3** (purple dotted) recorded in PhCN at 298 K.

To determine the absorption spectra of complex **3.4**, UV-Vis titrations were performed. These titrations consisted of adding a concentrated solution of **3.1** to a solution of **3.2** in PhCN. It is well known that the intensity of spectral changes produced upon the titration of one species into another can be correlated to the interaction between the two species and, therefore, the formation of the complex.[60] By plotting the change of

the spectral feature of **3.2** upon addition of **3.1** versus concentration of **3.1** a binding constant can be calculated for the interaction of the these two components to form complex **3.4**. Figure 3.3 depicts the changes in absorption of a solution of **3.2** (50 μM in PhCN) observed upon addition of **3.1**.

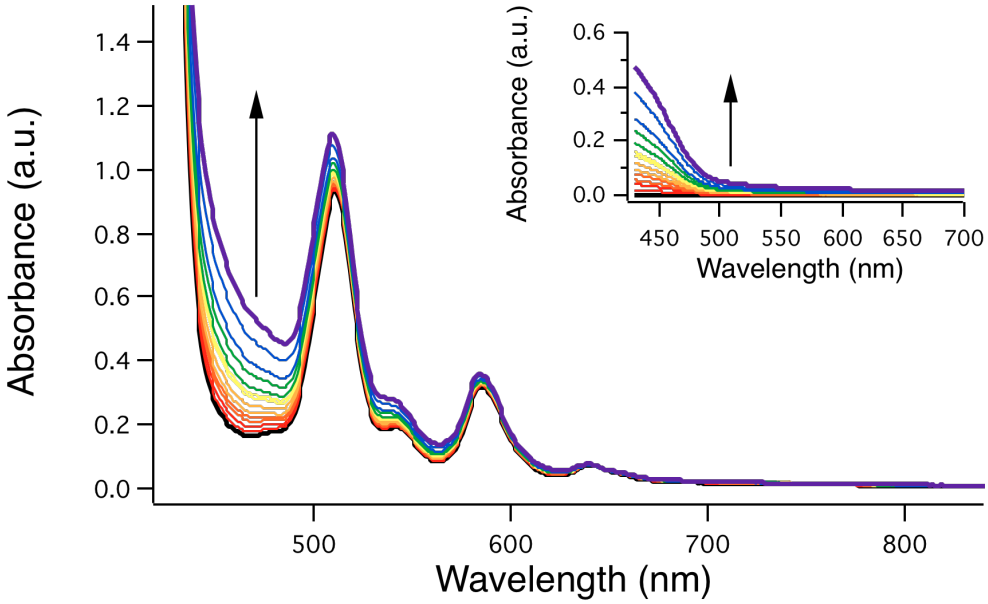

Figure 3.3 Absorption spectra of **3.2** (50 μM) upon the addition of 0 to 5 equiv of **3.1** at 298 K in PhCN. Inset: Absorption of **3.1** as its concentration increases from 0 to 0.25 mM in PhCN at 298 K.

Upon addition of **3.1** to **3.2**, the most notable spectral changes occur between 400 and 700 nm. It is noteworthy that there is no evidence of a charge transfer (CT) band, expected to appear around 700 nm, upon this addition. This absence is consistent with the lack of an appreciable electronic interaction between these species in the ground state. To determine the binding affinity for the carboxylate moiety of **3.2** for the NH protons of **3.1**, the changes in absorption at 585 nm were plotted as a function of concentration of **3.1**. The absorbance at 585 nm was chosen due to the minimal absorbance of **3.1** at this

wavelength. However, **3.1** does absorb minimally at this wavelength. Therefore, the absorbance of the calix[4]pyrrole at each indicated concentration was subtracted from the absorbance of the mixture at 585 nm. This correction allowed us to monitor quantitatively the absorbance changes that are solely due to binding events.

As a control, this titration analysis was also performed using **3.3** in place of **3.2**. Porphyrin **3.3** should not show any appreciable binding interaction with **3.1** due to the lack of anionic functionality needed for binding to the NH protons of the calix[4]pyrrole. The data for both titrations are plotted in Figure 3.4

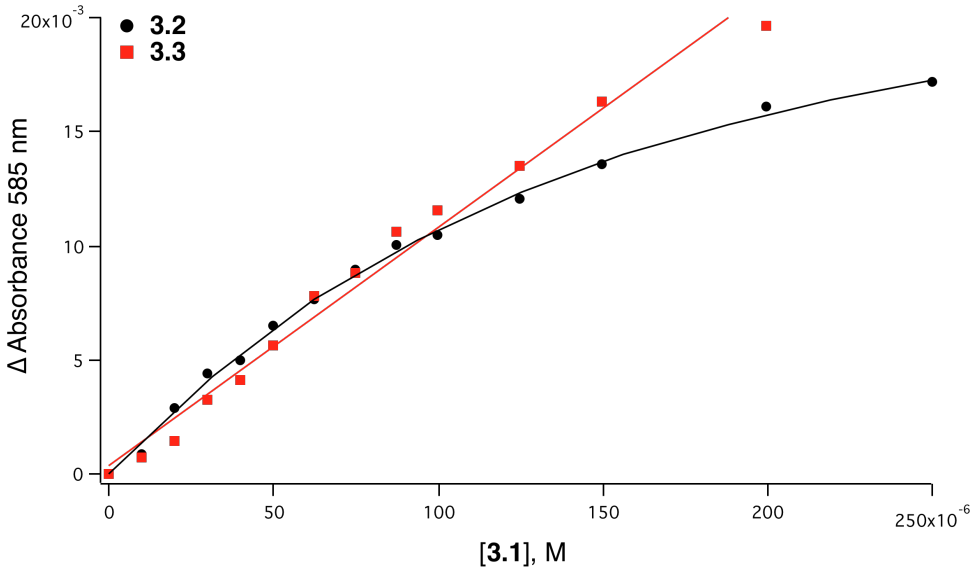

Figure 3.4 Change in absorption of **3.2** (black dot) and **3.3** (red square) at 585 nm seen upon addition of **3.1** in PhCN at 298 K. The absorption of **3.1** at each specified concentration has been subtracted as noted in the text.

As expected, the addition of **3.1** to **3.3** produced a change in absorption that was linear with respect to [**3.1**]. This is consistent with little appreciable interaction between the two species. On the other hand, porphyrin **3.2** showed saturation behavior, a feature

considered diagnostic of binding.[60] The formation constant for complex **3.4** was calculated using the following equations:

$$(\alpha^{-1} - 1)^{-1} = K([\mathbf{3.1}] - \alpha[\mathbf{3.2}]_0) \qquad (eqn.\ 3.1)$$

$$\alpha = (A - A_0)/(A_\infty - A_0) \qquad (eqn.\ 3.2)$$

wherein A is the absorbance at a given concentration, A_0 is the initial absorbance, A_∞ is the estimated absorbance under conditions of complete binding saturation, and K is the association constant. This analysis yielded a linear plot (Figure 3.5) which allowed for the determination of the association constant K,[61] which was found to be 1.1×10^4 M^{-1}. However, since the absorption of **3.1** and **3.2** overlap, this binding constant may have a large experimental error even after making a correction for the spectral overlap.

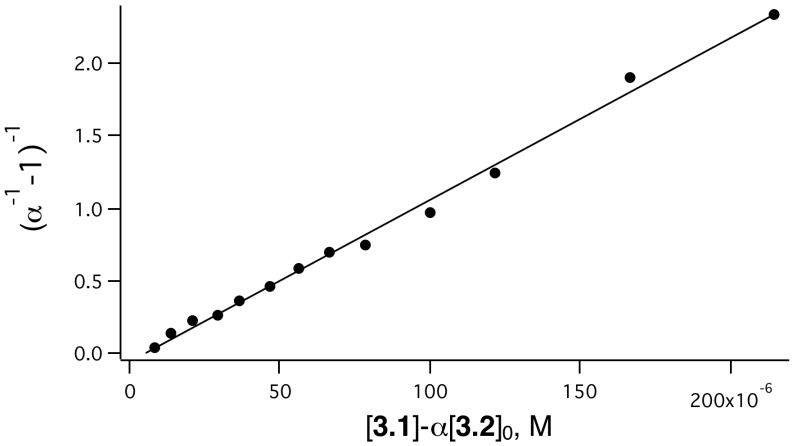

Figure 3.5 Linear plot used to determine binding constant (K_a) corresponding to the interaction of **3.1** with **3.2**. This plot is based on the observed changes in absorption as detailed in the text. The slope (K_a) is 11,000 ± 240 with an R^2 value of 0.99484. (Note: A_∞ was set to 2.45×10^{-2}; see text for definitions.)

To acquire a better indication of the formation constant of complex **3.4**, isothermal titration calorimetry (ITC) was performed in PhCN (Figure 3.6). For the ITC

titration, a 5 mM solution of **3.2** was titrated into a 0.5 mM solution of **3.1** in PhCN at 298 K. Using this technique, the binding constant corresponding to the interaction between **3.1** and **3.2** was found to be 6.3×10^4 M^{-1} with 6% error between runs. ITC also gave the Gibbs free energy, ΔG, of the binding event as –6.6 kcal·mol^{-1}, a value reflecting a thermodynamically favorable binding event. The enthalpy of binding, ΔH, was found to be −2.8 kcal·mol^{-1}, while the entropy of binding, ΔS, was found to be 13 cal·K^{-1}·mol^{-1}. Under the same conditions, porphyrin **3.2** showed no binding interaction with **3.1**.

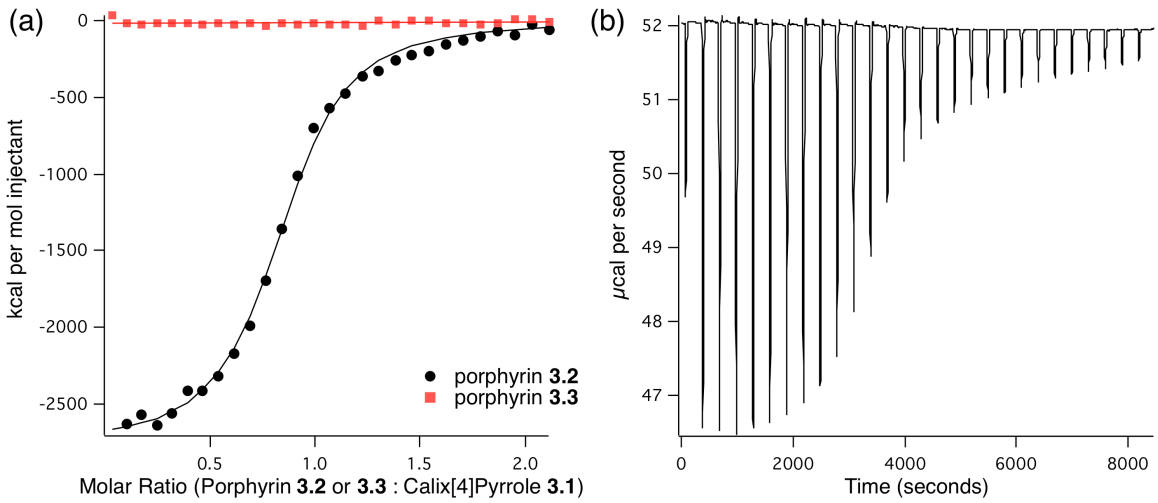

Figure 3.6 Isothermal titration calorimetry data for the addition of porphyrin **3.2** (5 mM, black dots) and porphyrin **3.3** (5 mM, red squares) into a PhCN solution of calix[4]pyrrole **3.1** (0.5 mM) at 298 K. The data are plotted as molar ratio vs µcal per second. Fitting the data for the interaction of porphyrin **3.2** with **3.1** to a 1:1 binding profile gave an association constant of $(6.3 \pm 0.5) \times 10^4$ M^{-1} in PhCN at 298 K. For the interaction of **3.2** with **3.1**, the energy values given by the fit were ΔG = −6.6 kcal·mol^{-1}, ΔH = −2.8 kcal·mol^{-1}, ΔS = 13 cal·K^{-1}·mol^{-1} in PhCN at 298 K. No evidence of binding was seen for the interaction of porphyrin **3.3** with **3.1**. (b) Raw ITC data for the addition of porphyrin **3.2** (5 mM) into a PhCN solution of calix[4]pyrrole **3.1** (0.5 mM) at 298 K. The data are plotted as µcal per second versus time.

To confirm further the binding interaction between **3.1** and **3.2** was between the carboxylate moiety of the porphyrin and the NH protons of the calix[4]pyrrole, ^{1}H NMR spectra were collected. The spectral changes seen in Figure 3.7 support the conclusion that anion binding is taking place between the suspected moieties of the complex. The NH proton shifts downfield which indicates its proximity to an anionic species and the increased shielding of the protons concurrently the proton signals corresponding tetraethylammonium counter cation to the carboxylate porphyrin anion shift upfield. This is as expected for the formation of a complex wherein the small tetraalkylammonium cation is bound within the cavity of the calix[4]pyrrole.

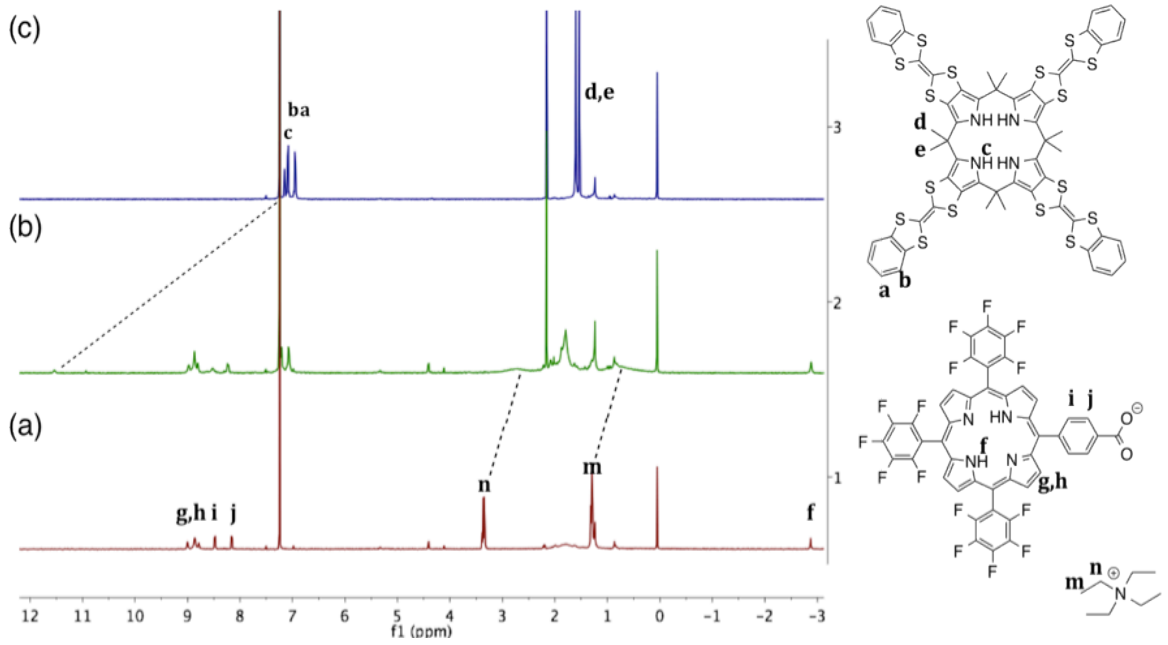

Figure 3.7 ^{1}H NMR spectra for (a) tetraethylammonium porphyrin carboxylate **3.2** (2.5 mM), (b) a 1:1 mixture of **3.1** and **3.2**, each at 2.5 mM, (c) calix[4]pyrrole **3.1** (2.5 mM). All spectra were recorded at 298 K in deuterated chloroform.

ET from a TTF moiety of **3.1** to the porphyrin core of **3.2** within complex **3.4** is expected to produce the radical species $\mathbf{3.1}^{\bullet+}$ and $\mathbf{3.2}^{\bullet-}$, respectively. To have spectra for

the purposes of comparison, chemical oxidations of each species were carried out in PhCN. The oxidant tris(4-bromophenyl)aminium hexachloridoantimonate, also known as "magic blue," was used to generate the radical cation **3.1**$^{\bullet+}$. Titration of **3.1** with up to 1 equiv of "magic blue" produced the spectral changes shown in Figure 3.8a. The emergence of absorption features at 430, 620, and 930 nm following oxidation of **3.1** is fully consistent with the oxidation of TTF to TTF$^{\bullet+}$.[38] Naphthalene radical anion was used to reduce porphyrin **3.2** chemically. The naphthalene radical anion was prepared in deoxygenated, anhydrous tetrahydrofuran (THF) following a literature procedure.[62] The UV spectrum for the titration of **3.2** with the naphthalene radical anion is shown in Figure 3.8b. The absorbance bands for the porphyrin radical anion **3.2**$^{\bullet-}$ are centered at 570, 618, and 850 nm. These spectral features produced from the chemical oxidation and reduction of **3.1** and **3.2**, respectively, provide important benchmarks for the identification of radical species formed under conditions of photoinduced ET.

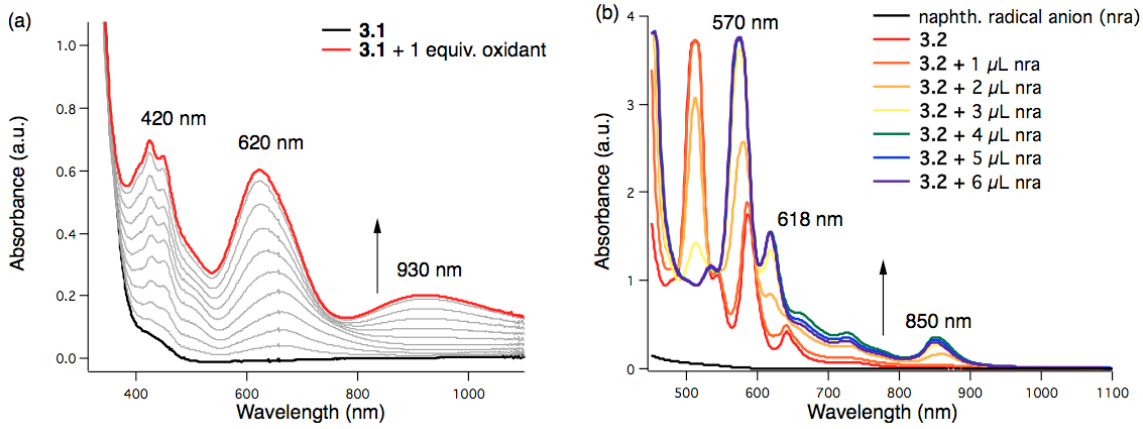

Figure 3.8. (a) Titration of **3.1** (50 mM, black line) with up to 1 equivalent of the chemical oxidant "magic blue" (final spectrum shown with a red line) at 298 K in benzonitrile. (b) Titration of **3.2** (0.3 mM, benzonitrile) with the naphthalene radical anion at 298 K.

3.3 Density Functional Theory Calculations

We considered it important to determine whether photoinduced electron transfer was possible within the supramolecular ensemble **3.4** and therefore performed theoretical calculations were performed. To determine the electronic structure of the complex, density functional theory (DFT) calculations were carried out on the optimized structure for complex **3.4** (Figure 3.10). The calculations indicate that the highest occupied molecular orbital (HOMO) is located on a tetrathiafulvalene moiety of calixpyrrole **3.1** while the lowest unoccupied molecular orbital (LUMO) is located on the porphyrin core of **3.2** (Figure 3.9).

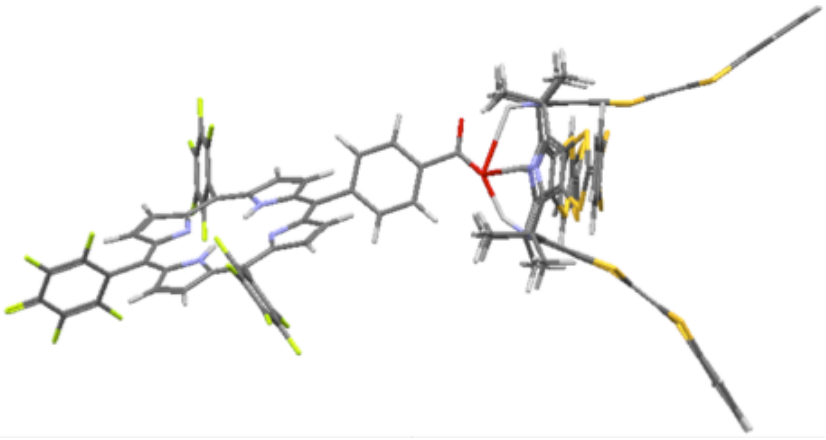

Figure 3.9 Optimized structure of complex **3.4** formed from **3.1** and **3.2** as calculated using density functional theory at the B3LYP/6-31G(d) level.

These results support the proposal that photoinduced ET from the electron rich TTF moiety to the electron deficient porphyrin upon photoexcitation will occur. The DFT studies also reveal little overlap of the HOMOs and LUMOs within complex **3.4**. This reduced overlap is reflected in a small electronic coupling constant, denoted as *V* in the Marcus theory equations, and is predictive of a long lived charge separation.[27]

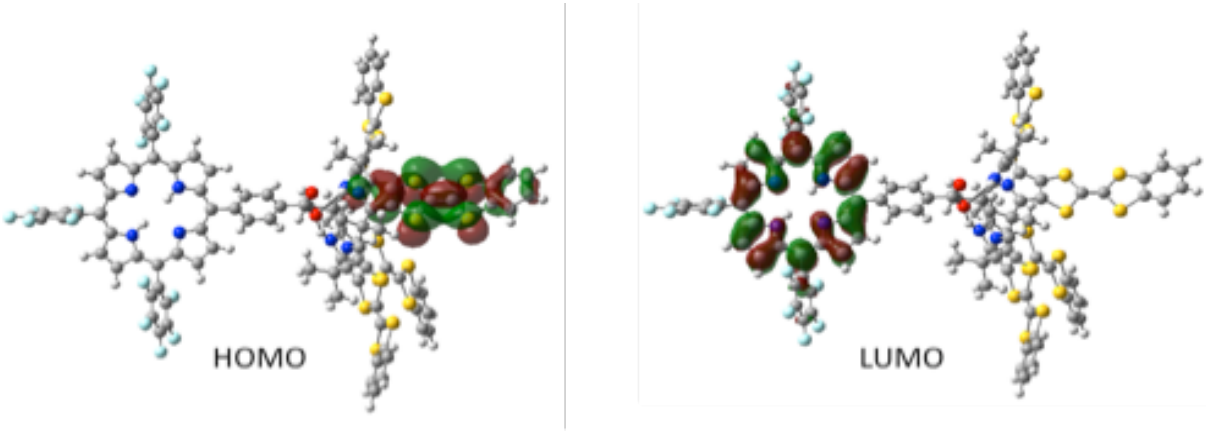

Figure 3.10 HOMO and LUMO of the optimized supramolecular ensemble formed upon mixing **3.1** and **3.2** to form complex **3.4**, as calculated by density functional theory at the B3LYP/6-31G(d) level.

3.4 Electrochemical Measurements

Electrochemical measurements were carried out with a view to determine the oxidation-reduction potentials for **3.1**, **3.2**, and complex **3.4**. Cyclic voltammetric (CV) analysis of **3.2** (0.3 mM), **3.1** (0.3 mM), and a mixture of **3.1** and **3.2** (0.5 mM and 0.1 mM, respectively) were performed in PhCN using 0.1 M tetra-*n*-butylammonium hexafluorophosphate ($TBAPF_6$) as the supporting electrolyte, platinum as the working electrode, a platinum wire as the counter electrode, and $Ag/AgNO_3$ as the reference electrode (Figure 3.11). Table 3.1 lists the CV half wave potentials for the three solutions subject to analysis.

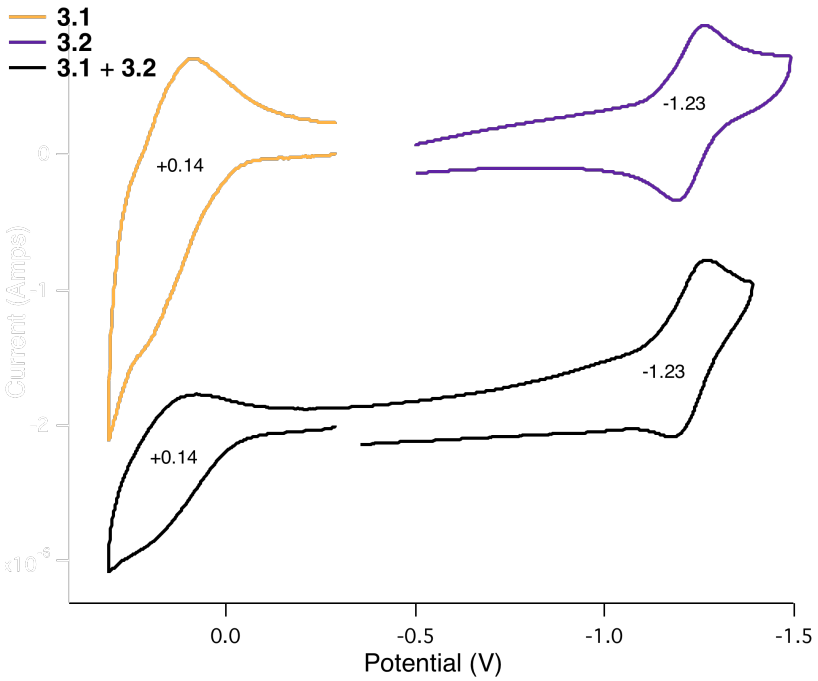

Figure 3.11 Cyclic voltammograms for **3.1** (a) (0.5 mM), (b) **3.2** (0.3 mM), and (c) complex **3.4** as produced from **3.1** (0.5 mM) and **3.2** (0.3 mM) recorded in PhCN using 0.1 M tetra-*n*-butylammonium hexafluorophosphate as the electrolyte. The reference electrode was $Ag/AgNO_3$, the working electrode was Pt, and the counter electrode was a Pt wire.

There is no noticeable difference between the oxidation potential of **3.1** and that of **3.4**. The same is true for the reduction of **3.2** and **3.4**. These findings support the suggestion that there is little interaction between the two components in **3.4** in the ground electronic state. The redox values obtained by CV measurements were used in equation 3.3 (wherein E_{ox} is the first one-electron oxidation potential, E_{red} is the first one-electron reduction potential, and e is the elementary charge) to calculate the CS state energy (E_{CS}) between **3.1** and **3.3** in complex **3.4**. This value was found to be 1.37 eV.

$$E_{CS} = e(E_{ox} - E_{red}) \qquad (eqn.\ 3.3)$$

Table 3.1 First One-Electron Oxidation and Reduction Potentials in PhCN as Determined by CV (V vs $Ag/AgNO_3$).

	E_{ox} (V)	E_{red} (V)
3.1 (0.5 mM)	+0.14	—
3.2 (0.3 mM)	+1.09	−1.23
3.1 (0.5 mM) + **3.2** (0.3 mM)	+0.14	−1.23

Since there was found to be no appreciable interaction of the two components in complex **3.4** in the ground state, the next step was to probe the excited states to determine if ET could occur upon photoexcitation.

3.5 Fluorescence Lifetime and Phosphorescence Measurements

To investigate whether ET was occurring from **3.1** to **3.2** via the singlet or triplet excited state of porphyrin **3.2**, the fluorescence lifetime of porphyrin **3.2** was studied. The fluorescence spectrum of porphyrin **3.2** in PhCN at room temperature is shown in Figure 3.12a. Since fluorescence is a feature of the decay of an electron from the singlet-excited state to the ground state, differences in the fluorescence lifetimes of **3.2** recorded in the presence and absence of **3.1** would indicate an electronic interaction within the singlet excited state of the porphyrin. For the lifetime measurements, the fluorescence at 710 nm was studied. The lifetime of **3.2** alone in PhCN was found to be 13.4 ns. A mixture of **3.1** and **3.2** in PhCN was found to have the same fluorescence lifetime (Figure 3.12b). This is taken as evidence that ET occurs from the triplet excited state (^{3}**3.2***) as opposed to the singlet excited state (^{1}**3.2***). If the singlet excited state were involved, the fluorescence lifetime and/or intensity of the fluorescence of **3.2** in the presence of **3.1** would be expected to be shorter/less than that of **3.2** in its absence.

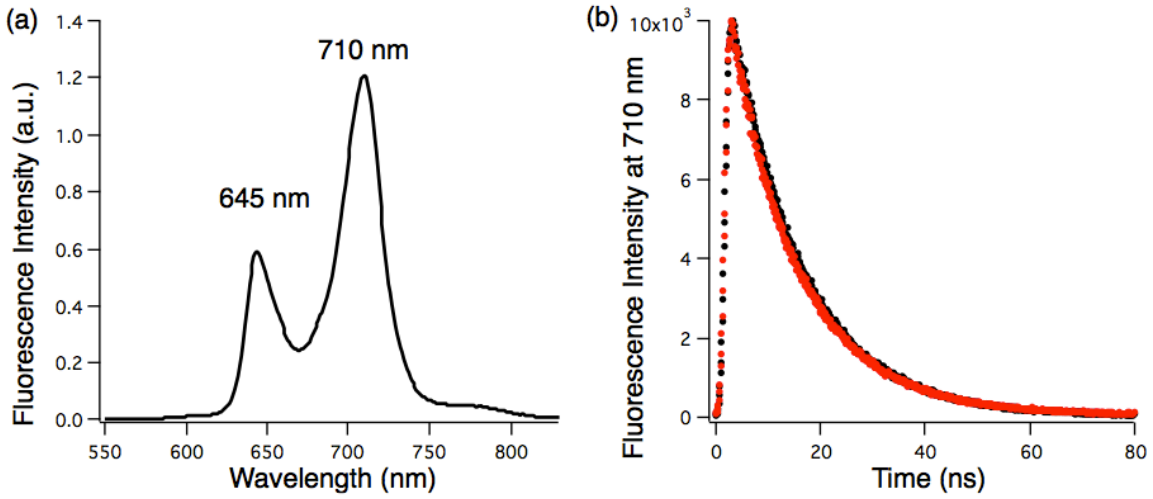

Figure 3.12 (a) Fluorescence spectrum of **3.2** (15 μM) recorded in PhCN at 298 K; excitation wavelength: 510 nm. (b) Fluorescence decay profiles of the singlet-excited state of **3.2** (^{1}**3.2***) observed upon excitation at 485 nm in the absence (black) and presence of **3.1** (0.5 mM) (red) in deoxygenated PhCN containing **3.2** (0.3 mM).

The absorbance maximum (640 nm, Figure 3.2) and fluorescence maximum (645 nm, Figure 3.12a) of **3.2** were used to determine the singlet energy level (E_S) of the porphyrin; using equation 3.4, the value was determined to be 1.93 eV.

$$E_S = ½[hc/\lambda_{Abs}) + (hc/\lambda_{Fl})] \qquad (eqn.\ 3.4)$$

In equation 3.4, λ_{Abs} is the longest wavelength of absorbance, λ_{Fl} is the shortest wavelength of fluorescence, h is Planck's constant, and c is the speed of light.

Since no evidence of an appreciable interaction in the singlet-excited state was found, interactions within the triplet state were investigated. The triplet energy level was determined from the phosphorescence of porphyrin **3.2**, recorded upon excitation at 435 nm in a mixture of ethyl iodide (EtI) and 2-methyltetrahydrofuran (2-MeTHF) in about a 1:1 ratio at 77 K. The phosphorescence of **3.2** was weak and required a large ratio of EtI to 2-MeTHF to utilize the heavy atom effect and increase the yield of intersystem

crossing to the triplet state. Free-base tetraphenylporphyrin derivatives, however, are known to have weak triplet emission and, therefore, low phosphorescence quantum yields.[63,64] Using equation 3.5 in which λ_{Phos} is the phosphorescence maximum, at 813 nm (Figure 3.13), the triplet excited state energy level was found to be 1.53 eV. This is a reasonable value for tetraphenylporphyrins. [63,64]

$$E=hc/\lambda_{Phos} \qquad (eqn.\ 3.5)$$

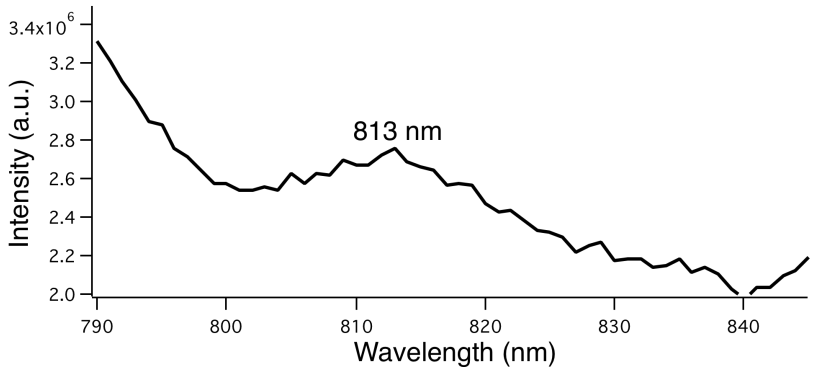

Figure 3.13 Phosphorescence spectrum of **3.2** recorded in a solution of ethyl iodide and 2-methyltetrahydrofuran in a 1:1 ratio, a mixture that was used to form a transparent glass upon cooling to $T = 77$ K. Measurements were made at this temperature via excitation at 435 nm.

Using the values obtained from equations 3.3, 3.4, and 3.5 for the CS state energy (1.37 eV), singlet excited state energy (1.93 eV), and triplet excited state energy (1.53 eV), respectively, an energy diagram was generated depicting the energetics associated with the expected ET pathway (Figure 3.14). This figure illustrates both the *inter*- and *intra*molecular ET pathways that could occur within complex **3.4** upon photoexcitation.

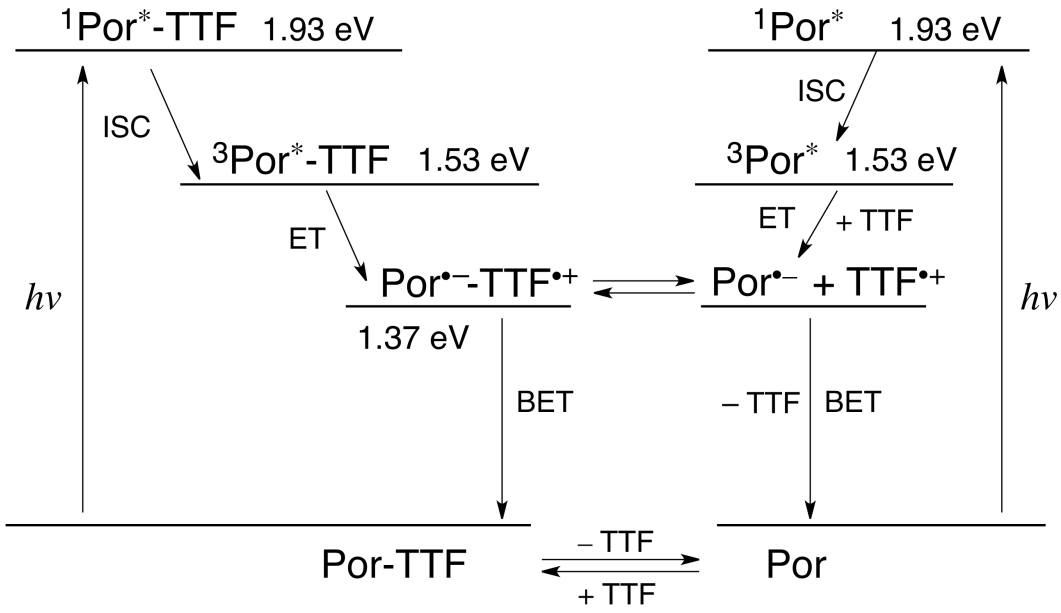

Figure 3.14 Energy diagram for the proposed photodynamics of the supramolecular complex (**3.4**, Por-TTF) formed between **3.1** (TTF) and **3.2** (Por) in PhCN. Photoinduced charge separation via *intra*molecular process (left panel) and *inter*molecular process (right panel).

After determining the energy levels for the species believed to be involved in the ET within complex **3.4**, the next step was to analyze the excited states of the complex. This was done using laser flash photolysis methods.

3.6 Femtosecond Laser Flash Photolysis Measurements

Femtosecond laser flash photolysis measurements, used to study singlet-excited states, were used to record the absorption spectra of ensemble **3.4**. More specifically, in order to analyze the ET expected to occur from a TTF moiety of **3.1** to the porphyrin **3.2** upon photoirradiation, the transient spectra of **3.2** were recorded. Upon photoexcitation at 400 nm, the porphyrin was promoted to the singlet-excited state ^{1}**3.2***. This excitation resulted in an increase in absorption at 620 nm and 670 nm in deoxygenated PhCN at 298

K as seen in Figure 3.15. The rate of intersystem crossing (k_{ISC}) was determined from a single exponential analysis for the decay of ^{1}**3.2***, found to be 3.3×10^8 sec^{-1}. Irradiation of **3.1** under the same conditions resulted in absorbance features at 620 and 834 nm that diminished with a decay rate of 1.6×10^9 sec^{-1} for the peak at 834 nm (Figure 3.16)

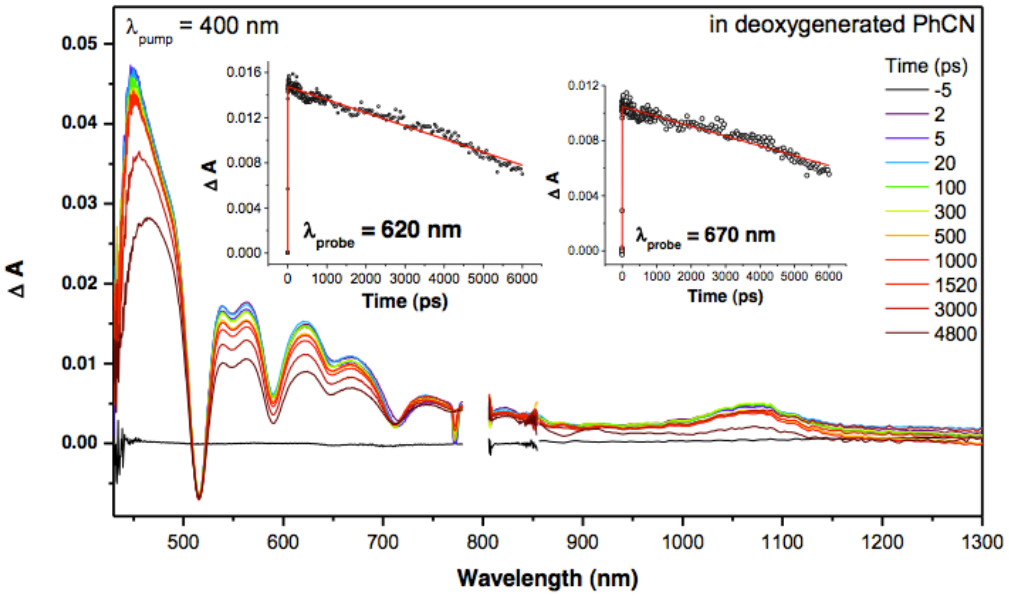

Figure 3.15 Femtosecond transient absorption spectra of ^{1}**3.2*** recorded after irradiation of **3.2** (0.1 mM) at 400 nm in deoxygenated PhCN at 298 K.

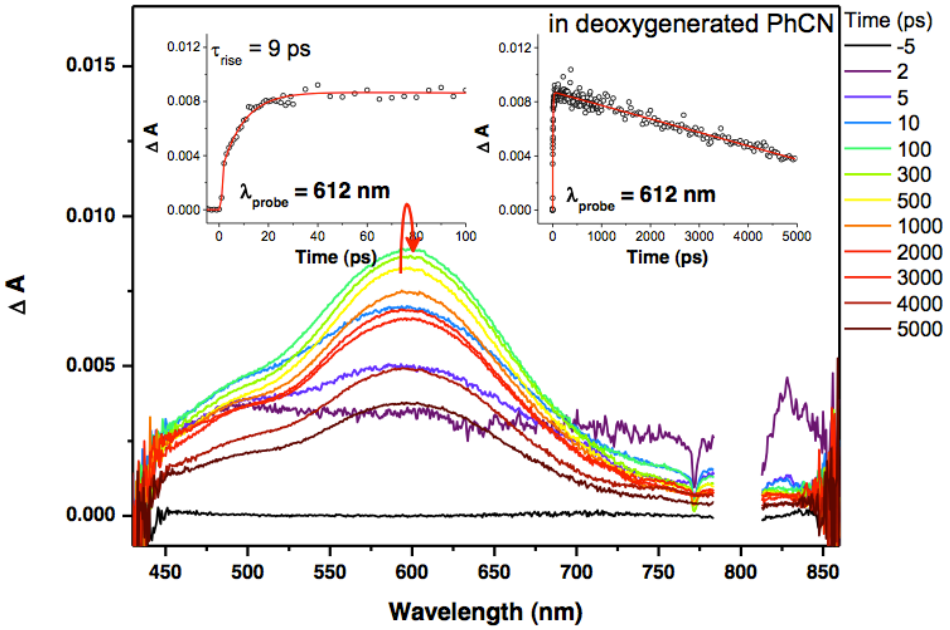

Figure 3.16 Femtosecond transient absorption features seen upon excitation of **3.1** (0.1 mM) at 400 nm. The changes shown after the sample is subject to laser pulse in deoxygenated PhCN at 298 K.

Upon excitation of a mixture of **3.1** and **3.2** (each at 50 μM) at 400 nm, the transient absorption spectra displayed the signature absorption from both species. The decay rate for the peak at 670 nm attributed to ^{1}**3.2***, 3.3 × 10^{8} s^{-1}, was found to be insensitive of the presence of **3.1** (Figure 3.17) Since the rate of decay for ^{1}**3.2*** remained the same in the presence and absence of **3.1**, it is believed that the formation of complex **3.4** does not increase the rate of intersystem crossings from ^{1}**3.2*** to ^{3}**3.2*** and that there is no reaction between **3.1** and the singlet excited state of **3.2**. This finding reiterates the conclusion reached based on the fluorescence lifetime studies, discussed above, wherein it was found no ET occurred from a TTF moiety of **3.1** to the singlet-excited state of the porphyrin acceptor **3.2**. It is therefore believed that ET processes within complex **3.4** take place primarily within the triplet-excited state with very little energy or electron transfer occurring within the singlet-excited state.

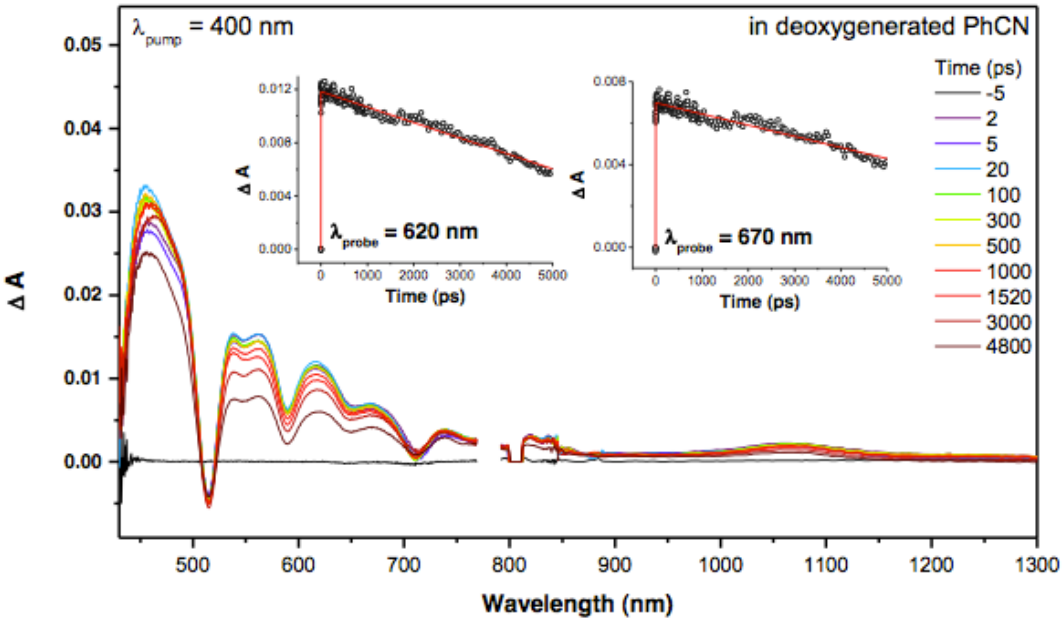

Figure 3.17 Femtosecond transient absorption spectra of a solution containing **3.1** (50 μM) and **3.2** (50 μM) as recorded following irradiation at 400 nm in deoxygenated PhCN at 298 K. Insets: Decay of the absorption spectral intensity seen for a mixture of **3.1** (50 μM) and **3.2** (50 μM) at 620 nm (left) at 670 nm (right) post excitation at 400 nm in deoxygenated PhCN at 298 K.

3.7 Nanosecond Laser Flash Photolysis Measurements

In order to study the triplet-excited state via transient absorption measurements, nanosecond laser flash photolysis was used. A pure sample of porphyrin **3.2** (0.1 mM) was irradiated with 532 nm light in deoxygenated PhCN. Under these conditions an absorption feature at 430 nm was seen to grow in (Figure 3.18a). This new feature is consistent with the formation of a triplet excited-state. The decay rate constant of this absorption feature, and therefore, the triplet, was found to be 1.1×10^4 sec^{-1}. There were no spectral changes observed upon irradiation of a sample of **3.1** (1.0 mM) in deoxygenated PhCN with a 355 nm laser pulse (not shown).

Upon irradiation at 532 nm in deoxygenated PhCN, a mixture of **3.1** (0.3 mM) and **3.2** (0.1 mM) showed a growth in the absorption feature at 450 nm, 670 nm, and 850 nm (Figure 3.18b). The absorbance band at 450 nm is attributed to the concurrent presence of ^{3}**3.2*** and **3.1**$^{\bullet+}$, species that had been independently characterized previously (cf. Figures 3.18a and 3.8a, respectively). The feature at 670 nm is attributed exclusively to **3.1**$^{\bullet+}$ based on the spectral changes observed upon chemical oxidation (Figure 3.8a) while the feature at 850 nm is attributed to **3.2**$^{\bullet-}$, based on the chemical reduction studies of **3.2** (cf. Figure 3.8b).

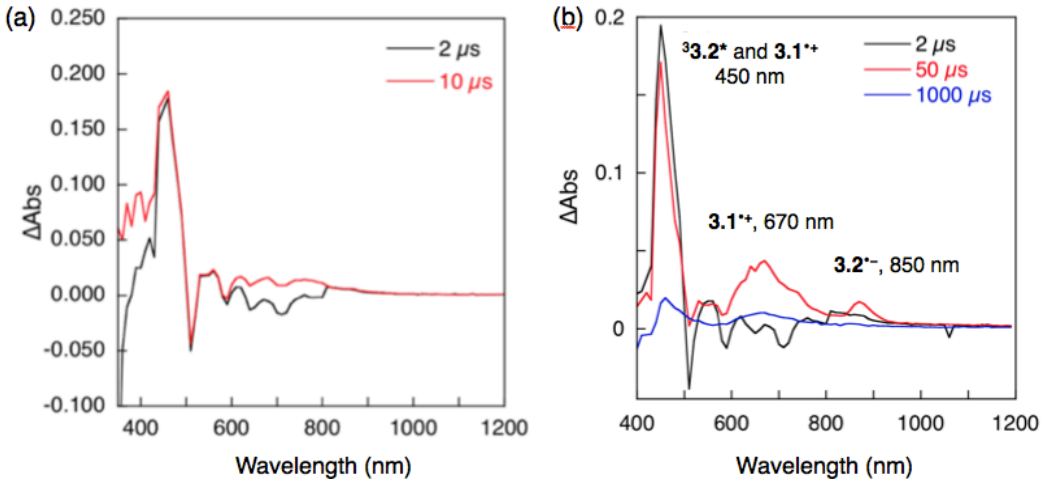

Figure 3.18 (a) Nanosecond laser flash photolysis absorption profile of ^{3}**3.2*** (0.1 mM) as observed 2 μs (black) and 10 μs (red) after excitation at 355 nm in deoxygenated benzonitrile at 298 K. (b) Nanosecond flash photolysis absorption spectra for a mixture of **3.1** (0.3 mM) and **3.2** (0.10 mM) observed upon excitation at 532 nm in deoxygenated PhCN at 298 K. Spectra were recorded 2 μs (black), 50 μs (red), and 1000 μs (blue) after the laser pulse.

The growth of the absorption feature at 670 nm as a function of [**3.1**] was monitored at room temperature (Figure 19a). Plotting the growth rate of growth of the absorbance at 670 nm versus the concentration of **3.1** gave a linear plot, seen in Figure

3.19b. The second-order rate constant was determined to be 4.4×10^8 M^{-1} s^{-1} from the slope of this plot. This rate constant corresponds to the *inter*molecular ET[27] and is smaller than that of the diffusion limiting value expected in PhCN, namely 5.6×10^9 M^{-1} s^{-1}.[65,66] The y-intercept of the line in Figure 3.19b gives the rate constant for the process of *intra*molecular forward ET; it was found to be 2.1×10^4 s^{-1}.[27]

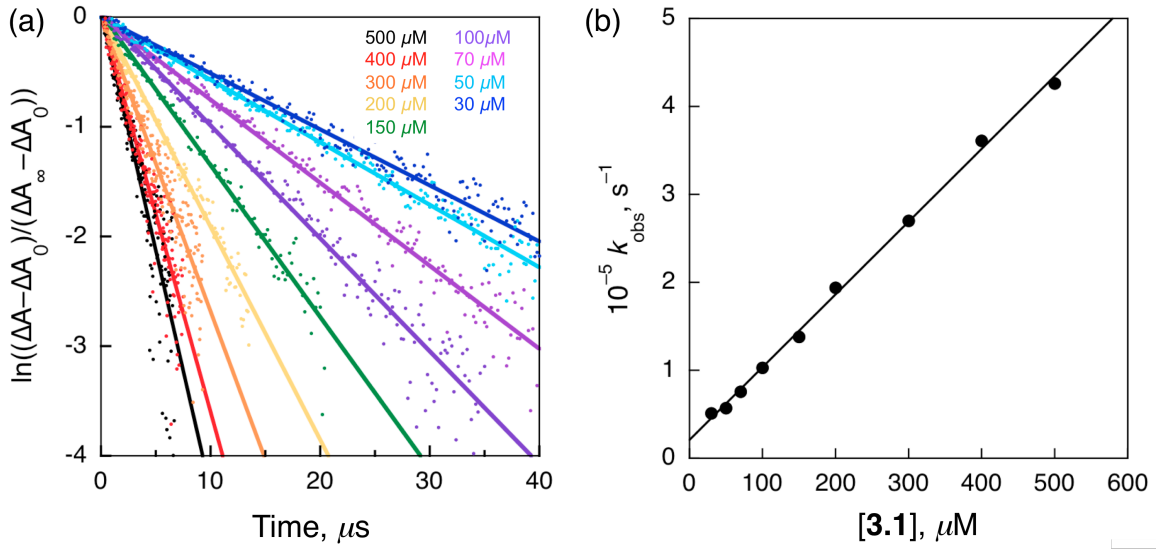

Figure 3.19 (a) Plot of the natural log of $(\Delta A\text{-}\Delta A_0)/(\Delta A_\infty\text{-}\Delta A_0)$ vs time using **3.1** at various concentrations and **3.2** at 0.1 mM (b) Plot of the rate constants for ET between **3.1** (various concentrations) and **3.2** (0.1 mM) vs concentrations of **3.1.** Experiments were performed in deoxygenated PhCN at 298 K.

The decay of the absorbance feature at 670 nm was found to fit well to a biexponential function, leading us to propose that the absorbance at 670 nm consists of two decay components. These are attributed to *inter*- and *intra*-molecular back ET, respectively. The first component is characterized by a decay rate that is independent of laser intensity (Figures 3.20a and 3.20b), as well as the concentration of **1** (Figure 3.20c). Such findings are consistent with intramolecular back ET. The rate constant of this

proposed intramolecular back ET event was determined to be 3.6×10^2 s^{-1}, while the corresponding CS lifetime was calculated to be 2.8 ms. This is one of the longest known CS lifetime for a photoinduced ET process within a noncovalenlty bound ensemble. The second component displays second-order kinetic features and is ascribed to intermolecular back ET. For this process, the rate constant was found to be 9.8×10^8 M^{-1} s^{-1}, which is also smaller than the diffusion limited value in PhCN (cf. Figures 3.21a and 3.21b).[65,66]

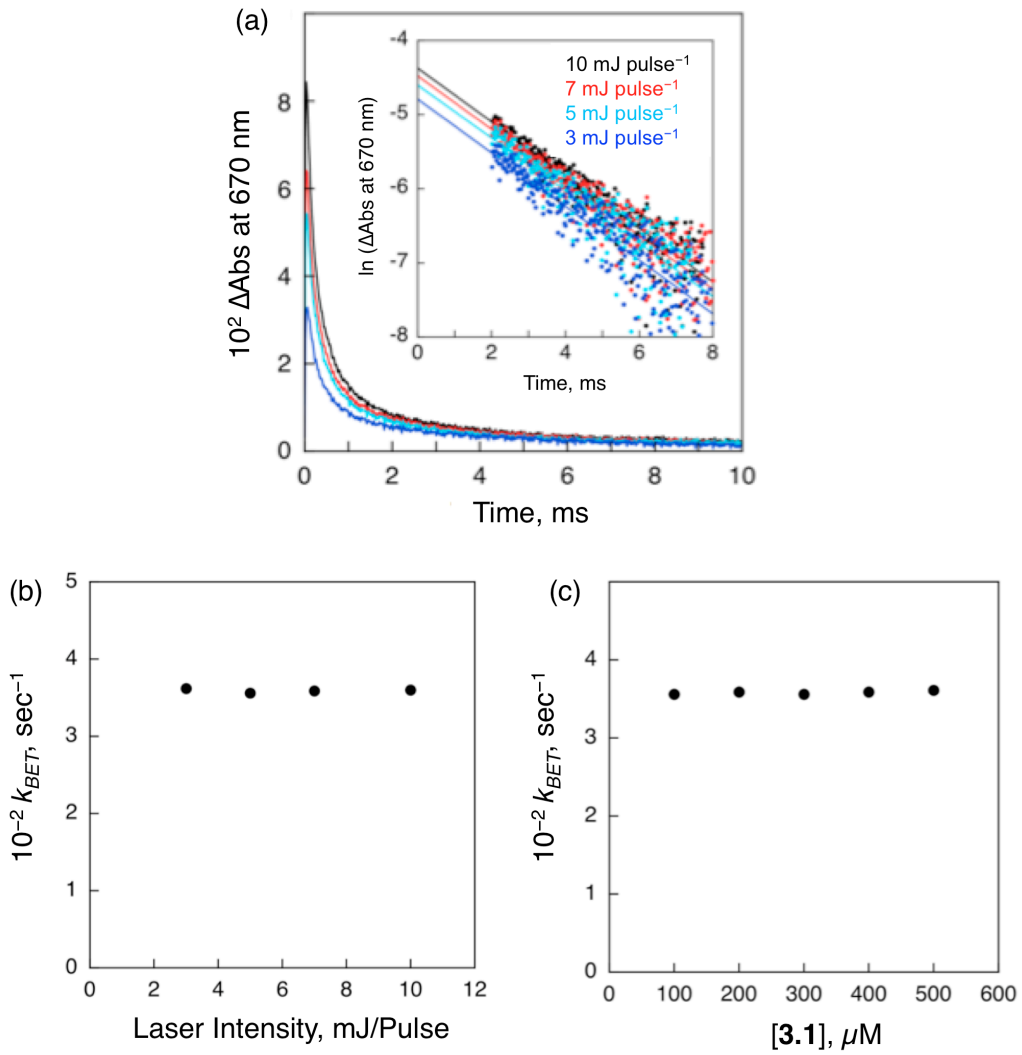

Figure 3.20 (a) Decay time profiles of the absorbance at 670 nm at various laser intensities. Inset: First-order plots. Rate of intramolecular back electron transfer (k_{BET}) (b) vs laser intensity for a sample containing 0.3 mM **3.1** and 0.1 mM **3.2** and (c) vs [**3.1**] for a sample containing 0.3 mM **3.2** in deoxygenated benzonitrile at 298 K.

Following Marcus theory, equations 3.6 and 3.7 predict that the rate constants of intramolecular forward and backward ET will be temperature dependent for a nonadiabatic system. This is what is expected for ET within ensemble **3.4**. In equations 3.6 and 3.7, k_{ET} is the rate constant of ET, T is the temperature, V is the electronic

coupling constant, λ is the reorganization energy, ΔG_{ET} is the Gibbs free energy of ET, k_B is the Boltzmann constant, and h is Planck's constant.[8,9]

$$k_{ET} = \left(\frac{4\pi^3}{h^2 \lambda k_B T}\right)^{1/2} V^2 \exp\left[-\frac{(\Delta G_{ET} + \lambda)^2}{4\lambda k_B T}\right] \qquad (eqn.\ 3.6)$$

$$\ln\left(k_{ET} T^{1/2}\right) = \ln\left(\frac{2\pi^{3/2} V^2}{h(\lambda k_B)^{1/2}}\right) - \frac{(\Delta G_{ET} + \lambda)^2}{4\lambda k_B T} \qquad (eqn.\ 3.7)$$

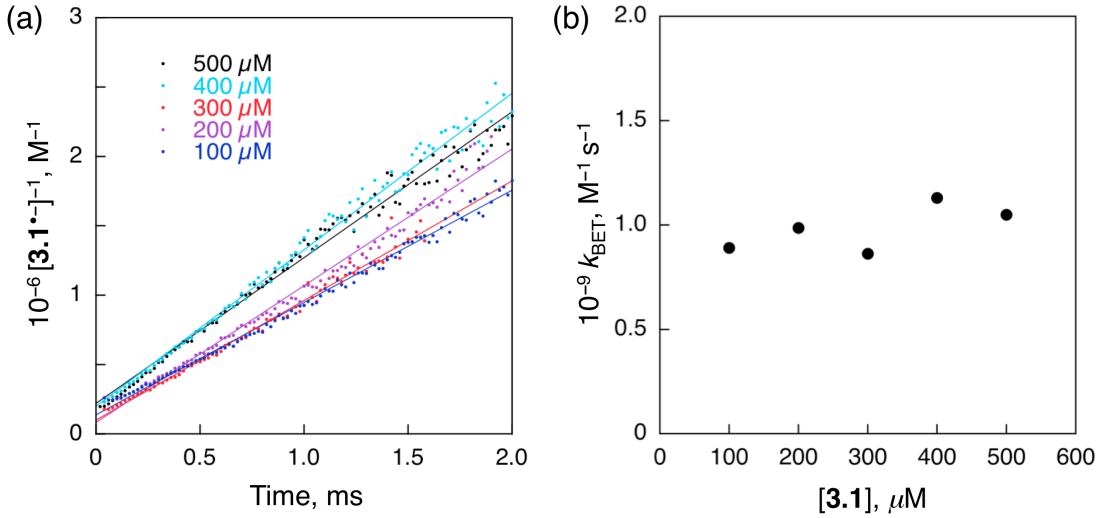

Figure 3.21 Second order decay analysis of the back electron transfer process at various concentrations of **3.1** as studied in the presence of 0.3 mM of **3.2** in deoxygenated benzonitrile at 298 K (left). Rate of back electron transfer versus concentration of **3.1** in a 0.3 mM solution of **3.2** in PhCN at 298 K. On the basis of these analyses, the intermolecular electron transfer rate was found to be 9.8×10^8 M^{-1} sec^{-1} (right).

Upon plotting the temperature dependence of the rate constant of intramolecular back ET in a Marcus plot (Figure 3.22a), the electronic coupling constant V is given by the intercept and the reorganization energy λ is given by the slope. These values were found to be 1.2×10^{-2} cm^{-1} and 0.76 eV, respectively. The V value is rather small, as

predicted by the DFT calculations. This reflects poor overlap of the HOMO and LUMO, as well as the long distance between the components **3.1** and **3.2** that make up the ET ensemble **3.4**. The small *V* value provides a rationale for the long-lived CS state, as observed via transient absorption spectroscopy. The temperature dependence of the rate constant of intramolecular back electron transfer was also analyzed using the Eyring plot, which is shown in Figure 3.22b. This analysis gives the Gibbs free energy of the transition state of ET, $\Delta G^{\neq}$, a value that was found to be 14 kcal·mol^{-1}. In a similar way the entropy of the transition state, $\Delta S^{\neq}$, and the enthalpy of the transition state, $\Delta H^{\neq}$, could be calculated as –40 cal·K^{-1}·mol^{-1} and 1.9 kcal·mol^{-1}, respectively.

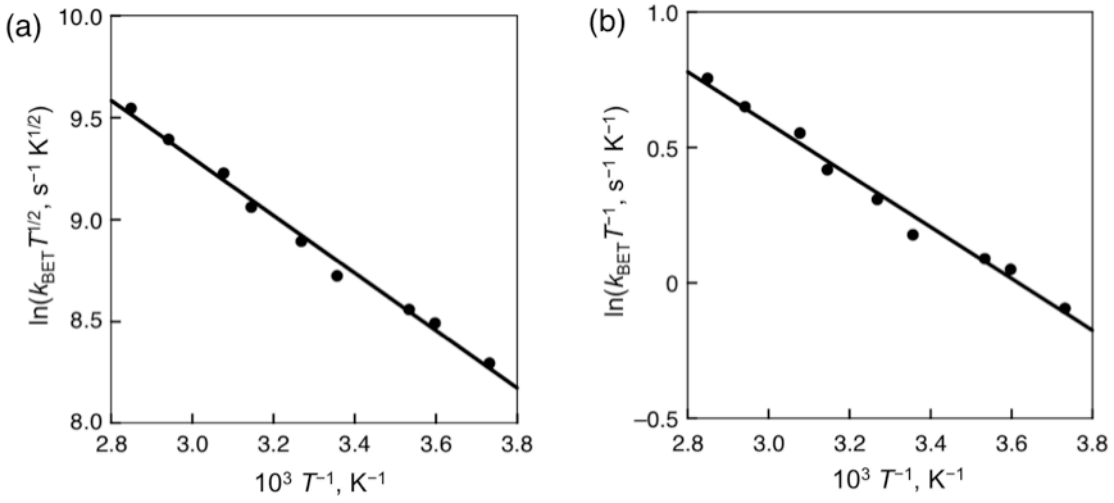

Figure 3.22 (a) Marcus plot of the change in the rate of intramolecular back ET (k_{BET}) vs temperature in PhCN. (b) Eyring plot constructed by plotting the observed changes in the rate of back electron transfer (k_{BET}) versus temperature in benzonitrile. The concentrations of **3.1** and **3.2** were 0.3 mM and 0.1 mM, respectively.

3.8 Electron Spin Resonance Spectroscopic Measurements

Typically, photoinduced ET from a neutral donor to a neutral acceptor results in the formation of radical species. For complex **3.4**, ET from a TTF moiety of **3.1** to porphyrin **3.2** upon photoirradiation of **3.2** should produce the radical species **3.1**$^{\bullet+}$ and **3.2**$^{\bullet-}$. To test this theory, calix[4]pyrrole **3.1** was chemically oxidized to the radical cation using one equivalent of the oxidant "magic blue" allowing us to characterize the radical cation. A spectroscopic technique used to determine whether radicals are present in solution is electron spin resonance spectroscopy (ESR, also known as electron spin resonance (EPR)); this instrumentation was used to obtain the ESR spectrum of in **3.1**$^{\bullet+}$ PhCN (Figure 3.23). Separately, porphyrin **3.2** was chemically reduced using naphthalene radical anion and the ESR spectrum of its radical anion, **3.2**$^{\bullet-}$, was collected (Figure 3.23).

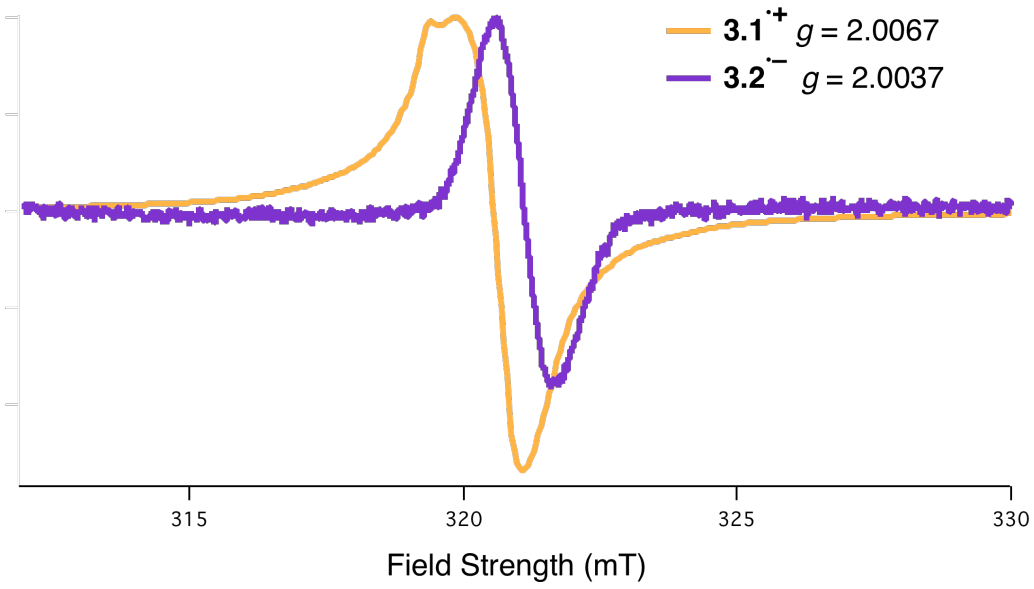

Figure 3.23 Normalized ESR spectra for chemically induced radicals of calix[4]pyrrole **3.1** (**3.1**$^{\bullet+}$) and porphyrin carboxylate **3.2** (**3.2**$^{\bullet-}$) in deaerated PhCN at 77 K.

With these spectra in hand, an ESR spectrum was taken of a sample containing **3.1** (0.5 mM) and **3.2** (0.3 mM) in PhCN at 4 K. Before irradiation, there was no significant ESR signal seen. However, upon photoirradiation with a 1000 W Hg high-pressure lamp, an ESR signal at g = 2.005 appeared (Figure 3.24). The g value in ESR is comparable to the chemical shift in NMR in that a specific compound will have a different value depending on what atoms the electron is located. For the radical cation $\mathbf{3.1}^{\bullet+}$, the ESR signal appears at g = 2.0067. The radical anion $\mathbf{3.2}^{\bullet-}$ is shifted further to the right and is seen at g = 2.0037.[38,45] The fact that the signal for the photoirradiated sample containing both **3.1** and **3.2**, and therefore complex **3.4**, has a g value between that of the individual radical components of the complex is good indication that both the radical species are produced upon photoirradiation and that light is necessary to induce the ET between the species.

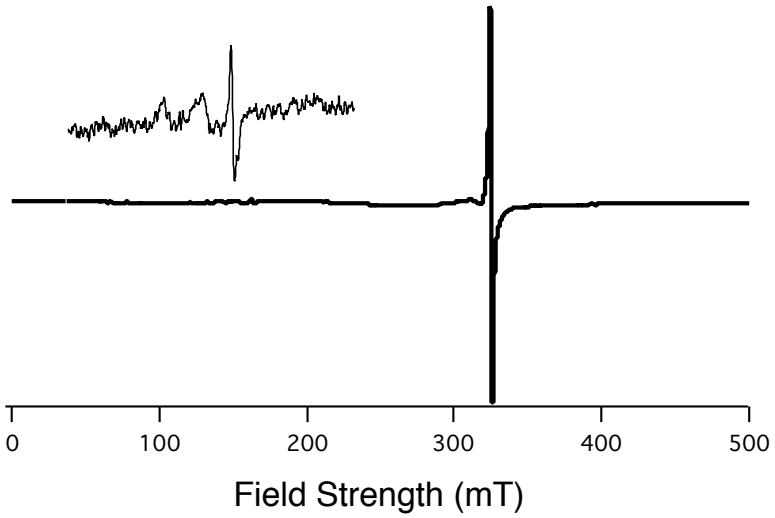

Figure 3.24 X-band ESR spectra for **3.1** (0.5 mM) and **3.2** (0.3 mM) in PhCN at 4 K under photoirradiation with a 1000 W high-pressure Hg lamp. The signal was observed at g = 2.005. Inset: Expanded region at g = 4. These results are consistent with formation of a triplet species under these experimental conditions.

The observed ESR signal in Figure 3.24 at g = 2.005 is a doublet signal, indicating singlet spin pairing. This finding thus supports the notion that an intermolecular CS state composed of doublet $\mathbf{3.1}^{\bullet+}$ and $\mathbf{3.2}^{\bullet-}$ is dominant under the ESR spectral conditions, most likely due to the relatively high concentrations of **3.1** and **3.2** used for the ESR measurements.

As can be seen from an inspection of the inset to Figure 3.24, a signal was seen at g = 4.18 that is ascribable to a triplet CS state.[27,38,40,66,67] Such an observation is consistent with the laser flash photolysis measurements that led to the conclusion that the charge separations goes through the triplet excited state. However, the zero-field splitting pattern around g = 2 that would be expected for the triplet CS state produced by intramolecular electron transfer at low temperature was not observed clearly in Figure 3.24. This absence of clear spectral features is ascribed to line broadening in frozen PhCN.

3.9 CONCLUSIONS

In summary, the ET events following photoexcitation of complex **3.4** formed from calix[4]pyrrole **3.1** and porphyrin carboxylate **3.2** were studied in depth. The 1:1 binding affinity corresponding to the interaction between **3.1** and **3.2** was found to be 6.3 $\times 10^4$ M^{-1} in PhCN at 298 K as determined from an analysis of UV-Vis spectral titrations, as well as ITC measurements. Density functional theory was used to provide support for the HOMO and LUMO being located on a TTF moiety of **3.1** and the porphyrin core of **3.2**, respectively. These theoretical studies also provide support for the suggestion that ET from **3.1** to **3.2** occurs upon photoirradiation of complex **3.4**. Photoinduced ET via the triplet excited state was confirmed using laser plash photolysis measurements, which allowed for the determination of both forward and backward ET rates. *Inter*- and

*intra*molecular ET was seen for complex **3.4** with intermolecular ET being dependent upon concentration of the species in solution. The triplet charge separated state produced upon photoirradiation of **3.2** was found to be 2.8 milliseconds, the longest known lifetime for a CS state generated via photoinduced ET within a non-covalently bound complex. The ability to create such a long-lived CS via simple mixing of appropriately chosen components provides a promising starting point for the future development of readily accessible artificial photosynthetic devices.

3.10 FUTURE DIRECTIONS

The next goal of this project was to combine the chemistry involving fullerene binding with the porphyrin—TTF-calix[4]pyrrole supramolecular ensemble described in this chapter. To do this, a tetrabutylammonium porphyrin carboxylate, **3.5** (Figure 3.25a), was synthesized in order to allow for the cavity of the calix[4]pyrrole to remain empty, as opposed to the use of the TEA^+ porphyrin carboxylate salt **3.2**. This change was done purposefully with the hopes that the TTF cavity would remain available for binding to fullerene, in analogy to what was detailed in Chapter 2 of this dissertation. To the extent this occurred it would allow formation of a assembly, **3.7**, to form.

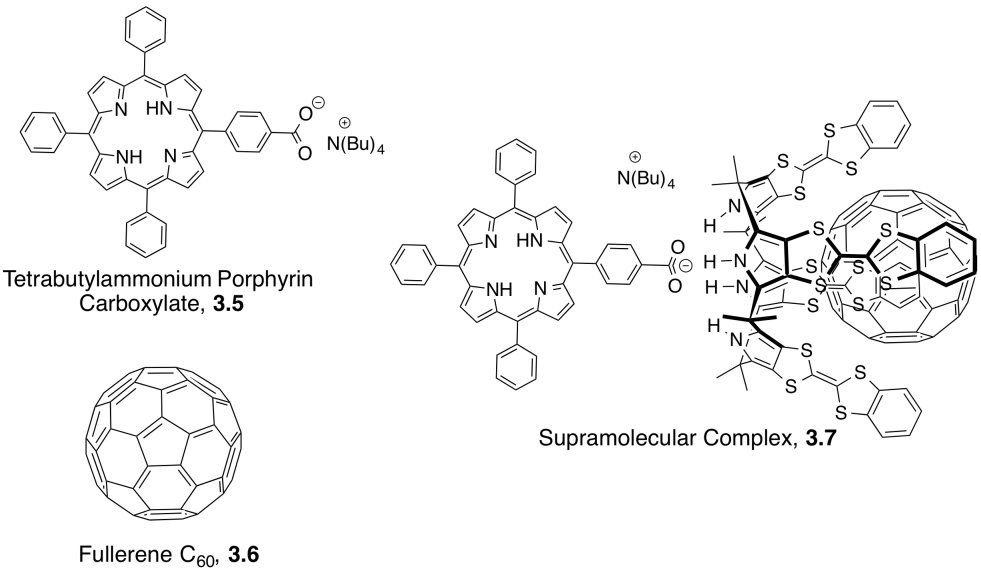

Figure 3.25 Structures of tetrabutylammonium porphyrin carboxylate **3.5** and proposed supramolecular complex **3.7** consisting of **3.5**, **3.1**, and fullerene C_{60} (**3.6**). Compound **3.5** was synthesized by Dr. Atanu Jana.

One of the major differences between porphyrin **3.5** and **3.2** is the substitution of the *meso*-position. In **3.2**, the pentafluorophenyl groups were used in order to make the porphyrin more electron deficient, therefore, easier to reduce by the TTF moieties of **3.1** upon photoirradiation. Porphyrin **3.5** consists of a phenyl group that remains un-substituted at the carbon positions. As shown in Figure 3.26, the use of pentafluorophenyl groups as the *meso*-substituents on the porphyrin shifts the reduction potential by –0.33 V vs $Ag/AgNO_3$ relative to the corresponding phenyl *meso*-substituted system. In other words, as compared to **3.2**, porphyrin **3.5** is harder to reduce and more likely to act as an electron donor.

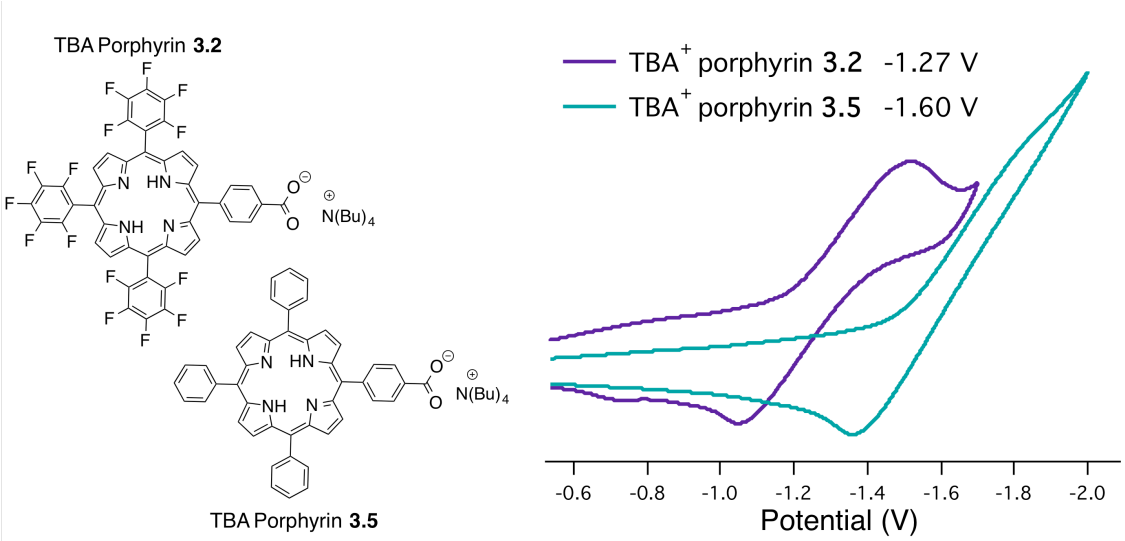

Figure 3.26 Cyclic voltammograms for **3.2** as the TBA^+ salt (0.1 mM, purple) and **3.5** (0.1 mM, teal) recorded in dichloromethane at room temperature using 0.1 M tetra-*n*-butylammonium hexafluorophosphate as the electrolyte. The reference electrode was $Ag/AgNO_3$, the working electrode was Pt, and the counter electrode was a Pt wire.

Preliminary UV-Vis-NIR studies in which porphyrin **3.5** was titrated into a solution of **3.1** and fullerene C_{60} (20 μM each) in dichloromethane resulted in what appears to be the formation of a CT band centered around 720 nm (Figures 3.27 a and b). This band reaches a maximum around 2.2 equivalents followed by a decrease in the absorbance in this region (Figure 3.27c). This behavior is currently being investigated to determine if **3.7** is in fact being formed and if there is CT within the complex that is subsequently "quenched" or if the complex undergoes dissociation upon the addition of more than 2 equivalents of **3.5**. Either event would lead to the observed decrease in absorbance.

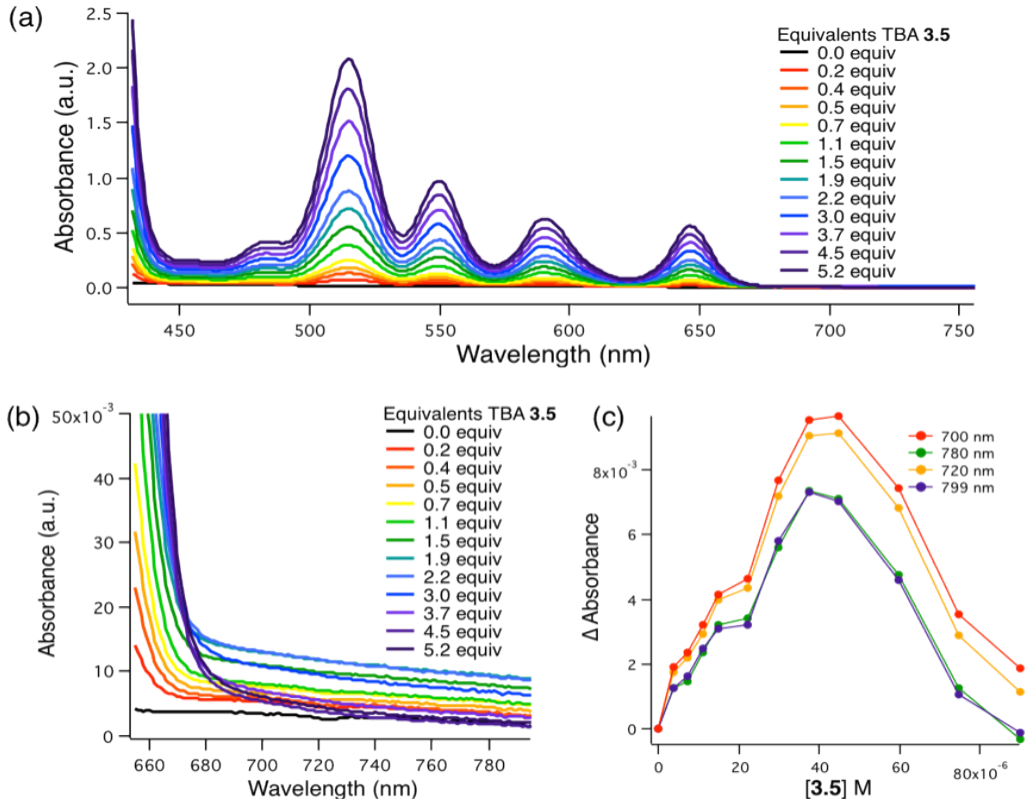

Figure 3.27 (a) UV-Vis-NIR titration for **3.1** and fullerene C_{60} (20 μM each) upon addition of **3.5** in dichloromethane at 298 K. The increase in absorbance below 700 nm is attributed to the addition of the porphyrin **3.5** to the solution. (a) Expanded view of the 650 and 799 nm spectral region of the titration (c) Plot of change in absorbance versus concentration of **3.5**.

The original intent behind forming complex **3.7** was to determine the plausibility of its use for what could become a self-assembled organic solar cell (Figure 3.28a). As seen in Figure 3.28b, the design of the desired self-assembled organic solar cell relies on the chemistry from both Chapter 2 and Chapter 3. The idea is that the polythiophene polymer backbone and the porphyrin will absorb light. The energy from the polymer will be transferred to the porphyrin, which will undergo electron transfer to the calix[4]pyrrole. From here, the calix[4]pyrrole will transfer an electron to the fullerene, resulting in a donor—bridge—acceptor (D-B-A) electron transfer ensemble. One of

issues that we expect to face in this ensemble is involves the electronics of the TTF calix[4]pyrrole. If the TTF calix[4]pyrrole is too electron rich it will not act as a bridge and stop ET from occurring from the porphyrin to the fullerene. To circumvent this issue, a calix[4]pyrrole that is not as electron rich but still has large binding affinity for fullerene would to be used. Such porphyrins are unknown at present.

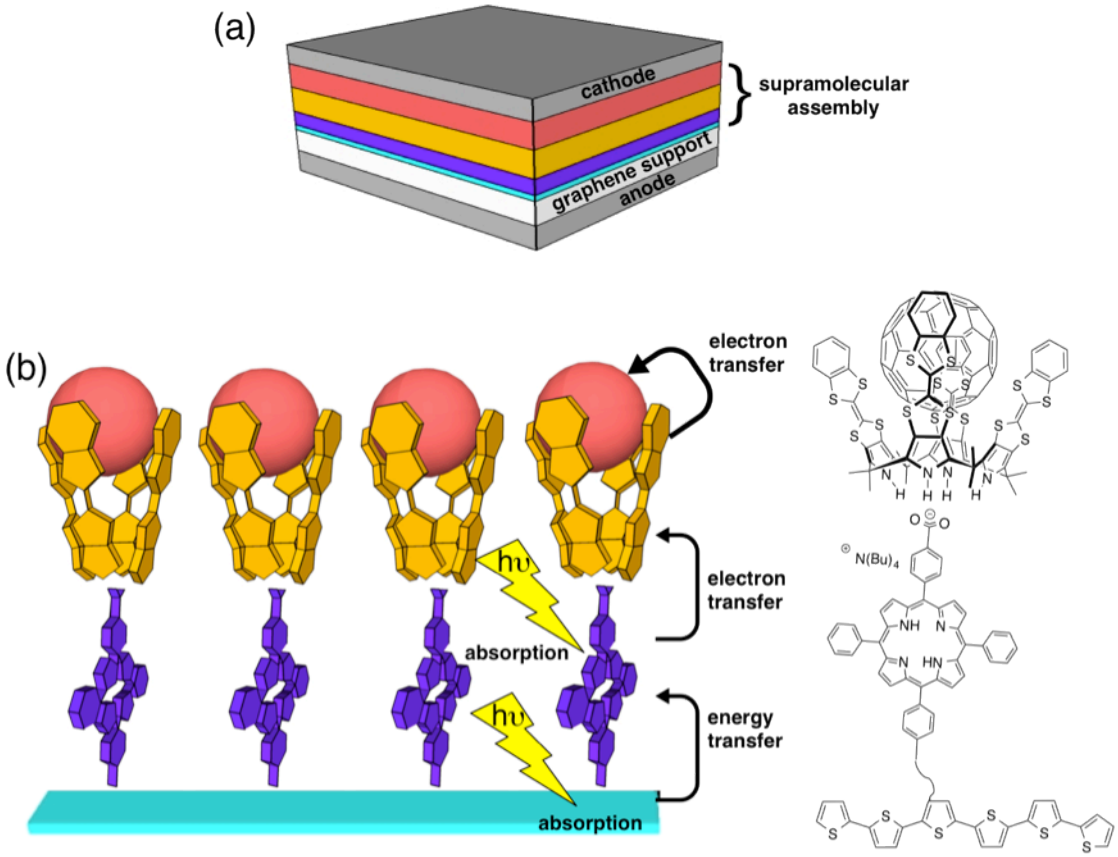

Figure 3.28 (a) Proposed organic solar cell consisting of a self-assembled supramolecular ensemble as the active layer. (b) Proposed supramolecular assembly based on a polythiophene polymer substituted with porphyrin carboxylates. These porphyrin units are expected to anion bind to a calix[4]pyrrole, inducing the conformational change to the cone conformer producing a cavity into which fullerene can bind to produce the proposed organic solar cell.

Attempts were made to synthesize a more electron deficient calix[4]pyrrole than **3.1** through the synthetic scheme depicted if Scheme 3.1 below.

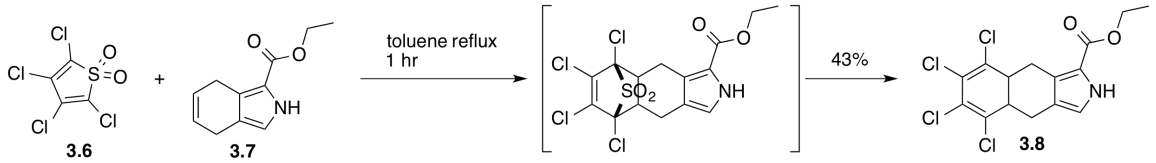

Scheme 3.1 Synthetic steps followed to synthesize extended pyrrole, 5,6,7,8-tetrachloro-4,4a,8a,9-tetrahydro-2*H*-benzo[*f*]isoindole, **3.8**.

Tetrachlorothiophene dioxide (**3.6**) and ethyl 4,7-dihydro-2*H*-isoindole-1-carboxylate (**3.7**) were made following literature procedure[68] and a modified literature procedure[69] detailed by Dr. Vladimir Roznyatovskiy,[70] respectively. Diels-Alder cyclization of the two precursors in toluene at reflux conditions gave ethyl 5,6,7,8-tetrachloro-4,4a,8a,9-tetrahydro-2*H*-benzo[*f*]isoindole-1-carboxylate (**3.8**) in 43% yield.[71]

The classical method for synthesizing calix[4]pyrroles involves condensation of the pyrrole with acetone in the presence of acid; however, for pyrroles containing sp^3 hybridized carbons at the β-position, this condensation approach is not possible due to steric hindrance (Figure 3.29).[72] Therefore, the ethylester pyrrole **3.8** was subjected to a different procedure in order to achieve the cyclization to the calix[4]pyrrole (**3.9**). The method, originally published by the Sessler group in 2009,[72] consists of subjecting β-substituted pyrroles to methyl lithium in diethyl ether followed by the addition of hydrochloric acid in diethyl ether as depicted in Figure 3.30.

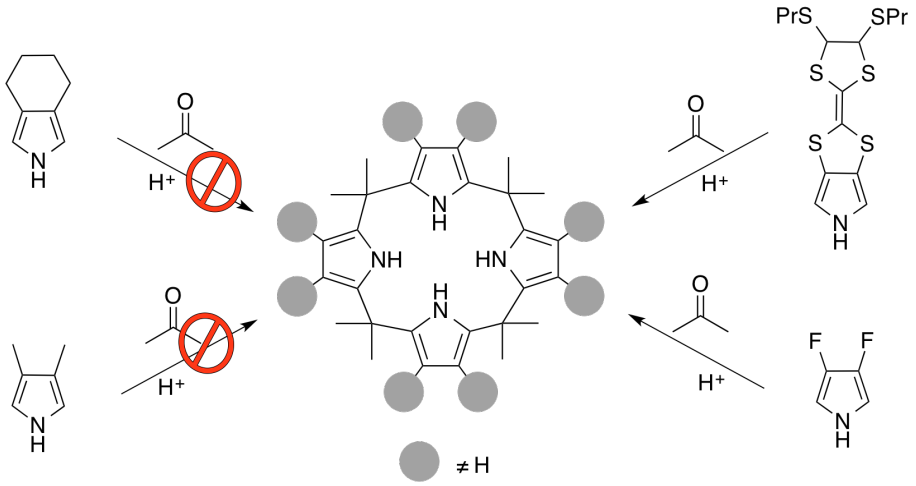

Figure 3.29 Classic protocol for the synthesis of calix[4]pyrroles containing substitution at the β-position of the pyrrole. The synthetic approach using condensation of the pyrrole with acetone in the presence of acid does not work effectively for pyrroles with steric bulk arising from the sp^3 carbons at the β-position.[72]

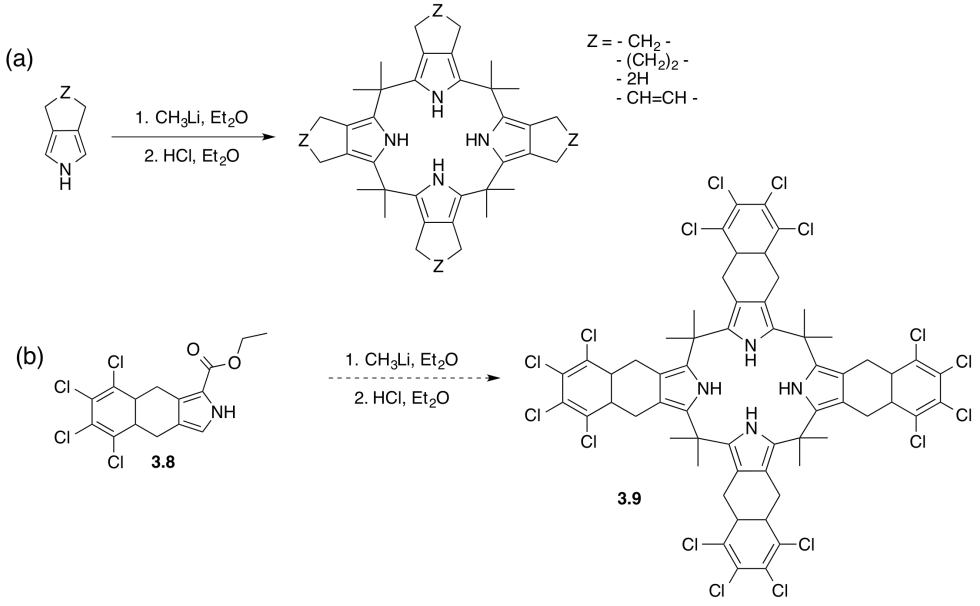

Figure 3.30 (a) Literature procedure for the synthesis of calix[4]pyrroles from β-substituted pyrroles.[72] (b) Procedure followed in attempt to get a calix[4]pyrrole from pyrrole **3.8**.

Unfortunately, all attempts to access calix[4]pyrrole **3.9** proved futile. Most likely this failure reflects the steric bulk from the extended rings of the pyrrole **3.8** added during the Diels-Alder cyclization of the **3.7** and **3.6**. To circumvent this potential problem, pyrrole **3.8** was subjected to oxidation conditions in an effort to aromatize the distal ring of the pyrrole. Though isoindoles are known to be extremely unstable upon aromatization, the candidate hoped that the most distal ring would be the only moiety to aromatize upon subjection of **3.8** to dichlorodicyanoquinone (DDQ). However, the ring never aromatized even when heated as refluxing solutions of dichloromethane, toluene, or chlorobenzene. Cheprakov et al. were able to remove the ester linkage of pyrrole **3.8** and get the porphyrin analogue to **3.9** fully aromatized using DDQ in naphthalene at 160 °C.[71] This route was also explored to aromatize the distal ring of **3.8** while in both the ester and de-esterified forms but proved unsuccessful. It is believed that upon subjection to the conditions of DDQ and refluxing naphthalene that the system may undergo complete aromatizaion through the three ring moieties and then decompose due to the known instability of isoindole.[71,73]

3.11 EXPERIMENTAL METHODS

Chemicals of the best grade available were purchased from commercial suppliers and were used without further purification. Unless otherwise noted, benzonitrile (PhCN) used during data collection was distilled over phosphorus pentoxide (P_2O_5) before use. Benzo-tetrathiafulvalene calix[4]pyrrole **3.1** was prepared using literature methods.[37] Porphyrin **3.3**, prepared using a modification of literature procedures,[74,75] was saponified using sodium hydroxide in aqueous tetrahydrofuran, followed by cation exchange using tetraethylammonium hydroxide, to yield the porphyrin carboxylate salt **3.2**. Extended pyrrole **3.8** was synthesized following a previous procedure detailed by Dr. Vladimir Roznyatovskiy.[70]

3.11.1 Instrumentation

^{1}H NMR spectra were recorded on a Varian MR 400 MHz spectrometer in deuterated chloroform at room temperature. UV-Vis-NIR absorption spectra were recorded on a Hewlett Packard 8453 diode array spectrophotometer. Fluorescent spectra were recorded on a Horiba FluoroMax-4 spectrophotometer. Isothermal titration calorimetry measurements were carried out on a VP-ITC MicroCalorimeter in 99% spectroscopic grade PhCN, purchased from Acros Organics and used without further purification.

3.11.2 Electrochemical Measurements

Cyclic voltammetry (CV) studies were carried out using an ALS-630B electrochemical analyzer in deoxygenated PhCN containing 0.1 M $TBAPF_6$ as a supporting electrolyte at 298 K. A conventional three-electrode cell was used with a

platinum working electrode (surface area = 0.3 mm^2) and a platinum wire as the counter electrode. The Pt working electrode, purchased from BAS, was routinely polished with a polishing alumina suspension from BAS and rinsed with distilled water and acetone before use. The potentials were measured with respect to a $Ag/AgNO_3$ (10 mM) reference electrode. All electrochemical measurements were carried out under a positive argon atmosphere.

3.11.3 Laser Flash Photolysis Measurements

The femtosecond time-resolved transient absorption (TA) spectra collected in Seoul were recorded on a spectrometer that consisted of NIR optical parametric amplifier (OPA) system (Quantronix, Pallitra) pumped by a Ti:sapphire regenerative amplifier system (Quantronix, Integra-C) operating at 1 kHz repetition rate and an optical detection system. The generated OPA output signals had a pulse width of ~ 100 fs which were used as pump pulses. White light continuum (WLC) probe pulses were generated using a sapphire window (3 mm of thickness) by focusing of small portion of the fundamental 800 nm pulses. The time delay between pump and probe beams was carefully controlled by making the pump beam travel along a variable optical delay (Newport, ILS250). Intensities of the spectrally dispersed WLC probe pulses are monitored by two miniature spectrographs (Ultrafast Systems, High Speed Spectrometers). To obtain the time-resolved transient absorption difference signal (ΔA) at a specific time, the pump pulses were chopped at 500 Hz and absorption spectra intensities were saved alternately with or without pump pulse. Typically, 6000 pulses were used excite samples so as to obtain the TA spectra at a particular delay time. The polarization angle between pump and probe beam was set at the magic angle (54.7°) in order to prevent polarization-dependent

signals. Cross-correlation fwhm in pump-probe experiments was less than 200 fs and chirp of WLC probe pulses was measured to be 800 fs in the 400-1200 nm region. To minimize chirp, non-reflection optics were used in the probe beam path and the cuvette was a 2 mm path length quartz cell. After the TA experiments, the absorption spectra of all compounds were carefully checked so as to avoid artifacts arising from, e.g., photo-degradation or photo-oxidation of the samples in question. HPLC grade solvents were used in all steady-state and time-resolved spectroscopic studies.

Femtosecond transient absorption spectroscopic experiments carried out in Osaka used in PhCN as the solvent. An ultrafast source consisting of an Integra-C (Quantronix Corp.), an optical parametric amplifier, TOPAS (Light Conversion Ltd.), and a commercially available optical detection system, Helios, provided by Ultrafast Systems LLC were also used.

Nanosecond time-resolved transient absorption measurements were carried out with a laser system provided by UNISOKU Co., Ltd. Measurements of nanosecond transient absorption spectra were performed according to the following procedure: A deoxygenated solution was excited by a Nd:YAG laser (Continuum, SLII-10, 4–6 ns fwhm) at λ = 532 nm. The photodynamics were monitored by continuous exposure to a xenon lamp (150 W) as a probe light and using a photomultiplier tube (Hamamatsu 2949) as the detector. These measurements were performed in Osaka.

3.11.4 Electron Spin Resonance Spectroscopy

Electron spin resonance (ESR) spectra were recorded on a JEOL X-band spectrometer (JES-RE1XE) with a quartz ESR tube. The ESR spectrum of the putative CS state in frozen PhCN was measured at 4 K using a liquid helium cryostat and 77 K

using a liquid nitrogen cryostat under conditions of photoirradiation with a high-pressure mercury lamp (USHIO LIGHTING USH–1005D) focused through a water filter at the sample cell in the ESR cavity. The g values were calibrated using a Mn^{2+} marker.

3.11.5 Theoretical Calculations

Density functional theory (DFT) calculations were performed using the Gaussian 09 program64 suite on a supercomputer (KISTI, IBM). The MO distribution diagram of complex **3.4**, the complex formed between calix[4]pyrrole **3.1** and porphyrin **3.2** was obtained via the B3LYP method employing 6-31G(d) basis set for all atoms.

3.11.6 Electron Spin Resonance Control Studies

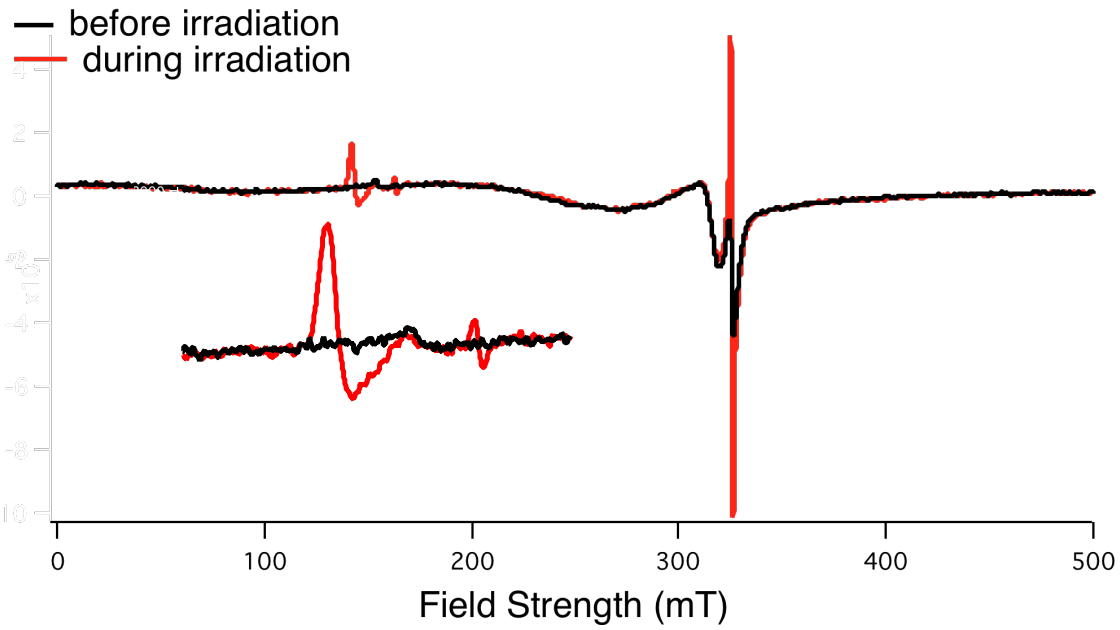

Figure 3.31 Full ESR spectra for porphyrin carboxylate **3.2** in deaerated PhCN at 4 K. (inset) Expanded view of the area near $g = 4$.

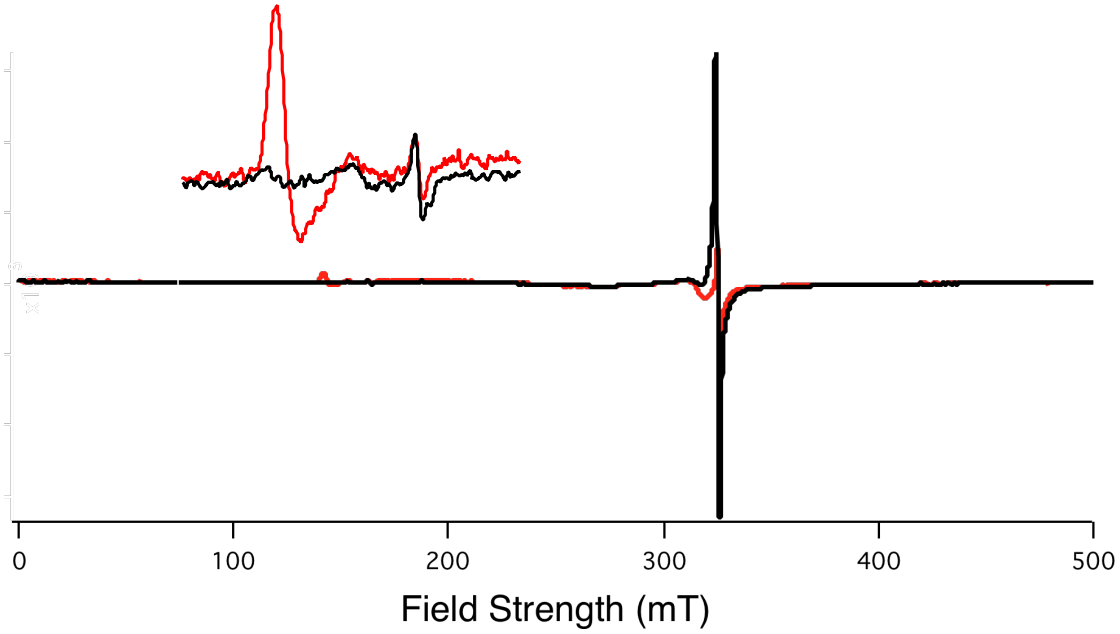

Figure 3.32 ESR spectrum of porphyrin **3.2** (red) recorded under conditions of photoirradiation overlaid with the ESR spectrum of **3.4** (**3.1** (0.5 mM) and **3.2** (0.3 mM)) (black) in solution under irradiation with a 1000 W high-pressure Hg lamp at 4 K in deaerated PhCN. Inset: Expanded view of the *g* = 4 region.

3.12 CHAPTER 3 REFERENCES

1. Lewis, N. S.; Nocera, D. G. *Proc. Natl. Acad. Sci.* **2006**, *103*, 15729-15735.
2. Fukuzumi, S. *Phys. Chem. Chem. Phys.* **2008**, *10*, 2283-2297.
3. Günes, S.; Neugebauer, H.; Sariciftci, N. S. *Chem. Rev.* **2007**, *107*, 1324-1338.
4. Nunzi, J.-M. *C. R. Physique* **2002**, *3*, 523-542.
5. Fukuzumi, S.; Ohkubo, K. *Dalton Trans.* **2013**, *42*, 15846-15858.
6. Kalowekamo, J.; Baker, E. *Solar Energy* **2009**, *83*, 1224-1231.
7. Heliatek Consolidates its Technology Leadership by Establishing a New World Record for Organic Solar Technology with a Cell Efficiency of 12%, http://www.heliatek.com/wp-content/uploads/2013/01/130116_PR_Heliatek_ achieves_record_cell_effiency_for_OPV.pdf, accessed June 2014.
8. Marcus, R. A.; Sutin, N. *Biochim. Biophys. Acta.* **1985**, *811*, 265-322.
9. Marcus, R. A. *Angew. Chem. Int. Ed.* **1993**, *32*, 1111-1121.
10. Fukuzumi, S. *Pure Appl. Chem.* **2007**, *79*, 981-991.
11. Fukuzumi, S. Electron Transfer of π-Functional Systems and Applications. In *Functional Organic Materials*, Wiley-VCH: Weinheim: 2007; pp 465-510.
12. Ohkubo, K.; Fukuzumi, S. *Bull. Chem. Soc. Jpn.* **2009**, 3279-3289.
13. Durrant, J. R.; Haque, S. A.; Palomares, E. *Chem. Comm.* **2006**, 3279-3289.
14. Martín, N.; Sánchez, L.; Herranz, M. a. Á.; Illescas, B.; Guldi, D. M. *Acc. Chem. Res.* **2007**, *40*, 1015-1024.
15. Wasielewski, M. R. *Acc. Chem. Res.* **2009**, *42*, 1910-1921.
16. Fukuzumi, S.; Ohkubo, K.; D'Souza, F.; Sessler, J. L. *Chem. Comm.* **2012**, *48*, 9801-9815.
17. Fukuzumi, S.; Ohkubo, K. *J. Mater. Chem.* **2012**, *22*, 4575.
18. Fukuzumi, S.; Saito, K.; Ohkubo, K.; Khoury, T.; Kashiwagi, Y.; Absalom, M. A.; Gadde, S.; D'Souza, F.; Araki, Y.; Ito, O.; Crossley, M. J. *Chem. Comm.* **2011**, *47*, 7980-7982.
19. de la Escosura, A.; Martínez-Díaz, M. V.; Guldi, D. M.; Torres, T. *J. Am. Chem. Soc.* **2006**, *128*, 4112-4118.
20. Ballardini, R.; Balzani, V.; Clemente-León, M.; Credi, A.; Gandolfi, M. T.; Ishow, E.; Perkins, J.; Stoddart, J. F.; Tseng, H.-R.; Wenger, S. *J. Am. Chem. Soc.* **2002**, *124*, 12786-12795.
21. Wessendorf, F.; Gnichwitz, J.-F.; Sarova, G. H.; Hager, K.; Hartnagel, U.; Guldi, D. M.; Hirsch, A. *J. Am. Chem. Soc.* **2007**, *129*, 16057-16071.
22. D'Souza, F.; Maligaspe, E.; Ohkubo, K.; Zandler, M. E.; Subbaiyan, N. K.; Fukuzumi, S. *J. Am. Chem. Soc.* **2009**, *131*, 8787-8797.
23. Molina-Ontoria, A.; Fernández, G.; Wielopolski, M.; Atienza, C.; Sánchez, L.; Gouloumis, A.; Clark, T.; Martín, N.; Guldi, D. M. *J. Am. Chem. Soc.* **2009**, *131*, 12218-12229.
24. D'Souza, F.; Amin, A. N.; El-Khouly, M. E.; Subbaiyan, N. K.; Zandler, M. E.; Fukuzumi, S. *J. Am. Chem. Soc.* **2011**, *134*, 654-664.

25. Bandi, V.; El-Khouly, M. E.; Nesterov, V. N.; Karr, P. A.; Fukuzumi, S.; D'Souza, F. *J. Phys. Chem. C.* **2013**, *117*, 5638-5649.
26. Wessendorf, F.; Grimm, B.; Guldi, D. M.; Hirsch, A. *J. Am. Chem. Soc.* **2010**, *132*, 10786-10795.
27. Kawashima, Y.; Ohkubo, K.; Kentaro, M.; Fukuzumi, S. *J. Phys. Chem. C.* **2013**, *117*, 21166-21177.
28. Bandi, V.; El-Khouly, M. E.; Ohkubo, K.; Nesterov, V. N.; Zandler, M. E.; Fukuzumi, S.; D'Souza, F. *J. Phys. Chem. C.* **2014**, *118*, 2321-2332.
29. Guldi, D. M.; Costa, R. D. *J. Phys. Chem. Lett.* **2013**, *4*, 1489-1501.
30. Sessler, J. L.; Wang, B.; Harriman, A. *J. Am. Chem. Soc.* **1993,** *115*, 10418-10419.
31. Sessler, J. L.; Jayawickramarajah, J. *Chem. Comm.* **2005**, 1939-1949.
32. Simonsen, K. B.; Becher, J. *Synlett* **1997**, 1211-1220.
33. Matsuo, Y.; Maruyama, M.; Gayathri, S. S.; Uchida, T.; Guldi, D. M.; Kishida, H.; Nakamura, A.; Nakamura, E. *J. Am. Chem. Soc.* **2009**, *131*, 12643-12649.
34. Brunetti, F. G.; Romero-Nieto, C.; López-Andarias, J.; Atienza, C.; López, J. L.; Guldi, D. M.; Martín, N. *Angew. Chem. Int. Ed.* **2013**, *52*, 2180-2184.
35. Romero-Nieto, C.; Medina, A.; Molina-Ontoria, A.; Claessens, C. G.; Echegoyen, L.; Martín, N.; Torres, T.; Guldi, D. M. *Chem. Comm.* **2012**, *48*, 4953-4955.
36. Nielsen, K. A.; Cho, W.-S.; Jeppesen, J. O.; Lynch, V. M.; Becher, J.; Sessler, J. L. *J. Am. Chem. Soc.* **2004**, *126*, 16296-16297.
37. Park, J. S.; Le Derf, F.; Bejger, C. M.; Lynch, V. M.; Sessler, J. L.; Nielsen, K. A.; Johnsen, C.; Jeppesen, J. O. *Chem. Eur. J.* **2010**, *16*, 848-854.
38. Park, J. S.; Karnas, E.; Ohkubo, K.; Chen, P.; Kadish, K. M.; Fukuzumi, S.; Bielawski, C. W.; Hudnall, T. W.; Lynch, V. M.; Sessler, J. L. *Science* **2010**, *329*, 1324-1327.
39. Kim, D. S.; Lynch, V. M.; Park, J. S.; Sessler, J. L. *J. Am. Chem. Soc.* **2013**, *135*, 14889-14894.
40. Fukuzumi, S.; Ohkubo, K.; Kawashima, Y.; Kim, D. S.; Park, J. S.; Jana, A.; Lynch, V. M.; Kim, D.; Sessler, J. L. *J. Am. Chem. Soc.* **2011**, *133*, 15938-15941.
41. Nielsen, K. A.; Levillain, E.; Lynch, V. M.; Sessler, J. L.; Jeppesen, J. O. *Chem. Eur. J.* **2009**, *15*, 506-516.
42. Jana, A.; Ishida, M.; Kwak, K.; Sung, Y. M.; Kim, D. S.; Lynch, V. M.; Lee, D.; Kim, D.; Sessler, J. L. *Chem. Eur. J.* **2013**, *19*, 338-349.
43. Becher, J.; Brimert, T.; Jeppesen, J. O.; Pedersen, J. Z.; Zubarev, R.; Bjornholm, T.; Reitzel, N.; Jensen, T. R.; Kjaer, K.; Levillain, E. *Angew. Chem. Int. Ed.* **2001**, *40*, 2497-2500.
44. Li, H.; Jeppesen, J. O.; Levillain, E.; Becher, J. *Chem. Comm.* **2003**, 846-847.
45. Bill, N. L.; Ishida, M.; Bähring, S.; Lim, J. M.; Lee, S.; Davis, C. M.; Lynch, V. M.; Nielsen, K. a.; Jeppesen, J. O.; Ohkubo, K.; Fukuzumi, S.; Kim, D.; Sessler, J. L. *J. Am. Chem. Soc.* **2013**, *135*, 10852-1085262.
46. Nielsen, K. A.; Cho, W. S.; Lyskawa, J.; Levillain, E.; Lynch, V. M.; Sessler, J. L.; Jeppesen, J. O. *J. Am. Chem. Soc.* **2006**, *128*, 2444-2451.

47. Custelcean, R.; Delmau, L. H.; Moyer, B. A.; Sessler, J. L.; Cho, W.-S.; Gross, D. E.; Bates, G. W.; Brooks, S. J.; Light, M. E.; Gale, P. A. *Angew. Chem. Int. Ed.* **2005**, *44*, 2537-2542.
48. Sessler, J. L.; Gross, D. E.; Cho, W.-S.; Lynch, V. M.; Schmidtchen, F. P.; Bates, G. W.; Light, M. E.; Gale, P. A. *J. Am. Chem. Soc.* **2006**, *128*, 12281-12288.
49. Kojima, T.; Honda, T.; Ohkubo, K.; Shiro, M.; Kusukawa, T.; Fukuda, T.; Kobayashi, N.; Fukuzumi, S. *Angew. Chem. Int. Ed.* **2008**, *47*, 6712-6716.
50. Osuka, A.; Noya, G.; Taniguchi, S.; Okada, T. *Chem. Eur. J.* **2000**, *6*, 33-46.
51. Winters, M. U.; Pettersson, K.; Mårtensson, J.; Albinsson, B. *Chemistry* **2005**, *11*, 562-573.
52. Kilså, K.; Kajanus, J.; Macpherson, a. N.; Mårtensson, J.; Albinsson, B. *J. Am. Chem. Soc.* **2001**, *123*, 3069-3080.
53. Andersson, M.; Linke, M.; Chambron, J.-C.; Davidsson, J.; Heitz, V.; Hammarström, L.; Sauvage, J.-P. *J. Am. Chem. Soc.* **2002**, *124*, 4347-4362.
54. Fukuzumi, S.; Ohkubo, K.; E, W.; Ou, Z.; Shao, J.; Kadish, K. M.; Hutchison, J. a.; Ghiggino, K. P.; Sintic, P. J.; Crossley, M. J. *J. Am. Chem. Soc.* **2003**, *125*, 14984-14985.
55. Ohkubo, K.; Sintic, P. J.; Lemmetyinen, H.; Ou, Z.; E, W.; Shao, J.; Kadish, K. M.; Crossley, M. J.; Fukuzumi, S. *Chem. Phys.* **2006**, *326*, 3-14.
56. Honda, T.; Nakanishi, T.; Ohkubo, K.; Kojima, T.; Fukuzumi, S. *J. Am. Chem. Soc.* **2010**, *132*, 10155-10163.
57. Hutchison, J. A.; Sintic, P. J.; Brotherhood, P. R.; Scholes, C.; Blake, I. M.; Ghiggino, K. P.; Crossley, M. J. *J. Phys. Chem. C.* **2009**, *113*, 11796-11804.
58. Takai, A.; Gros, C. P.; Barbe, J.-M.; Fukuzumi, S. *Phys. Chem. Chem. Phys.* **2010**, *12*, 12160-12168.
59. *The Porphyrin Handbook: Phthalocyanines: Spectroscpic and Electrochemical Characterization*. Elsevier Science: USA, 2003; Vol. 16.
60. Steed, J. W.; Atwood, J. L. *Supramolecular Chemistry*. John Wiley & Sons, LTD: USA, 2009.
61. Ohkubo, K.; Kawashima, Y.; Fukuzumi, S. *Chem. Comm.* **2012**, *48*, 4314-4316.
62. Corey, E. J.; Gross, A. W. *Org. Synth.* **1987**, *65*, 166-170.
63. Gouterman, M.; Khalil, G. E. *J. Mol. Spectroscopy* **1974**, *53*, 88.
64. Harriman, A. *J.C.S. Faraday I* **1980**, *76*, 1978-1985.
65. Kawashima, Y.; Ohkubo, K.; Fukuzumi, S. *J. Phys. Chem. A.* **2012**, *116*, 8942-8948.
66. Fukuzumi, S.; Ohkubo, K.; Zheng, X.; Chen, Y.; Pandey, R. K.; Zhan, R.; Kadish, K. M. *J. Phys. Chem. B.* **2008**, *112*, 2738-2746.
67. Murakami, M.; Ohkubo, K.; Nanjo, K.; Souma, K.; Suzuki, N.; Fukuzumi, S. *Chem. Phys. Chem.* **2010**, *11*, 2594-2605.
68. Lou, Y.; Chang, J.; Jorgensen, J.; Lemal, D. M. *J. Am. Chem. Soc* **2002**, *124*, 15302-15307.
69. Filatov, M. A.; Cheprakov, A. V.; Beletskaya, I. P. *J. Org. Chem.* **2007**, *2007*, 3468-3475.

70. Roznyatovskiy, V. *From Old Porphyrins to Novel Materials*. University of Texas at Austin, Texas, 2011.
71. Filatov, M. A.; Cheprakov, A. V. *Tetrahedron* **2011**, *67*, 3559-3566.
72. Sessler, J. L.; Roznyatovskiy, V.; Lynch, V. M. *J. Porphyr. Phthalocyan.* **2009**, *13*, 322-325.
73. Cheprakov, A. V. *J. Porphyr. Phthalocyan.* **2009**, *13,* 291.
74. Li, X.; Tanasova, M.; Vasileiou, C.; Borhan, B. *J. Am. Chem. Soc.* **2008**, *130*, 1885-1893.
75. Matile, S.; Berova, N.; Nakanishi, K. *J. Am. Chem. Soc.* **1995**, *117*, 7021-7022.

Chapter 4

Uses of Tetrathiafulvalene Derivatives as Redox Active Agents

4.1 Introduction

Tetrathiafulvalene (TTF), along with its derivatives, has attracted considerable interest for applications in molecular electronics,[1] superconducting materials,[1] electrochromic systems,[2] as well as effecting conformational control[3] and in stabilizing conductive states.[4] A more comprehensive background on TTF and its applications is included in Chapter 1 of this dissertation. This brief chapter will summarize collaborative work towards two of these uses, namely a TTF-modified Schiff-base calixpyrrole for the stabilization of a mixed-valence (MV) TTF dimer and a π-extended TTF BODIPY as a redox-switched emissive system.

4.2 Tetrathiafulvalene modified Schiff-base Calixpyrrole*

The ability to stabilize a TTF dimer would allow for multiple oxidations states of TTF to be achieved in addition to the radical cation and dication by allowing for interaction between two or more TTF moieties. These species include the MV dimer $[TTF_2]^{\bullet+}$ as well as the π-dimer $[TTF^{\bullet+}]_2$. The MV dimer is known to imitate the active

* Parts of this section were taken with permission from Bejger, C.; Davis, C. M.; Park, J. S.; Lynch, V. M.; Love, J. B.; Sessler, J. L. *Org Lett.,* **2011,** *13*, 4902-4905. Copyright 2011 American Chemical Society. Synthesis, UV-Vis, CV, and crystal growth were done by CB. EPR was done by CMD and CB. Crystallographic analysis was performed by VML. The first draft of this paper was written by CB with help from CMD. The final polishing was performed by JLS.

species seen in solid-state TTF-based conductive materials.[4-6] Therefore, the ability to stabilize such a state in solution would provide a step towards the development of supramolecular complexes that could act as switches to turn on or turn off the conductive properties of a synthetic assembly.[4,7-9] In order to achieve this stabilization, we decided to modify a Schiff-base calixpyrrole with TTF units, which, upon metal complexation, would allow for interactions between the TTF moieties.

The Schiff-base calixpyrrole used in this study (**4.1** in Figure 4.1) is an extended calix[4]pyrrole modified with four intervening azomethine groups, also known as Schiff-bases,[10] two on either side of each dipyrromethane component. This macrocycle, first reported independently by The Sessler[11] and Love[12] research groups in 2003, was designed by the Austin team to bind larger anions than its smaller analogue, calix[4]pyrrole.[11] This Schiff-base macrocycle became well known for its ability to coordinate transition metals,[12-14] lanthanides,[15] and actinides[15-17] via conformational changes to induce what is referred to as a "Pacman" conformation.[4,14]

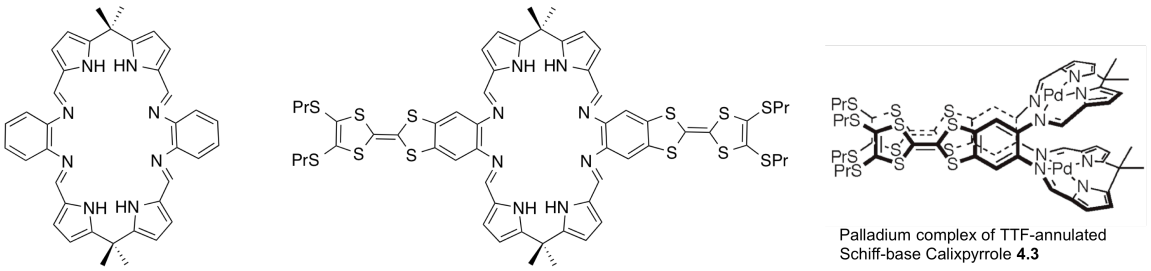

Figure 4.1 Structures of Schiff-base calixpyrrole **4.1** and the tetrathiafulvalene (TTF) derivative **4.2** as the free ligand and as the palladium complex **4.3**. Structure **4.3** reprinted with permission from *Org. Lett.* **2011**, *13*, 4902-4905. Copyright 2011 American Chemical Society.

In 2010, the Sessler group synthesized a Schiff-base calixpyrrole containing TTF moieties on either end of the azomethine group functionality in an effort to stabilize the mixed-valence dimer $[TTF_2]^{\bullet+}$ (**4.2** in Figure 4.1).[4] Palladium metalation of **4.2** using palladium acetate in the presence of triethylamine allowed for the formation of the bis-Pd(II) complex **4.3**. The metal complexation of palladium by the TTF-Schiff-base induced the conformational change to the Pacman conformation confirmed via X-ray crystallography, resulting in the two TTF units stacking in a face-to-face fashion with a distance of 3.65 Å between the TTF mean planes. Due to the close proximity of the TTF moieties, we believed it would prove possible to oxidize the TTF dimer by one electron to afford a stabilized MV radical dimer in solution.

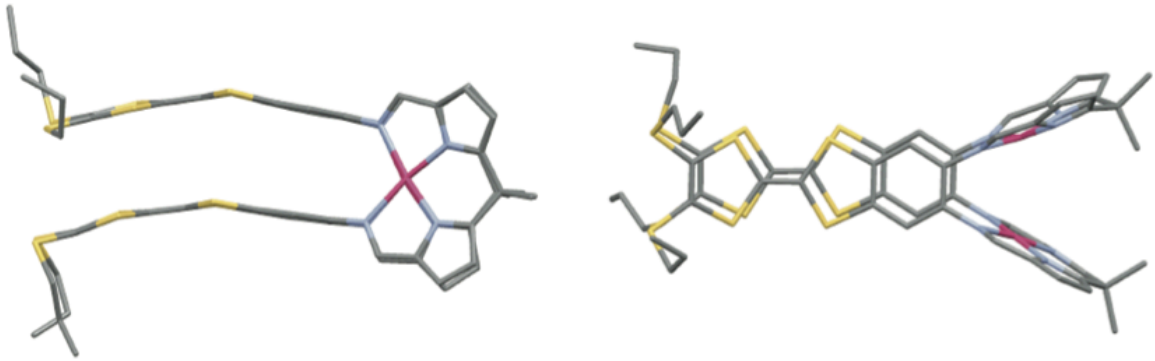

Figure 4.2 X-ray structure of **4.3**·CH_2Cl_2 (top and side views). Solvent and hydrogen atoms are omitted for clarity. Sulfur atoms are shown in yellow, nitrogen atoms in blue, carbon in gray, and palladium centers in magenta. Figures reprinted with permission from *Org. Lett.* **2011**, *13*, 4902-4905. Copyright 2011 American Chemical Society.

Evidence for the stabilization of the MV state came from an analysis of the electrochemical behavior of **4.2** and **4.3**. In the case of **4.2**, the TTF units are separated through space and do not interact with each other. Due to this lack of communication between the two TTF moieties, the first oxidation at 590 mV and second oxidation at 990

mV of both TTF moieties occur concurrently (Figure 4.3a). In contrast, the CV of **4.3** shows three peaks, one at 490, one at 600 and one at 1130 mV (Figure 4.3b). It was concluded that the two peaks at 430 and 600 mV corresponded to two one-electron oxidations, seen as one two-electron oxidation at 590 mV in the case of **4.2**. This assignment was rationalized in terms of structure. Specifically, it was suggested that due to the face-to-face orientation of the TTF units within **4.3** and the small distance separating these two TTF units intra-subunit communication would be possible. This, in turn, would allow the first oxidations of each TTF to occur in a stepwise manner.

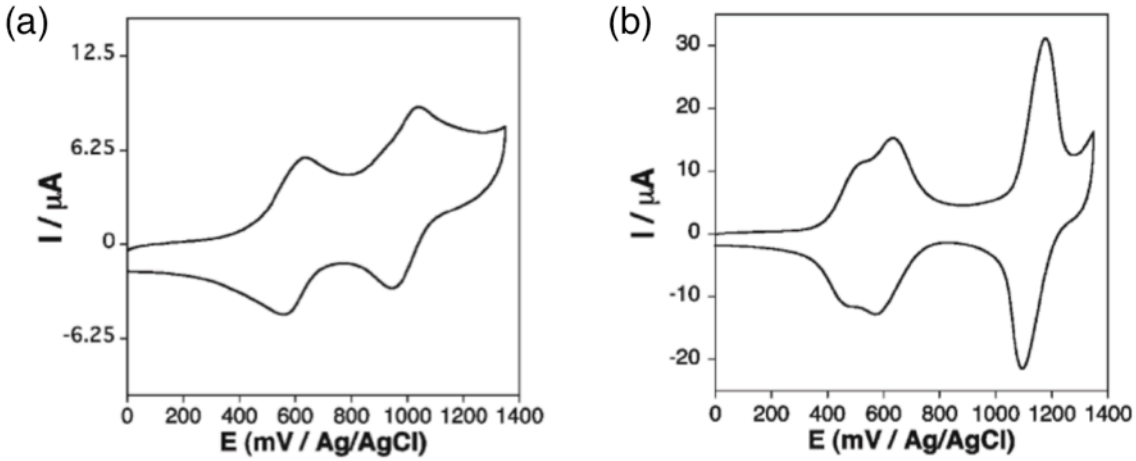

Figure 4.3 Cyclic voltammograms (CVs) of (a) **4.2** and (b) **4.3** at 2.5 mM in dichloromethane using tetrabutylammonium hexafluorophosphate as the supporting electrolyte, glassy carbon as the working electrode, and platinum as the counter electrode. Potentials measured against Ag/AgCl reference electrode at 100 mV/s. Figures reprinted with permission from *Org. Lett.* **2011**, *13*, 4902-4905. Copyright 2011 American Chemical Society.

Further support for the suggestion that a MV radical dimer is being formed came from ESR analysis of a solution of **4.3** in dichloromethane at 298 K upon addition of the oxidant tris(4-bromophenyl)aminium hexachloridoantimonate ("magic blue"). As can be

seen from an inspection of Figure 4.4, upon addition of magic blue from 0-4.0 equivalent a radical signal appears in the ESR spectrum. The maximum peak intensity is seen at 1 equivalent, a finding consistent with the formation of a one-electron oxidized species. Additional chemical oxidant up to 2 equivalents led to a decrease in signal intensity. This is consistent with the formation of an ESR silent spin-paired π-dimer $(TTF^{\bullet+})_2$. Adding more than 2 equivalents of magic blue resulted in "messy" ESR spectra. In particular, a shoulder type signature is seen. Such a feature is thought to reflect the presence of non-paired radical species within the complex.

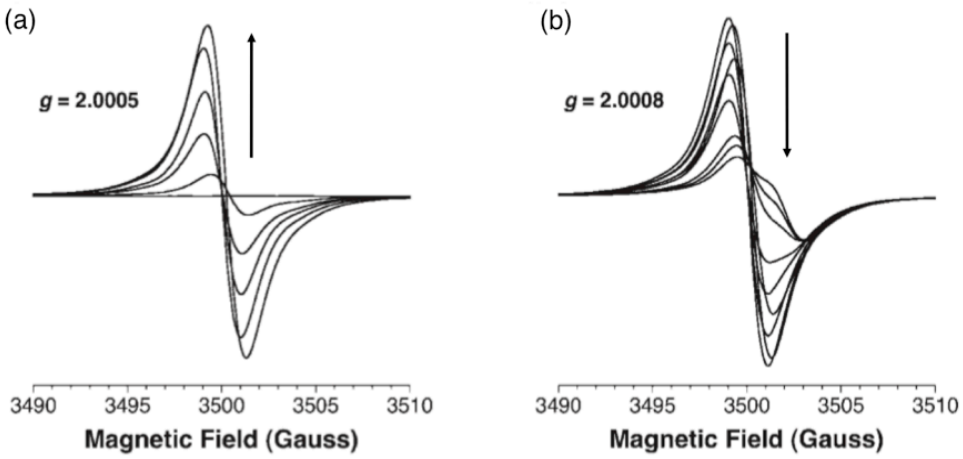

Figure 4.4 Electron spin resonance spectra of **4.3** (0.2 mM in dichloromethane at 295 K) recorded upon oxidation with (a) 0-1.0 equivalents and (b) 1.0-4.0 equivalents of magic blue. Figures reprinted with permission from *Org. Lett.* **2011**, *13*, 4902-4905. Copyright 2011 American Chemical Society.

Upon using the same titration conditions but employing **4.2** rather than **4.3**, a radical signal maximum was seen at 2 equivalents (Figure 4.5). This difference is due to the fact that in **4.2**, the two TTF moieties do not interact due to their spatial separation from one another; therefore, two equivalents are required in order to fully oxidize both TTF units to the radical cation since neither is oxidized preferentially over the other. This

behavior is also seen in the CV where the two one-electron oxidations take place at a single potential. However, in the case of **4.3**, since the two TTFs are close together they can interact and thereby stabilize the MV state. Such a conclusion is supported the CV analysis (*vide supra*), wherein a splitting of the first electron oxidation peak is seen.

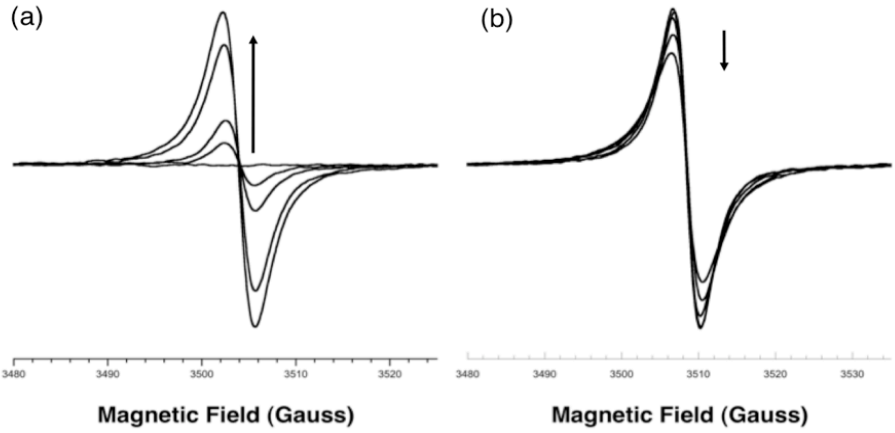

Figure 4.5 Electron spin resonance spectra of **4.2** (0.2 mM in dichloromethane at 295 K) recorded upon oxidation with (a) 0-2.0 equivalents and (b) 2.0-4.0 equivalents of magic blue. Figures reprinted with permission from *Org. Lett.* **2011**, *13*, 4902-4905. Copyright 2011 American Chemical Society.

The MV radical dimer was also detected by UV-Vis-NIR spectroscopic titrations. This was done by monitoring the signature absorption bands at 925 and 2000 nm[18] that appear upon oxidation of **4.3** with up to 1.0 equiv of magic blue. In contrast, only the TTF radical cation spectral feature at 925 nm was seen for **4.2** upon exposure to a maximum of 2 equiv of oxidant (Figure 4.6).

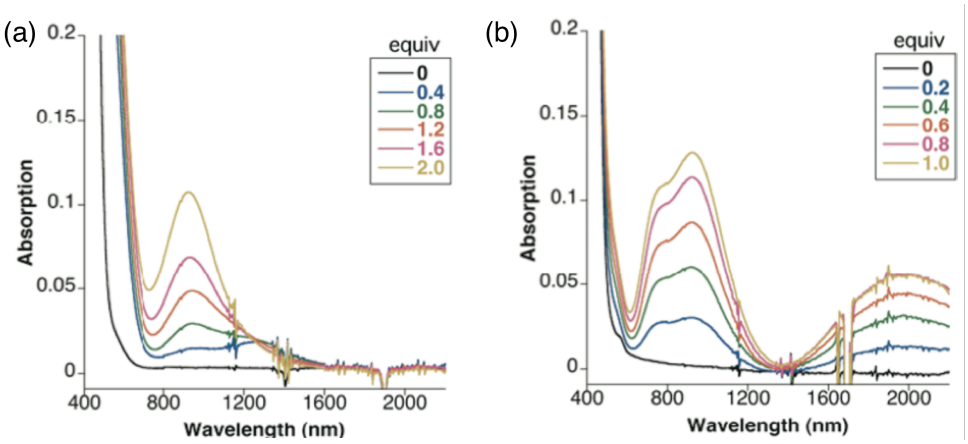

Figure 4.6 UV-Vis-NIR spectra of (a) **4.2** and (b) **4.3** as 0.2 mM solutions in dichloromethane recorded upon the stepwise oxidation with magic blue at room temperature. Figures reprinted with permission from *Org. Lett.* **2011**, *13*, 4902-4905. Copyright 2011 American Chemical Society.

4.2 π-Extended Tetrathiafulvalene BODIPY**

Materials that are able to absorb and/or emit light in the NIR region of the electromagnetic spectrum are of inherent interest due to their applicability in materials science, biochemistry, and medicinal applications.[19-21] NIR active systems with emission features that are tunable through external stimuli could be implemented as biological sensors or as light sources at useful telecommunication signaling wavelengths.[19-21] In this section efforts to create one such system are presented. Specifically as detailed below, upon substitution of a boradiazaindacene (BODIPY) with TTF units, it was found that a three-state organic system displaying redox-switchable "on—off—on" fluorescence in the NIR region could be created.

** Parts of this section were taken with permission from Bill, N. L.; Lim, J. M.; Davis, C. M.; Bähring, S.; Jeppesen, J. O.; Kim, D.; Sessler, J. L. *Chem. Comm.* **2014**, *50*, 6758-6761. Copyright 2014 The Royal Chemical Society. Synthesis was done by NBL and SB. CV was done by NLB. UV-Vis and fluorescence were done by NLB, JML, and CMD. The first draft of this paper was written by NLB. The final editing was done by JLS, DK, and JOJ.

BODIPYs are dyes that are well known for their large absorption coefficients, high fluorescent quantum yields, and photo-stability.[22] The addition of 2-methylene-1,3-dithiolidene rings at the alpha position of BODIPY pyrroles leads to a π-extended type moiety wherein the BODIPY core was imbedded within a TTF unit (**4.4**, Figure 4.7). The extension of the π-conjugated system within the dye moiety serves to lower the energy gap between the highest occupied and lowest unoccupied molecular orbitals (HOMO and LUMO), as seen by density functional theory (DFT) calculations. This decrease in band gap serves to shift the absorbance and fluorescence features of the dye well into the NIR spectral region. The resulting so-called ex-TTF-BODIPY was proved capable of undergoing one and two electron oxidations to the radical cation and dication, respectively. This feature, which mirrors what is seen with TTFs in general, allows for the manipulation of the fluorescent output of the dye.

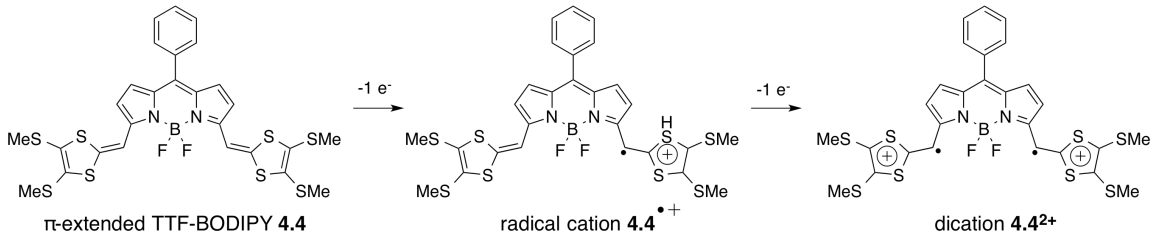

Figure 4.7 Stepwise oxidation of π-extended TTF-BODIPY **4.4** to the corresponding radical cation **4.4**$^{\bullet+}$ and dication **4.4**$^{2+}$.

The stepwise oxidation of **4.4** from 0-2 equiv of oxidant lead to dramatic changes in the UV-Vis-NIR absorption spectra of the molecule as seen in Figure 4.8a. These changes are attributed to the formation of the TTF radical cation upon treatment with one equiv of oxidant as seen by the increase in absorbance bands at 886 and 1572 nm.[18] The subsequent formation of the dication upon the addition of 1.0 more equiv of oxidant led to absorption at 1032 nm.

Upon photoexcitation of **4.4** at 754 nm in dichloromethane at 298 K a strong fluorescence at 803 nm was seen (in Figure 4.8b). The estimated quantum yield of this low energy fluorescence was calculated to be 0.43. The radical cation **4.4**$^{\bullet+}$ formed upon addition of one equivalent of magic blue produces no obvious fluorescent features upon photoexcitation at 442 nm. However, dication **4.4**$^{+}$ produced upon exposure to a second equiv of magic blue is characterized by a fluorescent feature that spans from the 950 nm to 1450 nm spectral region. However, the signal is relatively weak (quantum yield of 4.8×10^{-4}). The weak nature of the fluorescence is rationalized in terms of a heavy atom effect from the counter anion hexachloridoantimonate, as well as to an increase in molecular rotation and the charges present on the dithiolium rings.

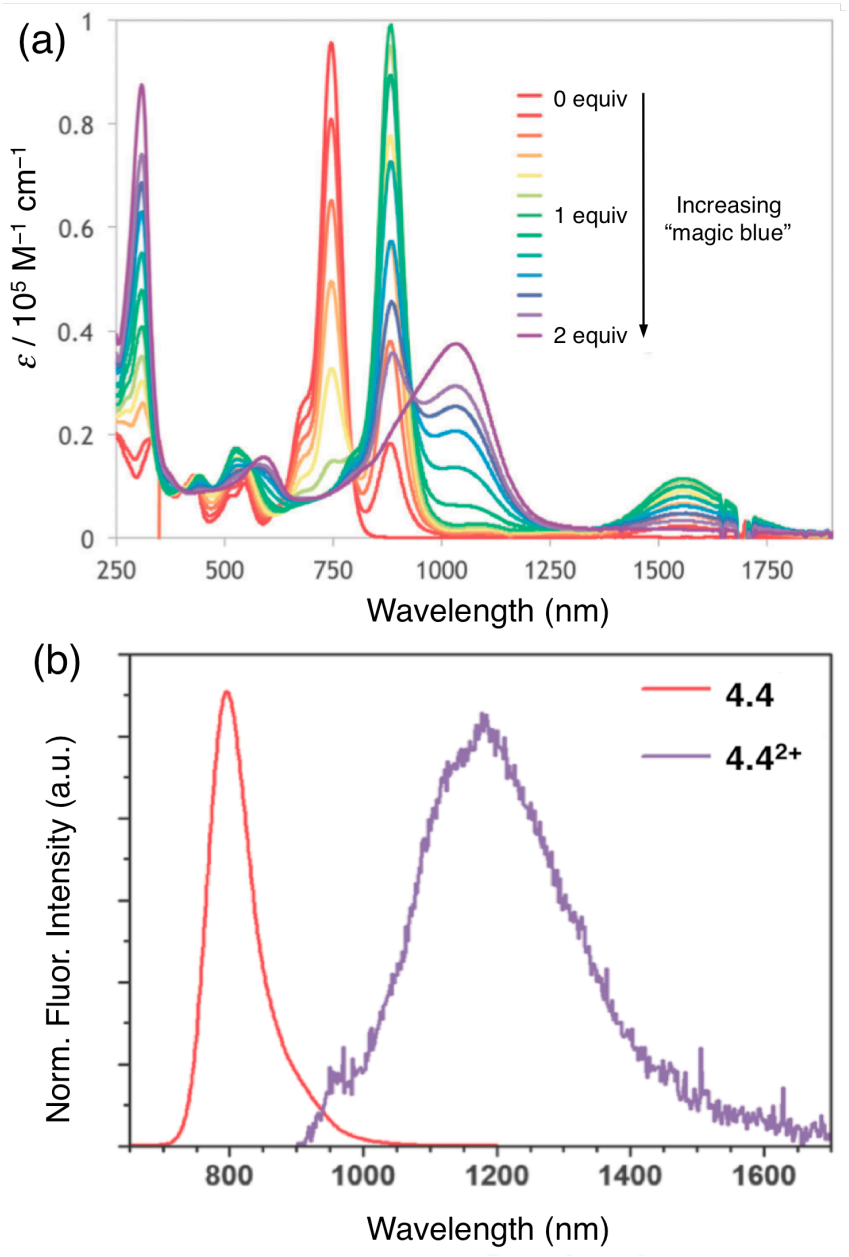

Figure 4.8 (a) Oxidative titrations of **4.4** with magic blue in dichloromethane at 298 K. Of particular note are the spectra of pristine **4.4** (red), recorded after one molar equivalent of oxidant yielding $\mathbf{4.4}^{\bullet+}$ (yellow), and that after two equivalents of oxidant yielding $\mathbf{4.4}^{2+}$ (violet). (b) Emission spectra of **4.4** (red) and $\mathbf{4.4}^{2+}$ (violet) recorded in dichloromethane at 298 K upon excitation at 442 nm. Figures reprinted with permission from *Chem. Comm.* **2014**, *50*, 6758-6761. Copyright 2014 The Royal Society of Chemistry.

This π-extended TTF-BODIPY displays electro-chromic and electro-fluorochromic behavior that extends well into the NIR region of the electromagnetic spectrum. Moreover, to the best of our knowledge, it has the longest wavelength emission and one of the longest wavelength absorptions for a BODIPY derivative reported to date.[23-26]

4.3 CONCLUSIONS

In summary, by substituting TTF onto various molecular systems, one can use oxidation and reduction of TTF for applications such as molecular stabilization, conformational control, and electrochromic manipulation. Two such examples were described in this chapter.

The addition of TTF units onto a Schiff-base calixpyrrole allowed for the stabilization of a TTF mixed valence radical state under solution phase conditions upon oxidation. As the free base, the two TTF units acted as independent species. However, insertion of palladium led to preorganization of the macrocycle and resulted in vastly different electrochemical behavior. Specifically, the binding of two palladium atoms within the Schiff-base core serves to stabilize the "Pacman" conformer of the macrocycle. In this arrangement the TTF units are stalked next to one another allowing them to interact. As a consequence, a MV radical state is stabilized, as detected via CV as well as ESR and UV-Vis-NIR spectral studies.

By substituting a well-known fluorescent dye, BODIPY, with TTF moieties, a redox active dye was produced. This ex-TTF-BODIPY dye displayed electro-chromic and electro-fluorochromic behavior that was drastically red shifted from the corresponding unsubstituted BODIPY. Upon one-electron oxidation the initial

fluorescent compound lost its luminescence. Some of the emission features were regained upon subjecting the initial oxidized species to a further one-electron oxidation. Both fluorescent outputs were in the NIR region of the electromagnetic spectrum. This makes the ex-TTF-BODIPY attractive for use in biochemical sensing or telecommunication applications where NIR emissive features are desirable. The behavior of this redox switched "on—off—on" fluorescence was studied via CV, UV-Vis-NIR and fluorescence spectroscopies, and theoretical analyses.

4.4 EXPERIMENTAL METHODS

General chemicals of the best grade available were purchased from commercial suppliers and used without further purification. Syntheses of TTF-annulated Schiff-base calix[4]pyrrole **4.2** and its palladium complex **4.3** were performed by Christopher Bejger following a published procedure.[4] The ex-TTF-BODIPY **4.4** was synthesized by Nathan Bill following a published procedure.[2]

4.4.1 Instrumentation

UV-Vis-NIR absorption spectra were recorded on a BECKMAN DU 630B (**4.2** and **4.3**) and a Cary 5000 spectrometer (**4.4**) in a 1 cm quartz cuvette. Cyclic voltammetry (CV) studies were carried out using a CV-50W Voltammetric Analyzer in deaerated dichloromethane containing either 0.2 M (for **4.2** and **4.3**) or 0.1 M (for **4.4**) $TBAPF_6$ as the a supporting electrolyte at 298 K. A conventional three-electrode cell was used with a glassy carbon probe as the working electrode and a platinum wire as the counter electrode. The potentials were measured with respect to an Ag/AgCl reference electrode. Electron spin resonance (ESR) spectra were recorded on a Bruker EMX Plus spectrometer at room temperature in dichloromethane. Steady-state fluorescence spectra in NIR region were recorded using photomultiplier tubes (Hamamatsu, H9170-75 and R5108), a lock-in amplifier (EG&G, 5210) combined with a mechanical chopper and a CW He-Cd laser (Melles Griot, Omnichrome 74) for photo-excitation at 442 nm. Quantum mechanical calculations were performed with the Gaussian 09 program suite. All optimization calculations were carried out using density functional theory (DFT) B3LYP employing the 6-31G(d,p) basis set. In the cases of oxidized forms ($\mathbf{4.4^{\bullet+}}$ and $\mathbf{4.4^{2+}}$), the possible spin states and multiplicities were estimated.

4.5 CHAPTER 4 REFERENCES

1. Becher, J.; Li, Z.-T.; Blanchard, P.; Svenstrup, N.; Lau, J.; Nielsen, K. A.; Leriche, P. *Pure Appl. Chem.* **1997**, *69*, 465-470.
2. Bill, N. L.; Lim, J. M.; Davis, C. M.; Bähring, S.; Jeppesen, J. O.; Kim, D.; Sessler, J. L. *Chem. Comm.* **2014**, *50*, 6758-6761.
3. Jana, A.; Ishida, M.; Cho, K.; Ghosh, S. K.; Kwak, K.; Ohkubo, K.; Sung, Y. M.; Davis, C. M.; Lynch, V. M.; Lee, D.; Fukuzumi, S.; Kim, D.; Sessler, J. L. *Chem. Comm.* **2013**, *49*, 8937-8939.
4. Bejger, C.; Davis, C. M.; Park, J. S.; M Lynch, V.; Love, J. B.; Sessler, J. L. *Org. Lett.* **2011,** *13*, 4902-5.
5. Batail, P., Ed. *Chem. Rev.* **2004**, *104*, 4887-5781.
6. Tanaka, K.; Matsumoto, T.; Ishiguro, F.; Chujo, Y. *J. Mater. Chem.* **2011,** *21*, 9603-9607.
7. Cheng, P. N.; Chiang, P. T.; Chiu, S. H. *Chem. Comm.* **2005**, 1285-1287.
8. Frei, M.; Diederich, F.; Tremont, R.; Echegoyen, L. *Helv. Chim. Acta.* **2006**, *89*, 2040-2058.
9. Park, J. S.; Karnas, E.; Ohkubo, K.; Chen, P.; Kadish, K. M.; Fukuzumi, S.; Bielawski, C. W.; Hudnall, T. W.; Lynch, V. M.; Sessler, J. L. *Science* **2010**, *329*, 1324-1327.
10. IUPAC, Compendium of Chemical Terminology, 2nd ed. (the "Gold Book") (1997). Online corrected version: (2006–).
11. Sessler, J. L.; Cho, W.-S.; Dudek, S. P.; Hicks, L.; Lynch, V. M.; Huggins, M. T. *J. Porphyrins Phthalocyanines* **2003**, *7*, 97-104.
12. Givaja, G.; Blake, A. J.; Wilson, C.; Schröder, M.; Love, J. B. *Chem. Comm.* **2003**, 2508-2509.
13. Veauthier, J. M.; Tomat, E.; Lynch, V. M.; Sessler, J. L.; Mirsaidov, U.; Markert, J. T. *Inorg. Chem.* **2005,** *44*, 6736-6743.
14. Love, J. B. *Chem. Comm.* **2009**, 3154-3165.
15. Arnold, P. L.; Potter, N. A.; Carmichael, C. D.; Slawin, A. M. Z.; Roussel, P.; Love, J. B. *Chem. Comm.* **2010**, 1833-1835.
16. Arnold, P. L.; Blake, A. J.; Wilson, C.; Love, J. B. *Inorg. Chem.* **2004**, *43*, 8206-8208.
17. Arnold, P. L.; Patel, D.; Pécharman, A.-F.; Wilson, C.; Love, J. B. *Dalton Trans.* **2010**, *39*, 3501-3508.
18. Spanggard, H.; Prehn, J.; Nielsen, M. B.; Levillain, E.; Allain, M.; Becher, J. *J. Am. Chem. Soc* **2000**, *122*, 9486-9494.
19. Qian, G.; Wang, Z. Y. *Chem. - Asian J.* **2010**, *5*, 1006-1029.
20. Luo, S.; Zhang, E.; Su, Y. Q.; Cheng, T.; Shi, C. *Biomaterials* **2011**, *32*, 7127-7138.
21. Pansare, V. J.; Hejazi, S.; Faenza, W. J.; Prud'homme, R. K. *Chem. Mater.* **2012**, *24*, 812-827.

22. Loudet, A.; Burgess, K. *Chem. Rev.* **2007**, *107*, 4891-4932.
23. McDonnel, S. O.; O'Shea, D. F. *Org. Lett.* **2006**, *8*, 3493-3496.
24. Jiao, C.; Huwant, K.-W.; Wu, J. *Org. Lett.* **2011**, *13*, 632-635.
25. Nakamura, M.; Tahara, H.; Takahashi, K.; Nagata, T.; Uoyama, H.; Kuzuhara, D.; Mori, S.; Okujima, T.; Yamada, H.; Uno, H. *Org Biomol. Chem.* **2012**, *10*, 6840-6849.
26. Wakamiya, A.; Murakami, T.; Yamaguchi, S. *Chem. Sci.* **2013**, *4*, 1002-1007.

References

1. Andersson, M.; Linke, M.; Chambron, J.-C.; Davidsson, J.; Heitz, V.; Hammarström, L.; Sauvage, J.-P. J. *Am. Chem. Soc.* **2002**, *124*, 4347-4362.
2. Anslyn, E. V.; Dougherty, D. A. Modern Physical Organic Chemistry. University Science Books: USA, 2006.
3. Arnold, P. L.; Blake, A. J.; Wilson, C.; Love, J. B. *Inorg. Chem.* **2004**, *43*, 8206-8208.
4. Arnold, P. L.; Patel, D.; Pécharman, A.-F.; Wilson, C.; Love, J. B. *Dalton Trans.* **2010**, *39*, 3501-3508.
5. Arnold, P. L.; Potter, N. A.; Carmichael, C. D.; Slawin, A. M. Z.; Roussel, P.; Love, J. B. *Chem. Comm.* **2010**, 1833-1835.
6. Baeyer, A. *Ber. Dtsch. Chem. Ges.* **1886**, 19.
7. Ballardini, R.; Balzani, V.; Clemente-León, M.; Credi, A.; Gandolfi, M. T.; Ishow, E.; Perkins, J.; Stoddart, J. F.; Tseng, H.-R.; Wenger, S. *J. Am. Chem. Soc.* **2002**, *124*, 12786-12795.
8. Bandi, V.; El-Khouly, M. E.; Nesterov, V. N.; Karr, P. A.; Fukuzumi, S.; D'Souza, F. *J. Phys. Chem. C.* **2013**, *117*, 5638-5649.
9. Bandi, V.; El-Khouly, M. E.; Ohkubo, K.; Nesterov, V. N.; Zandler, M. E.; Fukuzumi, S.; D'Souza, F. J. *Phys. Chem. C.* **2014**, *118*, 2321-2332.
10. Batail, P., Ed. *Chem. Rev.* **2004**, *104*, 4887-5781.
11. Becher, J.; Brimert, T.; Jeppesen, J. O.; Pedersen, J. Z.; Zubarev, R.; Bjornholm, T.; Reitzel, N.; Jensen, T. R.; Kjaer, K.; Levillain, E. *Angew. Chem. Int. Ed.* **2001**, *40*, 2497-2500.
12. Becher, J.; Li, Z.-T.; Blanchard, P.; Svenstrup, N.; Lau, J.; Nielsen, K. A.; Leriche, P. *Pure Appl. Chem.* **1997**, *69*, 465-470.
13. Bechgaard, K.; Jérome, D. *Sci. Am.* **1982**, 247, 50.
14. Beer, P. D.; Rothin, A. S. J. Chem. Soc., *Chem. Comm.* **1988**, 52-54.
15. Bejger, C.; Davis, C. M.; Park, J. S.; M Lynch, V.; Love, J. B.; Sessler, J. L. *Org. Lett.* **2011**, *13*, 4902-5.
16. Berera, R.; Grondelle, R.; Kennis, J. T. M. *Photosynth. Res.* **2009**, *101*, 105-118.
17. Berg, J. M.; Tymoczko, J. L.; Stryer, L. Biochemistry. 6 ed.; W. H. Freeman and Company: USA, 2007.
18. Bill, N. L.; Ishida, M.; Bähring, S.; Lim, J. M.; Lee, S.; Davis, C. M.; Lynch, V. M.; Nielsen, K. a.; Jeppesen, J. O.; Ohkubo, K.; Fukuzumi, S.; Kim, D.; Sessler, J. L. *J. Am. Chem. Soc.* **2013**, *135*, 10852-1085262.
19. Bill, N. B.; Ishida, M.; Kawashima, Y.; Ohkubo, K.; Sung, Y. M.; Lynch, V. M.; Lim, J. M.; Kim, D.; Sessler, J. L.; Fukuzumi, S. *Chem. Sci.* **2014**, *5*, 3888-3896.
20. Bill, N. L.; Lim, J. M.; Davis, C. M.; Bähring, S.; Jeppesen, J. O.; Kim, D.; Sessler, J. L. *Chem. Comm.* **2014**, *50*, 6758-6761.
21. Brunetti, F. G.; Romero-Nieto, C.; López-Andarias, J.; Atienza, C.; López, J. L.; Guldi, D. M.; Martín, N. *Angew. Chem. Int. Ed.* **2013**, *52*, 2180-2184.

22. Canevet, D.; Sallé, M.; Zhang, G.; Zhang, D.; Zhu, D.-B. *Chem. Comm.* **2009**, 2245-2269.
23. Cheng, P. N.; Chiang, P. T.; Chiu, S. H. *Chem. Comm.* **2005**, 1285-1287.
24. Cheprakov, A. V. *J. Porphyr. Phthalocyan.* **2009**, *13*, 291.
25. Coffen, D. L.; Q., C. J.; Williams, D. R.; Garret, P. E.; Canfield, N. D. J. *J. Am. Chem. Soc.* **1971**, *93*, 2258-2268.
26. Connors, K. A. *Binding Constants: The Measurement of Molecular Complex Stability*. John Wiley & Sons, Inc.: 1987.
27. Corey, E. J.; Gross, A. W. *Org. Synth.* **1987**, *65*, 166-170.
28. Costero, A. M.; Rodriguez, S. *Tetrahedron* **1992**, *48*, 6265-6272.
29. Crystal Clear 1.40, R. A. C., The Woodlands, Tx; 2008. DENZO-SMN. Otwinowski, Z.; Minor, W. Methods in Enzymology, 276: Macromolcular Crystallography, part A. 307-326, C. W. Carter, Jr. and R. M. Sweets, Editors, Academic Press; 1997.
30. Curiel, D.; Ohkubo, K.; Reimers, J. R.; Fukuzumi, S.; Crossley, M. *J. Phys. Chem. Chem. Phys.* **2007**, *9*, 5260-5266.
31. Custelcean, R.; Delmau, L. H.; Moyer, B. A.; Sessler, J. L.; Cho, W.-S.; Gross, D. E.; Bates, G. W.; Brooks, S. J.; Light, M. E.; Gale, P. A. *Angew. Chem. Int. Ed.* **2005**, *44*, 2537-2542.
32. D'Souza, F.; Amin, A. N.; El-Khouly, M. E.; Subbaiyan, N. K.; Zandler, M. E.; Fukuzumi, S. *J. Am. Chem. Soc.* **2011**, *134*, 654-664.
33. D'Souza, F.; Maligaspe, E.; Ohkubo, K.; Zandler, M. E.; Subbaiyan, N. K.; Fukuzumi, S. *J. Am. Chem. Soc.* **2009**, *131*, 8787-8797.
34. D'Souza, F.; Smith, P. M.; Rogers, L.; Zandler, M. E.; Islam, S. D.-M.; Araki, Y.; Ito, O. *Inorg. Chem.* **2006**, *45*, 5057-5065.
35. Davis, C. M.; Kawashima, Y.; Ohkubo, K.; Lim, J. M.; Kim, D.; Fukuzumi, S.; Sessler, J. L. *J. Phys. Chem. C.* **2014**, *118*, 13503-13513.
36. de la Escosura, A.; Martínez-Díaz, M. V.; Guldi, D. M.; Torres, T. *J. Am. Chem. Soc.* **2006**, *128*, 4112-4118.
37. Durrant, J. R.; Haque, S. A.; Palomares, E. *Chem. Comm.* **2006**, 3279-3289.
38. El-Khouly, M. E.; Kim, J. H.; Kay, K.-Y.; Choi, C. S.; Ito, O.; Fukuzumi, S. *Chem. Eur. J.* **2009**, *15*, 5301-5310.
39. Ferraris, J.; Cowan, D. O.; Walatka, V.; Peristein, J. H. *J. Am. Chem. Soc.* **1973**, *95*, 948-949.
40. Filatov, M. A.; Cheprakov, A. V. *Tetrahedron* **2011**, *67*, 3559-3566.
41. Filatov, M. A.; Cheprakov, A. V.; Beletskaya, I. P. *J. Org. Chem.* **2007**, *2007*, 3468-3475.
42. Frei, M.; Diederich, F.; Tremont, R.; Echegoyen, L. *Helv. Chim. Acta.* **2006**, *89*, 2040-2058.
43. Fritsky, I. O.; Ott, R.; Krämer, R. *Angew. Chem. Int. Ed.* **2000**, *39*, 3255-3258.
44. Fukuzumi, S. *Bull. Chem. Soc. Jpn.* **2006**, *79*, 177-195.
45. Fukuzumi, S. *Electron Transfer of π-Functional Systems and Applications*. In Functional Organic Materials, Wiley-VCH: Weinheim: 2007; pp 465-510.

46. Fukuzumi, S. *Phys. Chem. Chem. Phys.* **2008**, *10*, 2283-2297.
47. Fukuzumi, S. *Pure Appl. Chem.* **2007**, *79*, 981-991.
48. Fukuzumi, S.; Kojima, T. *J. Mater. Chem.* **2007**, *18*, 1427-1439.
49. Fukuzumi, S.; Ohkubo, K. *Dalton Trans.* **2013**, *42*, 15846-15858.
50. Fukuzumi, S.; Ohkubo, K. *J. Mater. Chem.* **2012**, *22*, 4575.
51. Fukuzumi, S.; Ohkubo, K.; D'Souza, F.; Sessler, J. L. *Chem. Comm.* **2012**, *48*, 9801-9815.
52. Fukuzumi, S.; Ohkubo, K.; E, W.; Ou, Z.; Shao, J.; Kadish, K. M.; Hutchison, J. a.; Ghiggino, K. P.; Sintic, P. J.; Crossley, M. J. *J. Am. Chem. Soc.* **2003**, *125*, 14984-14985.
53. Fukuzumi, S.; Ohkubo, K.; Kawashima, Y.; Kim, D. S.; Park, J. S.; Jana, A.; Lynch, V. M.; Kim, D.; Sessler, J. L. *J. Am. Chem. Soc.* **2011**, *133*, 15938-15941.
54. Fukuzumi, S.; Ohkubo, K.; Zheng, X.; Chen, Y.; Pandey, R. K.; Zhan, R.; Kadish, K. M. *J. Phys. Chem. B.* **2008**, *112*, 2738-2746.
55. Fukuzumi, S.; Saito, K.; Ohkubo, K.; Khoury, T.; Kashiwagi, Y.; Absalom, M. A.; Gadde, S.; D'Souza, F.; Araki, Y.; Ito, O.; Crossley, M. J. *Chem. Comm.* **2011**, *47*, 7980-7982.
56. Gale, P. A.; Anzenbacher, P.; Sessler, J. L. *Coord. Chem. Rev.* **2001**, *222*, 57-102.
57. Gale, P. A.; Sessler, J. L.; Kral, V. *Chem. Comm.* **1998**, *1*, 1-8.
58. Gale, P. A.; Sessler, J. L.; Král, V.; Lynch, V. *J. Am. Chem. Soc.* **1996**, *118*, 5140-5141.
59. Givaja, G.; Blake, A. J.; Wilson, C.; Schröder, M.; Love, J. B. *Chem. Comm.* **2003**, 2508-2509.
60. Gouterman, M.; Khalil, G. E. *J. Mol. Spectroscopy* **1974**, *53*, 88.
61. Guldi, D. M.; Costa, R. D. *J. Phys. Chem. Lett.* **2013**, *4*, 1489-1501.
62. Guldi, D. M.; Prato, M. *Acc. Chem. Res.* **2000**, *33*, 695-703.
63. Günes, S.; Neugebauer, H.; Sariciftci, N. S. *Chem. Rev.* **2007**, *107*, 1324-1338.
64. Harriman, A. J.C.S. Faraday I 1980, 76, 1978-1985.
65. Harriman, A.; Kubo, Y.; Sessler, J. L. *J. Am. Chem. Soc.* **1992**, *114*, 388-390.
66. Hasobe, T.; Saito, K.; Kamat, P. V.; Troiani, V.; Qui, H.; Solladié, N.; Kim, K. S.; Park, J. K.; Kim, D.; D'Souza, F.; Fukuzumi, S. *J. Mater. Chem.* **2007**, *17*, 4160-4170.
67. Heliatek Consolidates its Technology Leadership by Establishing a New World Record for Organic Solar Technology with a Cell Efficiency of 12%, http://www.heliatek.com/wp-content/uploads/2013/01/130116_PR_Heliatek_achieves_record_cell_effiency_for_OPV.pdf, accessed June 2014.
68. Honda, T.; Nakanishi, T.; Ohkubo, K.; Kojima, T.; Fukuzumi, S. *J. Am. Chem. Soc.* **2010**, *132*, 10155-10163.
69. Zahradnik, R.; Carsky, P.; Hünig, S.; Kiesslich, G.; Scheutzow, D. *Int. J. Sulfur. Chem. Part C.* **1971**, *6*, 109-122.
70. Hurtley, W. R. H.; Smiles, S. *J. Chem. Soc.* **1926**, 2263-2270.

71. Hutchison, J. A.; Bell, T. D. M.; Ganguly, T.; Ghiggino, K. P.; Langford, S. J.; Lokan, N. R.; Paddon-Row, M. N. J. *Photochem. Photobiol., A* **2008**, *197*, 220-225.
72. Hutchison, J. A.; Sintic, P. J.; Brotherhood, P. R.; Scholes, C.; Blake, I. M.; Ghiggino, K. P.; Crossley, M. J. *J. Phys. Chem. C*. **2009**, *113*, 11796-11804.
73. Imahori, H.; Sekiguchi, Y.; Kashiwagi, Y.; Sato, T.; Araki, Y.; Ito, O.; Yamada, H.; Fukuzumi, S. *Chem. Eur. J*. **2004**, *10*, 3184-3196.
74. IUPAC, Compendium of Chemical Terminology, 2nd ed. (the "Gold Book") (1997). Online corrected version: (2006-).
75. Jana, A.; Ishida, M.; Cho, K.; Ghosh, S. K.; Kwak, K.; Ohkubo, K.; Sung, Y. M.; Davis, C. M.; Lynch, V. M.; Lee, D.; Fukuzumi, S.; Kim, D.; Sessler, J. L. *Chem. Comm*. **2013**, *49*, 8937-8939.
76. Jana, A.; Ishida, M.; Kwak, K.; Sung, Y. M.; Kim, D. S.; Lynch, V. M.; Lee, D.; Kim, D.; Sessler, J. L. *Chem. Eur. J*. **2013**, *19*, 338-349.
77. Jérome, D.; Mazaud, A.; Ribault, M.; Bechaard, K. *J. Physique. Lett*. **1980**, *41*, 95-98.
78. Jiao, C.; Huwant, K.-W.; Wu, *J. Org. Lett*. **2011**, *13*, 632-635.
79. Kalowekamo, J.; Baker, E. *Solar Energy* **2009**, *83*, 1224-1231.
80. Kashiwagi, Y.; Ohkubo, K.; McDonald, J. A.; Blake, I. M.; Crossley, M. J.; Araki, Y.; Ito, O.; Imahori, H.; Fukuzumi, S. *Org. Lett*. **2003**, *5*, 2719-2721.
81. Kavarnos, G. J. *Fundamentals of Photoinduced Electron Transfer*. VCH Publishers, Inc.: USA, 1993.
82. Kawashima, Y.; Ohkubo, K.; Fukuzumi, S. J. *Phys. Chem. A*. **2012**, *116*, 8942-8948.
83. Kawashima, Y.; Ohkubo, K.; Kentaro, M.; Fukuzumi, S. *J. Phys. Chem. C*. **2013**, *117*, 21166-21177.
84. Kilså, K.; Kajanus, J.; Macpherson, a. N.; Mårtensson, J.; Albinsson, B. *J. Am. Chem. Soc*. **2001**, *123*, 3069-3080.
85. Kim, D. S.; Lynch, V. M.; Park, J. S.; Sessler, J. L. *J. Am. Chem. Soc*. **2013**, *135*, 14889-14894.
86. Kojima, T.; Honda, T.; Ohkubo, K.; Shiro, M.; Kusukawa, T.; Fukuda, T.; Kobayashi, N.; Fukuzumi, S. *Angew. Chem. Int. Ed*. **2008**, *47*, 6712-6716.
87. Konarev, D. V.; Khasanov, S. S.; Otsuka, A.; Maesato, M.; G., S.; Lyubovskaya, R. M. *Angew. Chem. Int. Ed*. **2010**, *49*, 4829-4832.
88. Konarev, D. V.; Kuzmin, A. V.; Simonov, S. V.; Khasanov, S. S.; Yudanova, E. I.; Lyubovskaya, R. M. *Dalton Trans*. **2011**, *40*, 4453-4458
89. Kovbasyuk, L.; Krämer, R. *Chem. Rev*. **2004**, *104*, 3161-3188.
90. Kremer, C.; Lützen, A. *Chem. Eur. J*. **2013**, *19*, 6162-6196.
91. Kubik, S. *J. Am. Chem. Soc*. **1999**, *121*, 5846-5855.
92. Lewis, N. S.; Nocera, D. G. *Proc. Natl. Acad. Sci*. **2006**, *103*, 15729-15735.
93. Li, H.; Jeppesen, J. O.; Levillain, E.; Becher, J. *Chem. Comm*. **2003**, 846-847.
94. Li, X.; Tanasova, M.; Vasileiou, C.; Borhan, B. *J. Am. Chem. Soc*. **2008**, *130*, 1885-1893.

95. Lou, Y.; Chang, J.; Jorgensen, J.; Lemal, D. M. *J. Am. Chem. Soc.* **2002**, *124*, 15302-15307.
96. Loudet, A.; Burgess, K. *Chem. Rev.* **2007**, *107*, 4891-4932.
97. Love, J. B. *Chem. Comm.* **2009**, 3154-3165.
98. Luo, S.; Zhang, E.; Su, Y. Q.; Cheng, T.; Shi, C. *Biomaterials* **2011**, *32*, 7127-7138.
99. Marcus, R. A. *Angew. Chem. Int. Ed.* **1993**, *32*, 1111-1121.
100. Marcus, R. A. *J. Chem. Phys* **1956**, *24*, 966-978.
101. Marcus, R. A.; Sutin, N. *Biochim. Biophys. Acta.* **1985**, *811*, 265-322.
102. Martín, N.; Sánchez, L.; Herranz, M. a. Á.; Illescas, B.; Guldi, D. M. *Acc. Chem. Res.* **2007**, *40*, 1015-1024.
103. Matile, S.; Berova, N.; Nakanishi, K. *J. Am. Chem. Soc.* **1995**, *117*, 7021-7022.
104. Matsuo, Y.; Maruyama, M.; Gayathri, S. S.; Uchida, T.; Guldi, D. M.; Kishida, H.; Nakamura, A.; Nakamura, E. *J. Am. Chem. Soc.* **2009**, *131*, 12643-12649.
105. McDonnel, S. O.; O'Shea, D. F. *Org. Lett.* **2006**, *8*, 3493-3496.
106. Molina-Ontoria, A.; Fernández, G.; Wielopolski, M.; Atienza, C.; Sánchez, L.; Gouloumis, A.; Clark, T.; Martín, N.; Guldi, D. M. *J. Am. Chem. Soc.* **2009**, *131*, 12218-12229.
107. Murakami, M.; Ohkubo, K.; Nanjo, K.; Souma, K.; Suzuki, N.; Fukuzumi, S. *Chem. Phys. Chem.* **2010**, *11,* 2594-2605.
108. Nabeshima, T. *Coord. Chem. Rev.* **1996**, *148*, 151-169.
109. Nabeshima, T.; Hashiguchi, A.; Yazawa, S.; Haruyama, T.; Yano, Y. *J. Org. Chem.* **1998**, *63*, 2788-2789.
110. Nakamura, M.; Tahara, H.; Takahashi, K.; Nagata, T.; Uoyama, H.; Kuzuhara, D.; Mori, S.; Okujima, T.; Yamada, H.; Uno, H. *Org Biomol. Chem. 2012*, *10*, 6840-6849.
111. Nielsen, K. A.; Cho, W. S.; Lyskawa, J.; Levillain, E.; Lynch, V. M.; Sessler, J. L.; Jeppesen, J. O. *J. Am. Chem. Soc.* **2006**, *128*, 2444-2451.
112. Nielsen, K. A.; Cho, W.-S.; Jeppesen, J. O.; Lynch, V. M.; Becher, J.; Sessler, J. L. *J. Am. Chem. Soc.* **2004**, *126*, 16296-16297.
113. Nielsen, K. A.; Cho, W.-S.; Sarova, G. H.; Petersen, B. M.; Bond, A. D.; Becher, J.; Jensen, F.; Guldi, D. M.; Sessler, J. L.; Jeppesen, J. O. *Angew. Chem. Int. Ed.* **2006**, *45*, 6848-6853.
114. Nielsen, K. A.; Levillain, E.; Lynch, V. M.; Sessler, J. L.; Jeppesen, J. O. *Chem. Eur. J.* **2009**, *15*, 506-516.
115. Nielsen, K. A.; Martín-Gomez, L.; Sarova, G. H.; Sanguinet, L.; Gross, D. E.; Fernández-Lázaro, F.; Stein, P. C.; Levillain, E.; Sessler, J. L.; Guldi, D. M.; Sastre-Santos, Á.; Jeppesen, J. O. *Tetrahedron* **2008**, *64*, 8449-8463.
116. Nielsen, K. A.; Sarova, G. H.; Martín-Gomez, L.; Fernandez-Lazaro, F.; Stein, P. C.; Sanguinet, L.; Levillain, E.; Sessler, J. L.; Guldi, D. M.; Sastre-Santos, Á.; Jeppesen, J. O. *J. Am. Chem. Soc.* **2008**, *130*, 460-462.
117. Nunzi, J.-M. *C. R. Physique* **2002**, *3*, 523-542.
118. Ohkubo, K.; Fukuzumi, S. *Bull. Chem. Soc. Jpn.* **2009**, 3279-3289.

119. Ohkubo, K.; Kawashima, Y.; Fukuzumi, S. *Chem. Comm.* **2012**, *48*, 4314-4316.
120. Ohkubo, K.; Kawashima, Y.; Sakai, H.; Hasobe, T.; Fukuzumi, S. *Chem. Comm.* **2013**, *49*, 4474-4476.
121. Ohkubo, K.; Kotani, H.; Shao, J.; Ou, Z.; Kadish, K. M.; Li, G.; Pandey, R. K.; Fujitsuka, M.; Ito, O.; Imahori, H.; Fukuzumi, S. *Angew. Chem. Int. Ed.* **2004**, *43*, 853-856.
122. Ohkubo, K.; Sintic, P. J.; Lemmetyinen, H.; Ou, Z.; E, W.; Shao, J.; Kadish, K. M.; Crossley, M. J.; Fukuzumi, S. *Chem. Phys.* **2006**, *326*, 3-14.
123. Osuka, A.; Noya, G.; Taniguchi, S.; Okada, T. *Chem. Eur. J.* **2000**, *6*, 33-46.
124. Pansare, V. J.; Hejazi, S.; Faenza, W. J.; Prud'homme, R. K. *Chem. Mater.* **2012**, *24*, 812-827.
125. Park, J. S.; Karnas, E.; Ohkubo, K.; Chen, P.; Kadish, K. M.; Fukuzumi, S.; Bielawski, C. W.; Hudnall, T. W.; Lynch, V. M.; Sessler, J. L. *Science* **2010**, *329*, 1324-1327.
126. Park, J. S.; Le Derf, F.; Bejger, C. M.; Lynch, V. M.; Sessler, J. L.; Nielsen, K. A.; Johnsen, C.; Jeppesen, J. O. *Chem. Eur. J.* **2010**, *16*, 848-854.
127. Peracchi, A.; Mozzarelli, A. *Biochim. Biophys. Acta* **2011**, *1814*, 922-33.
128. Pierre, J.-L.; Gagnaire, G.; Chautemps, P. *Tetrahedron Lett.* **1992**, *33*, 217-220.
129. Qian, G.; Wang, Z. Y. *Chem. - Asian J.* **2010**, *5*, 1006-1029.
130. Rebek, J.; Costello, T.; Wattley, R. *J. Am. Chem. Soc.* **1985**, *107*, 7487-7493.
131. Rebek, J.; Wattley, R. V. *J. Am. Chem. Soc.* **1980**, *102*, 4853-4854.
132. Romero-Nieto, C.; Medina, A.; Molina-Ontoria, A.; Claessens, C. G.; Echegoyen, L.; Martín, N.; Torres, T.; Guldi, D. M. *Chem. Comm.* **2012**, *48*, 4953-4955.
133. Roznyatovskiy, V. *From Old Porphyrins to Novel Materials*. University of Texas at Austin, Texas, 2011.
134. Schneider, H.-J.; Werner, F. *J. Chem. Soc., Chem. Comm.* **1992**, 490-491.
135. Sessler, J. L.; Cho, W.-S.; Dudek, S. P.; Hicks, L.; Lynch, V. M.; Huggins, M. T. *J. Porphyrins Phthalocyanines* **2003**, *7*, 97-104.
136. Sessler, J. L.; Gross, D. E.; Cho, W.-S.; Lynch, V. M.; Schmidtchen, F. P.; Bates, G. W.; Light, M. E.; Gale, P. A. *J. Am. Chem. Soc.* **2006**, *128*, 12281-12288.
137. Sessler, J. L.; Jayawickramarajah, J. *Chem. Comm.* **2005**, 1939-1949.
138. Sessler, J. L.; Roznyatovskiy, V.; Lynch, V. M. *J. Porphyr. Phthalocyan.* **2009**, *13*, 322-325.
139. Sessler, J. L.; Wang, B.; Harriman, A. *J. Am. Chem. Soc.* **1993**, *115*, 10418-10419.
140. Sheldrick, G. M. SHELXL97. Program for the Refinement of Crystal Structures. University of Gottingen, Germany. 1994.
141. Sheldrick, G. M. SHELXTL/PC (Version 5.03). Siemens Analytical X-ray Insruments, Inc., Madison Wisconsin, USA; 1994.
142. Simonsen, K. B.; Becher, J. *Synlett* **1997**, 1211-1220.
143. Spanggard, H.; Prehn, J.; Nielsen, M. B.; Levillain, E.; Allain, M.; Becher, J. *J. Am. Chem. Soc.* **2000**, *122*, 9486-9494.

144. Steed, J. W.; Atwood, J. L. Supramolecular Chemistry, 2nd Edition. John Wiley & Sons, Ltd. USA, 2009.
145. Supur, M.; El-Khouly, M. E.; Seok, J. H.; Kay, K.-Y.; Fukuzumi, S. *J. Phys. Chem. A.* **2011**, *115*, 14430-14437.
146. Takai, A.; Gros, C. P.; Barbe, J.-M.; Fukuzumi, S. *Phys. Chem. Chem. Phys.* **2010**, *12*, 12160-12168.
147. Takeuchi, M.; Ikeda, M.; Sugasaki, A.; Shinkai, S. *Acc. Chem. Res.* **2001**, *34*, 865-873.
148. Tanaka, K.; Matsumoto, T.; Ishiguro, F.; Chujo, Y. *J. Mater. Chem.* **2011**, *21*, 9603-9607.
149. The Porphyrin Handbook: Phthalocyanines: Spectroscpic and Electrochemical Characterization. Elsevier Science: USA, 2003; Vol. 16.
150. Tompa, P. *Chem. Rev.* **2014**, *114*, 6715-6732.
151. Traylor, T. G.; Mitchell, M. J.; Ciccone, J. P.; Nelson, S. *J. Am. Chem. Soc.* **1982**, *104*, 4986-4989.
152. Tsai, C.-J.; del Sol, A.; Nussinov, R. *J. Mol. Biol.* **2008**, *378*, 1-11.
153. Veauthier, J. M.; Tomat, E.; Lynch, V. M.; Sessler, J. L.; Mirsaidov, U.; Markert, J. T. *Inorg. Chem.* **2005**, *44*, 6736-6743.
154. Wakamiya, A.; Murakami, T.; Yamaguchi, S. *Chem. Sci.* **2013**, *4*, 1002-1007.
155. Wang, F.; Schwabacher, A. W. *J. Org. Chem.* **1999**, *64*, 8922-8928.
156. Wasielewski, M. R. *Acc. Chem. Res.* **2009**, *42*, 1910-1921.
157. Wasielewski, M. R. *Chem. Rev.* **1992**, *92*, 435-461.
158. Wessendorf, F.; Gnichwitz, J.-F.; Sarova, G. H.; Hager, K.; Hartnagel, U.; Guldi, D. M.; Hirsch, A. *J. Am. Chem. Soc.* **2007**, *129*, 16057-16071.
159. Wessendorf, F.; Grimm, B.; Guldi, D. M.; Hirsch, A. *J. Am. Chem. Soc.* **2010**, *132*, 10786-10795.
160. Winters, M. U.; Pettersson, K.; Mårtensson, J.; Albinsson, B. *Chemistry* **2005**, *11*, 562-573.
161. Wudl, F.; Smight, G. M.; Hufnagel, E. J. *Chem. Comm.* **1970**, 1453-1454.

Vita

Christina Marie Davis was born in Virginia in 1988, the daughter of Marie and David Davis. In 2006, she graduated from Brooke Point High School and began to pursue her bachelor's degree in chemistry at The College of William and Mary. In 2010, she received her B.Sc. in Chemistry with Highest Honors after which she moved to Austin, Texas to begin her Ph.D. program under the guidance of Prof. Jonathan L. Sessler at the University of Texas at Austin. During the fall of 2011 she was a visiting researcher at Yonsei University in Seoul, South Korea where she worked with Prof. Dongho Kim and Dr. Sessler for the semester. She has also been a visiting scholar at Osaka University where she worked with Prof. Shunichi Fukuzumi during the months of February (2012), July (2012), and November (2013). Christina received Honorable Mention in the National Science Foundation Graduate Research Program in 2011 and a Graduate School Continuing Fellowship in the summer of 2014.

Permanent email: cmdav2@gmail.com

This dissertation was typed by the author.